Copper Based Nanomaterials for Potential Biomedical Applications

By

Madhumita Das
Roll No. 146153008

A Thesis

Submitted in Partial Fulfillment of the Requirements for the Degree of

DOCTOR OF PHILOSOPHY

at the

Indian Institute of Technology Guwahati

Centre for Nanotechnology
Indian Institute of Technology Guwahati
Guwahati- 781039, Assam, India
July, 2019

Copper Based Nanomaterials for Potential Biomedical Applications

A thesis by ***Madhumita Das***

Thesis Supervisors,

Prof. Siddhartha Sankar Ghosh and Prof. Arun Chattopadhyay

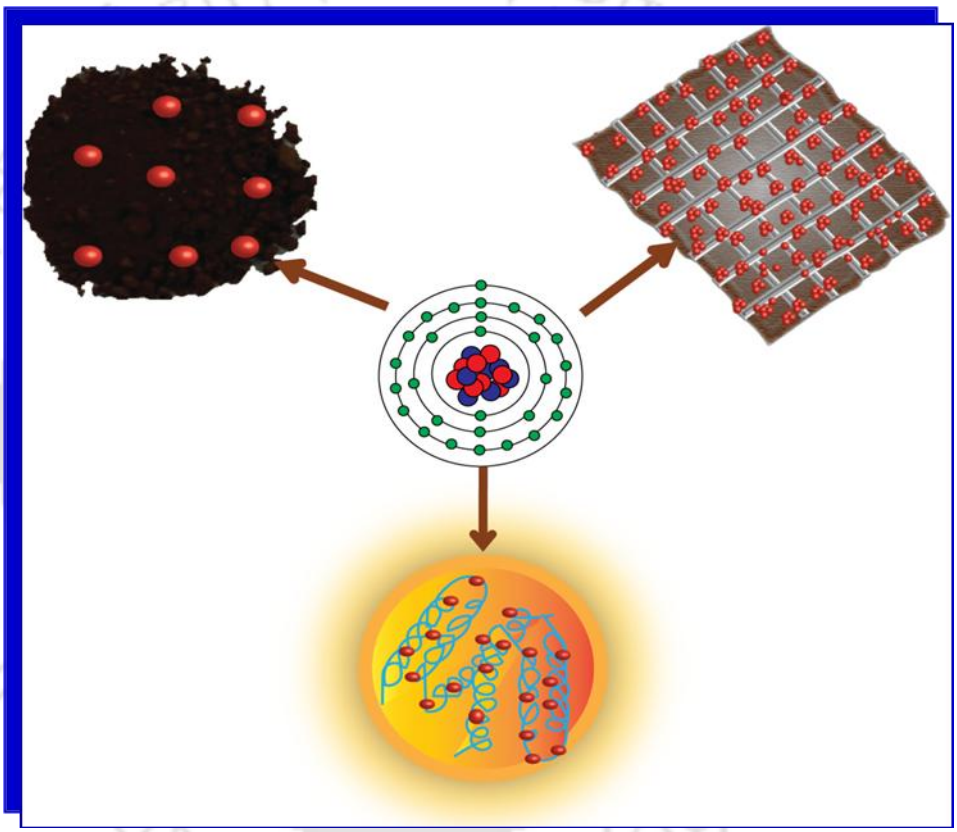

Centre for Nanotechnology
IIT Guwahati, Assam, India.

DECLARATION

I hereby declare that the results and discussions embodied in the thesis titled "**Copper Based Nanomaterials for Potential Biomedical Applications"** is the outcome of research work carried out by me under the supervision of ***Prof. Siddhartha Sankar Ghosh*** and ***Prof. Arun Chattopadhyay***, **Centre for Nanotechnology**, **Indian Institute of Technology Guwahati**, **Guwahati**, **Assam**, **India** for the award of the degree of Doctor of Philosophy. To the best of my knowledge and belief, the present thesis has not been submitted for any degree, diploma, associate ship etc. of any Institute or University elsewhere.

Date:
Place: Guwahati

Madhumita Das
Centre for Nanotechnology
IIT Guwahati, Guwahati-781039
Assam, India

भारतीय प्रौद्योगिकी संस्थान गुवाहाटी
INDIAN INSTITUTE OF TECHNOLOGY GUWAHATI

CERTIFICATE

This is to certify that the thesis entitled "**Copper Based Nanomaterials for Potential Biomedical Applications"** being submitted to the **Indian Institute of Technology Guwahati** by ***Madhumita Das*** (Roll No. **146153008**) for the award of the degree of **Doctor of Philosophy** in ***Nanotechnology*** is a bonafide record of research work carried by her. The information and data reported by her are solely the results of her original findings. She has meticulously carried out the investigations and followed the guideline of the laboratory. This work has not been submitted elsewhere for any degree or diploma.

Prof. Siddhartha Sankar Ghosh

Thesis Supervisor
Department of Biosciences and Bioengineering, Indian Institute of Technology Guwahati, Guwahati-781039, Assam, India

Prof. Arun Chattopadhyay

Thesis Supervisor
Department of Chemistry, Indian Institute of Technology Guwahati, Guwahati-781039, Assam, India

Dedicated to my Family

ACKNOWLEDGEMENT

Here I am facing the end of a journey and what a journey it has been. It started with an audacious dream of being a student again, of learning and of reliving a part of my life I had left way behind. It is nothing short of a miracle to me that I have somehow managed to complete the race. There have been some obstacles and hurdles but they certainly made the race more entertaining. This journey that I must now see to its inevitable conclusion has not always been smooth sailing but definitely a fulfilling one. Now that I am standing at the edge of the precipice I must look back to my guides and my companions. This is the time for farewells and words of gratitude, of thankfulness and acknowledgement.

I am a full time professional, a doctor with the responsibilities and working hours that leave no time for anything outside of the ordinary. Yet, I ventured into pursuing after research, after a whole new world that could open up new possibilities for me and at the same time make my life a whole lot more challenging. And the biggest support behind my unorthodox choice was my family. My daughter who had by now completed her post graduation became my tutor. She persevered when I wanted to give up and doggedly ensured that I was prepared for the big challenge ahead. My first big hurdle was the entrance test. I passed it thanks to my own unrelenting stubbornness and my daughter's tutoring only to be met with the herculean task of convincing the Institute that I could be an asset to them. This is where I was introduced to the two people who not only showed immense trust on a virtual stranger but also made possible for me to turn my dream into reality. Once what was only a vague idea suddenly became a part of my life. These two people are my supervisors, Prof. Siddhartha Sankar Ghosh and Prof. Arun Chattopadhyay. I owe them my place in the institute and everything that came after. Their support and guidance have carried me through my research and I will be forever grateful to them for everything they have taught me. Their unstinting confidence in my abilities gave me the encouragement I needed to keep going when times got tough. They were my mentors, my moral support and my guiding light. I must also express my sincere

thanks and gratitude to Prof. Pranab Goswami for his support and guidance. He was the man who provided me with all the study materials to prepare for the entrance examination. He was also the first person who encouraged me to appear for the interview to get admitted in to the Centre for Nanotechnology.

I am also thankful to my doctoral committee members Dr. Sunanda Chatterjee (Chairperson), Dr. Lal Mohan Kundu, Dr. Partho Sarathi Gooh Pattader**,** Prof. Parameswar Krishnan Iyer for their valuable suggestions and their patience during all of my seminars. They were instrumental in assuring my progress throughout my research period.

It would be a grave injustice and unforgivable of me not to extend my special thanks to Dr. Upashi Goswami, my lab mate and collaborator. She was the teacher who taught me everything that was foreign to me in this endeavor and the friend who supported me when I needed it. Without her, I cannot imagine a fitting end to this journey.

I must thank my collaborators from IASST, Dr. Raghuram Kandimalla and Dr. Sanjeeb Kalita for their help and expertise in my work with *in vivo* systems. Thanks to my other collaborator Ms. Srirupa Bhattacharyya for pitching in whenever I needed her.

I would like to thank Central Instrumental Facility (CIF), Centre for Excellence in Nanoelectronics & Theranostic Devices (CENTD) and DBT Programme Support (Centre for Excellence) for providing me with the much needed instrumental facilities. I am thankful to all the staff members of Centre of Nanotechnology and CENTD, especially, Mr. Kaustubh Acharyya, Mr. Paran Dutta, Mrs. Pranjoli Das and Mr. Indrajit Talukdar for their help and support. Mr. Indrajit Talukdar in particular must be given a special mention for carrying out all the TEM experiments with so much patience and care. I am thankful to my lab mates Dr. Amaresh Kumar Sahoo, Dr. Aditi Banerjee, Dr. Bandhan, Dr. Upashi, Dr. Deepanjalee, Anitha, Debashree, Konika for providing me with a healthy work environment. I am also indebted to Anitha and Debashree who helped me a number of times by babysitting my experiments. I also offer my sincere thanks to Namami, Anushree, Srestha, Ujjwal, Kasturi and Somorjit for their help and support.

Last but not the least; I must thank my family members for all their encouragement, love, and support.

Madhumita Das

TABLE OF CONTENTS

Thesis Abstract

Copper Based Nanomaterials for Potential Biomedical Applications

By

Madhumita Das

Submitted to the Indian Institute of Technology Guwahati in July, 2019 in Partial Fulfillment of the Requirements for the Degree of Doctor of Philosophy in Centre for Nanotechnology

With the advent of nanoscience and nanotechnology, several new approaches have been developed to design materials at the nanoscale level. Recently, metallic nanoclusters have emerged as new nanoscale materials with multitude of promising applications in the health care system. As a relatively safe material with wide functionality; copper was chosen as a primary platform to fabricate some therapeutic tools for potential applications in cancer therapy, annihilation of multidrug resistant clinical isolates, development of point of use water filtration device for house hold use, and fabrication of dressing materials for assisting in healing of infected diabetic wound. The present thesis is divided into six chapters.

Chapter 1 of the thesis describes about nanoscience and nanotechnology. It also provides information about nanomaterials along with their synthesis and multi-dimensional applications. Salient features of this current thesis work have been mentioned in brief.

Chapter 2 explains a facile, novel process of fabrication of a luminescent bovine serum albumin (BSA)-copper nanocluster (BSA-Cu NC) customized ibuprofen nanodrug (BSA-CuNC-Ibf). As malignancy has covered a major portion of the health ailments of our society, cancer chemotherapy with the prepared nanodrug has been pesuaded in *in vivo* system. The as synthesized BSA-CuNC-Ibf exhibited incomparable chemotherapeutic efficiency on Dalton's lymphoma ascites (DLA) bearing Swiss

albino mice with significant reduction of tumour growth. It also inhibited metastasis of the cancer cells and thus enhances the life expectancy of mice.

Chapter 3 of the thesis reports a novel facile method for synthesis of a bimetallic Fe-Cu-nanocomposite on the surface of fine sand particles. Looking at the potential antimicrobial role of copper nanoparticles, a broad spectrum antimicrobial agent was fabricated as an effective tool against multidrug resistant bacteria, as emergence of drug resistant bacteria is a major cause of concern in treating infections. The prepared bimetallic nanocomposite exhibited antimicrobial activity against multidrug resistant bacteria as well as fungus isolated from different human biological samples like blood, urine, pus and wound swab. The observed broad spectrum antimicrobial property of the nanocomposite was applied next for purification of water.

Chapter 4 reports fabrication of a portable water filter utilizing the bimetallic nanocomposite for point-of-use water filtration. The nanocomposite could easily be used to filter a wide range of bacteria along with hazardous metals. Therefore, the prepared nanocomposite could be beneficial as a hand hold simple and cost effective water filtration device.

The multifaceted role of copper in nanoplatform was also implemented to treat infected diabetic wound, as diabetes mellitus is one of the most prevalent health problems of the community with high risk of developing various alarming complications if not controlled properly.

Chapter 5 of this thesis describes fabrication of a nanomaterial based dressing material in dual form, which exhibited broad spectrum antimicrobial activity. The wound healing ability of both the dressing materials was also carried out in Wistar albino rats with infected diabetic wounds. Remarkably, they have also been found to assist in healing of infected diabetic wounds and show a promising prospect in the management of other infected wounds.

Chapter 6 of this thesis gives an overview of the whole work along with future prospects of the prepared materials. The composition reported in the thesis mainly emphasized on development of novel metal nanoplatform and functionalizing with different materials for their biomedical applications. The current work has multifaceted application potential in the field of nanomedicine.

Glossary of Acronyms

a.u.	Arbitaray Units
ALP	Alkaline Phosphatase
ALT	Alanine Transaminase
AST	Aspartate Transaminase
BSA	Bovine Serum Albumin
CFU	Colony Forming Unit
CI	Combination Index
CLSM	Confocal Laser Scanning Microscope
Cu	Copper
Cu NCs	Copper Nanoclusters
Cu NPs	Copper Nanoparticles
DCFH-DA	2, 7-Dichlorofluoresceindiacetate
DLA	Dalton's Lymphoma Ascites
DLC	Differential Leukocyte Count
DMSO	Dimethyl Sulphoxide
EDX	Energy Dispersive X-ray Spectrum
EtBr	Ethidium Bromide
Fe	Iron
Fe NPs	Iron Nanoparticles
FESEM	Field-Emission Scanning Electron Microscopy
GFP	Green Fluorescent protein
Hb	Hemoglobin
HeLa	Human Cervical Cancer Cell Line
LFT	Liver Function Tests
NB	Nutrient Broth
Plt	Platelet
PBS	Phosphate Buffered Saline
RBC	Red Blood Cell
ROS	Reactive Oxygen Species
TEM	Transmission Electron Microscope
WBC	White Blood Cell

CHAPTER-1

Introduction and Review of Literature

Chapter 1 introduces a concise description about nanoscience and its impact in nanomedicine. It also describes about importance of nanoparticles in the field of nanomedicine, their synthesis, property and applications. It gives brief illustrations about applications of metal nanoplatform in various biomedical fields.

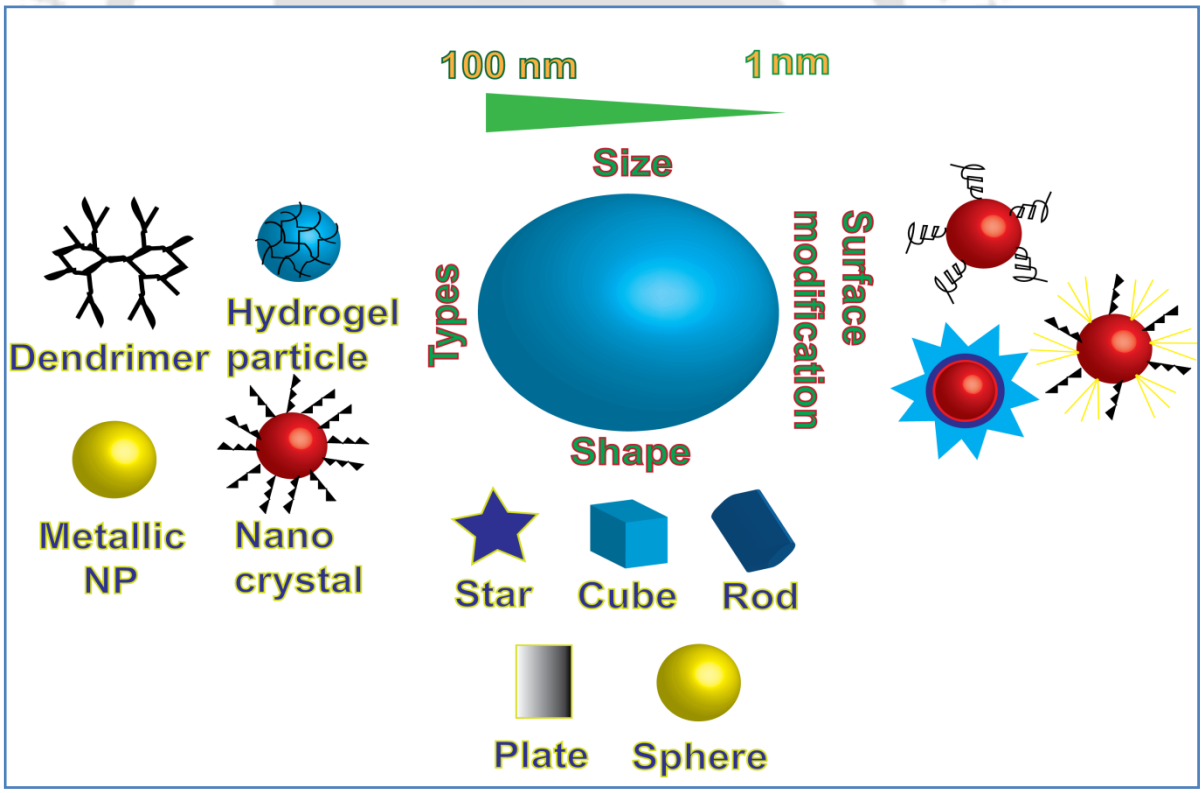

CHAPTER -1

1.1. Introduction

The term nano (originate from Greek word *nanos*, which means dwarf) refers to a factor of 10^{-9} (one billionth) a unit prefix[1-2] both in the International System of Units (SI) and in the non SI units. Nanoscience is the branch of science that deals with the study of materials at the scale of nanometer (1-100 nm) at least in one dimension.[3] Nanotechnology on the other hand, concerns itself with tools and techniques of manipulating the nanoscale objects at molecular level.[4] Nanoscale objects or nanomaterials attain immense importance because of their superior chemical, physical, optical, magnetic, thermal, electrical, imaging and mechanical properties compared to their conventional counterparts.[5-7] Because of these unique properties they are highly desirable for applications in various disciplines like agriculture, catalysis, chemistry, commercial, electronics, environmental sectors, food industry, physics, solar cells and also in biomedical healthcare.[6] Acquiring the knowledge from nanoscience about the material behavior of nanoscale objects, nanotechnology focuses on engineering various nanomaterials for widespread applications[1,4] in the field of photonics, electronics and medicines.[8] Specially in the field of medicine, numerous nanoplatforms have been explored extensively for biosensing,[9] bioimaging[9] drug delivery, gene therapy, tissue engineering and nanomedicine.[10]

1.2. Nanoscale Materials

Nanoscale materials or nanomaterials refer to a group of substances which have a diameter of 100 nanometers or less, at least in one dimension.[5] Materials after obtaining the nanometer scale in size, attain distinct behavior due to increase surface to volume ratio, increased reactivity and mechanical strength.[6] They may present in different forms like single, fused, aggregated or agglomerated with spherical, tubular, and irregular shapes.[6,11] They are classified on the basis of number of dimensions into four

classes. (1) zero dimensional (0-D), where all dimensions (x,y,z) are at nanoscale i.e. ≤ 100 nm. These are mostly atomic clusters. (e.g. nanoparticles), (2) one dimensional (1-D), where two dimensions (x,y) are at nanoscale level but the other dimension (z) is not (e.g. nanowires, nanotubes, nanorods, ceramic crystals and polymer nanofibers), (3) two dimensional (2-D), where one dimension (z) is at nanoscale level but the other two dimensions (x,y) are not (e.g. grapheme, nanofilms, nanoplates nanocoatings), and (4) three dimensional (3-D) which are not limited to nanoscale level in any dimensions (e.g. polycrystals and spherical particles). This classification is not confined to 1-100 nm of nanoscale range.[6,12] Nanomaterials attain immense importance because of their superior chemical, physical, optical, magnetic, thermal, electrical, imaging and mechanical properties compared to their conventional counterparts.[5-7] Because of these unique properties they are highly desirable for applications in various disciplines like agriculture, catalysis, chemistry, commercial, electronics, environmental sectors, food industry, physics, solar cells and also in biomedical healthcare.[6] Nanomaterials may be of several varities, for example, nanoclusters, nanoparticles, nanocomposites, nanocapsules, nanoporous materials, nanofibres, fullerenes, nanowires, single-walled and multi-walled (Carbon) nanotubes etc.[13]

1.3. Nanoparticles

As an elementary module of nanotechnology, nanoparticles have gained enormous importance in the recent years. Nanoparticles are broadly classified into three groups like organic, inorganic and carbon based nanoparicles.

1.3.1. Organic Nanoparticles

Organic nanoparticles are harmless and eco-friendly. Examples of organic nanoparticles are dendrimers, micelles, liposomes etc. They are suitable candidate for packing with drug and gene for delivery, as some of the organic nanoparticles (micelles and liposomes) have unique property of forming a nanocapsule, entrapping substance in their hollow core.[6,14] Few examples of organic nanopartcles are illustrated in **Figure 1.1.**

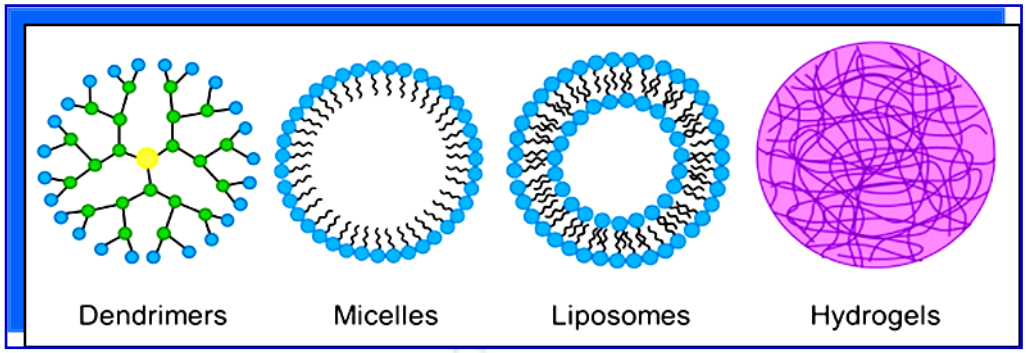

Figure 1.1. Schematic examples of some common types of organic nanoparticles. [Reprinted with permission from **reference 15**. Copyright 2017, American Chemical Society].

1.3.2. Inorganic Nanoparticles

Inorganic nanoparticles are mostly metal based or metal oxide based. Metal based nanoparticles are synthesized from metals. On the other hand, metal oxide nanoparticles are prepared from their respective metallic nanopartcles. Inorganic nanoparticles are better candidates for imaging and cancer treatment because of the plasmonic and magnetic properties of some inorganic nanoparticles.[6] Inorganic nanoparticles embedded within organic components can be used for next-generation theranostics as they reveal properties of both types of nanoparticles.[15] In **Figure 1.2.** schematic illustrations of some common inorganic nanoparticles are depicted.

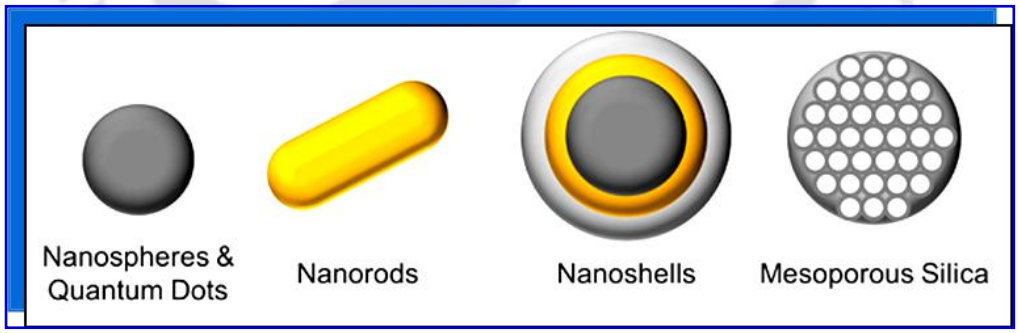

Figure 1.2. Schematic examples of some common types of inorganic nanoparticles. [Reprinted with permission from **reference 15.** Copyright 2017, American Chemical Society].

1.3.3. Carbon based Nanoparticles

Carbon based nanoparticles are synthesized from carbons. Different carbon based nanoparticles are carbon nanotubes (CNT), carbon nanofibers, carbon black, fullerenes, graphenes and nano sized activated carbon.[6,16] Schematic examples of some common types of carbon based nanoparticles are depicted in **Figure 1.3.**

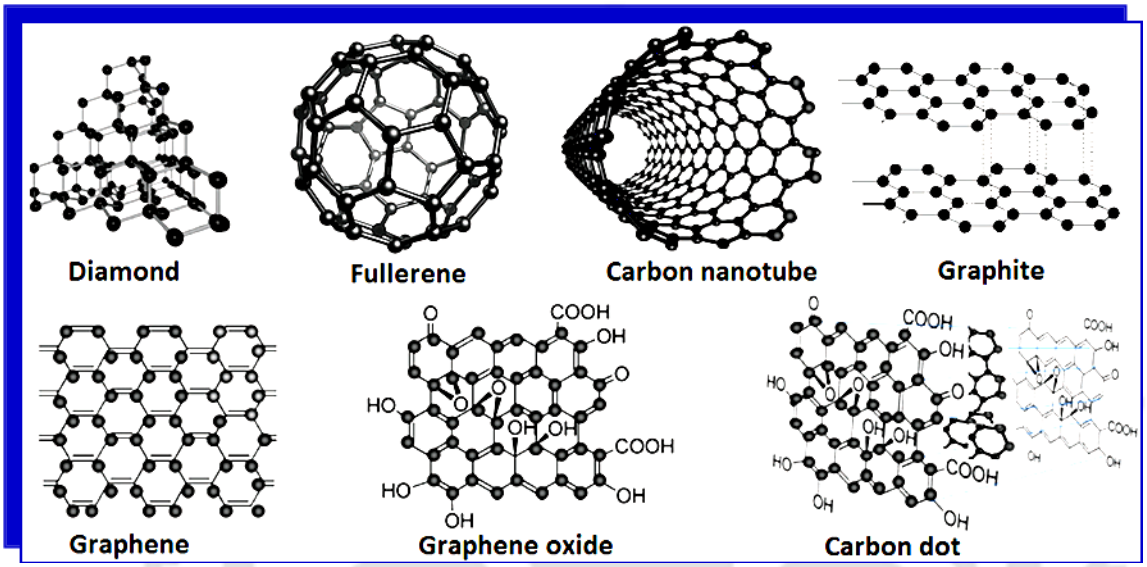

Figure 1.3. Schematic examples of some common types of carbon based nanoparticles. [Reprinted with permission from **reference 7.** Copyright 2016, Royal Society of Chemistry].

1.4. Metallic Nanoparticles

Metallic nanoparticles have attracted significant attention in the field of material science because they exhibit distinctive quantum properties, different from that of the corresponding bulk materials.[17] Also they are more reactive compared to their metal counterparts.[6] Common metallic nanoparticles are silver (Ag NPs), gold (Au NPs), iron (Fe NPs), copper (Cu NPs), zinc (Zn NPs), cobalt (Co NPs), aluminium (Al NPs) and lead (Pb NPs) nanoparticles.[6,18] They have unique properties like crystalline and amorphous structures, high surface area to volume ratio, surface charge, and sensitive to air, moisture, heat and light. Metallic nanoparticles are extremely expedient for applications in optical, thermal, magnetic and sensor devices.[19]

1.4.1. Copper Nanoparticles

Copper nanoparticles have drawn much attention because of their natural abundance, good electrical conductivity, high melting point, minimal electrochemical migration, excellent soldering ability, catalytic activity and affordabillity.[17,19] Copper has substituted the place of other metals such as Ag, Au and Pt, in many applications like, heat transfer and inkjet printing[19,20] because of its low cost, high conductivity,[19] small size, high surface/volume ratio, improvement of size, shape and oxidation resistance, etc.[19] Moreover, high boiling point of copper helps to withstand high-temperature and-pressure chemical reactions and thus helps in various organic transformations.[17] All these distinctive properties, have made copper one of the most precious metals in recent years.

1.4.1.1. Synthesis of Copper Nanoparticles

The techniques of copper nanoparticles synthesis are basically classified as chemical or bottom-up and physical or top-down method.[19] In bottom-up method, materials are build-up from atom to clusters and then to nanoparticles. Whereas in top-down method, materials are shrink down from bulk to nano scale.[6,19] Chemical reduction, sonochemical reduction, sol-gel, micro emulsion, electrochemical, hydrothermal, polyol, pyrolysis, biological synthesis and microwave supported techniques are few examples of chemical methods of copper nanoparticle synthesis. Few examples of physical techniques are laser ablation, nanolithography, vapor phase synthesis, mechanical milling, spinning, sputtering, thermal decomposition and pulsed wire discharge.[19]

Among all these methods, chemical treatment is the most widely accepted method and even many of the recently used techniques to manipulate the shape and/or size of the NPs are considered as a modified protocol of the chemical method. It is simple, flexible and most importantly size and shape of the Cu NPs can be controlled by optimizing the reaction conditions. Chemical method for preparing Cu NPs is centered on reduction, hydrolysis, condensation and oxidation reactions. Selection of any one and/or combination of the above chemical reactions basically depends on the type of materials to be prepared.[17,19]

Cu-based materials are highly reactive as they remain in a wide range of oxidation states like Cu^{0}, Cu^{+1}, Cu^{+2}, Cu^{+3}. Because of the inherent tendency to get oxidized under atmospheric conditions, synthesis of copper nanoparticles is much more difficult than the other noble metal nanoparticles. To overcome this problem, many efforts have been made to prepare stable Cu NPs by using different stabilizers (like BSA,[21] SiO_2 shell[22]) during synthesis or by exploring new techniques to prepare Cu NPs with more complex structures. Trials are also conducted to anchor Cu NPs (e.g., Cu, CuO, or Cu_2O) on supports such as iron oxides,[23] SiO_2,[24] polymers[25] to increase the stability Cu NPs.[17] These support materials may interact with the Cu NPs and may also confer their properties resulting in alterations in final material's physical and chemical properties. Therefore, by selecting an appropriate support, it is possible to fabricate a novel Cu NPs suitable for selected application.

In this regard, a variety of metals and metal oxides have been tried and tested as supporting materials for Cu based NPs synthesis. Recently, use of magnetic nanoplatform in different research area have attracted a lot of attention because of their easy recovery with the help of an external magnetic field.[17]

1.4.2. Iron nanoparticles

Chemically inert superparamagnetic iron oxide nanoparticles (IONPs) such as magnetite (Fe_3O_4), hematite (α-Fe_2O_3) and maghemite (γ-Fe_3O_4) are extensively studied due to their unique properties such as biocompatibility, surface to volume ratio, greater surface area, potent magnetic and catalytic behavior, easy separation technique, low toxicity, and superior colloidal stability.[26] Currently, IONPs are customized by polymers, inorganic metal/metal oxides or bioactive molecules to fabricate engineered NPs with enhance efficacy[27] This can be achieved by several techniques like layering a coating material over the iron oxide core, to form core–shell structure or the NPs are dispersed in a matrix to form the beads.[28]

Many methods are adopted for synthesis of IONPs by modifying the conventional protocols in order to achieve the best physicochemical properties.[29] Selection of synthesizing method is crucial because it affects the size, surface chemistry, magnetic behavior and most importantly degree of biocompatibility in living

organisms ascertained by way they interact with biological barrier and lipid bilayer of cell membrane.[29,30] Broadly, there are three main ways of IONP preparation.[31]

1. Chemical: Chemical methods are the most commonly employed methods. These are simple, and efficient. Moreover, size and shape of the NPs can be manipulated. Examples of chemical methods are coprecipitation, hydrothermal, microemulsion, sol-gel, thermal decomposition, electrochemical decomposition, polyol etc. The size and shape of the prepared Fe NPs depend on the nature and ratios of precursors used.[31,32]
2. Physical: Physical methods are elaborate and they do not have control over the manipulation of the size of the particles. Examples are aerosol, gas phase deposition, pulsed laser ablation, laser induced pyrolysis, power ball milling, electron beam lithography.[31,33]
3. Biological: Biological methods may be protein mediated, bacteria mediated, fungi mediated and plant mediated.[31,34]

A comparison of the synthesis of IONPs by three main methods currently existing for the synthesis of IONPs is illustrated in **Figure 1.4.**

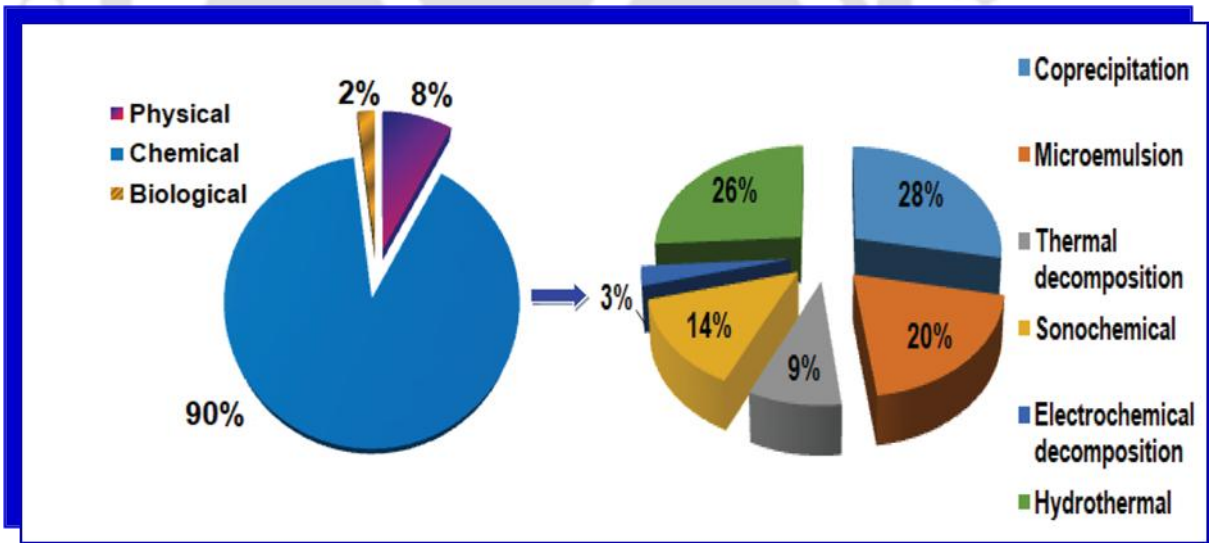

Figure 1.4. Scematic representation of comparison among the prevalence of the main methods of IONPs synthesis.

Amongst all these methodologies, chemical methods are mostly employed because of high yield with low operating expense. And out of all the chemical methods, co-precipitation method is the most widely used method. The beauty of this method is that, it allows IONPs to be fabricated in an inert nitrogen atmosphere at room temperature. By this method, it is likely to get smaller IONPs in scale size of 5 - 40 nm. Usually, size, shape, and magnetic properties of the resulting IONPs depend on reaction conditions such as the type of salts used, pH, and ionic strength.[29]

1.4.3. Applications of metal nanoparticles (Cu NPs and Fe NPs)

Copper nanoparticles have gained significant interest because of their physicochemical properties such as small dimensions, high surface-to-volume ratio, easy interaction with other particles, high melting point, electrical and thermal conductivity, highly reactive compared to other metallic nanoparticles, light absorption and high heat transfer ability. On account of these unique properties, copper nanoparticles are widely used in heat transfer systems,[35] as biosensors,[36] in high strength materials,[37] as catalysts,[38] as biolabel, cancer therapeutics,[39] promising industrial tools as gas sensors, high temperature superconductors and in solar cells.[40] Cu NPs are also established as a potent antimicrobial agent.[19,41] A major proportion of the health hazards in India are due to different types of pathogens and water plays a major role in their transmission. Poor water quality and lack of adequate disposal of wastes are contributing to waterborne diseases.[42] The major contaminant of water is the microorganism, and removal of pathogenic microorganism is the most crucial step of water treatment.[14] On the other hand; large-scale use of conventional antibiotics has led to generation of new strains of pathogens with increasing levels of antibiotic resistance. Therefore, development of a new antimicrobial agent in the form of nanoparticles which can be used as a device to evade multidrug resistant mechanisms[43] has now become a crucial objective. There are reports stating the potentiality of Cu NPs in purification of wastewater.[39,44]

In addition, they also have attracted interest as wound healing matrix because of their biocidal properties.[40,45] Usually, the wound healing is a self-liming, very well-organized process and it starts instantaneously after the injury and accomplished within

a period of 1−12 weeks by the process of cell proliferation followed by tissue remodeling and regeneration.[46] However clinical challenges arise when there are superadded microbial infections resulting in delayed healing[47] which is very common phenomenon in chronic wounds like pressure ulcers, diabetic ulcers, and vascular ulcers.[46] Out of these, diabetic ulcer is more common. Worldwide almost 285 million adult (6.4%) in the age group of 20-85 yrs are reported to have diabetes in 2010, which is likely to touch 7.7% (439 million) by 2030. So from 2010 to 2030, there will be a 69% increase in numbers of adults with diabetes in developing countries like India. This prediction, which is based on a large number of studies indicate a rising burden of diabetes in developing countries.[48] Long standing diabetes is always associated with numerous complications and foot ulceration is the most common complication which affects almost 15% of diabetic patients.[49] Secondary infection in an unhealed diabetic foot ulcer is the most dreaded complication that may end up with amputation of the limb.[50] Therefore, research endeavors to remodel a value-added dressing material targeting both infection control and faster wound healing by a biocompatible, affordable and potent material is the need of the hour.

At the same time, the unique physicochemical properties of the IONPs make them one of the most promising tools for biomedical applications.[29] By virtue of their ultrafine size, magnetic properties, and biocompatible quality, the superparamagnetic iron oxide nanoparticles (SPION) have emerged as a potential contrast agent for MRI and an imminent nanoplatform for targeted drug delivery, bioimaging, hyperthermia, gene therapy, stem cell tracking, molecular/cellular tracking, antibacterial agent, early detection of inflammation, cancer, diabetes, and atherosclerosis.[51] It is worth mentioning that, because of magnetic driving via an external field, IONPs are used for easy separation of biological products and also used to add magnetic properties to other engineered particles.[29,31] The ability of IONPs to remove contaminants is utilized for industrial scale wastewater treatment which applies its nanosorbent or photocatalytic properties.[52]

1.5. Nanoclusters

Nanoclusters (NCs) are quite newcomer as a group of functional materials in the field of nanomedicine. They are made up of several to tens of atoms with a core size usually less than 2 nm.[53,54] The ultra-small size of the NCs, which is very close to the Fermi wavelength of electrons, offer them distinct energy levels and a multitude of molecular-like properties,[55,56] such as highest occupied molecule orbital-lowest unoccupied molecule orbital (HOMO-LUMO) transition, tunable luminescence, large Stokes shift, quantized charging, molecular chirality and magnetism.[55,57] Nanoclusters (NCs) have been acknowledged as a promising nanoscale materials in catalysis,[53,58] biosensors,[53,59] detection of biomolecules[53,60] and heavy metals,[53,61] and solar cells.[53,62] Lately, much emphasis has been given in cancer theranostics due to their easy synthesis, good stability, biocompatibility, trouble-free conjugation, and better renal clearance.[53,63] A range of metallic NCs like silver (Ag), gold (Au) and copper (Cu) are put into practice in the field of biosensing, biolabelling, bioimaging as well as nanotherapy.[55,64] They link the breach between nanoparticles and bulk compound and demonstrate molecule like properties.[65] Because of their light-emission and other unique attributes, metallic NCs have proved superior to other nanoscale materials in the theranostic platforms.[55,66] Recently, a number of strategies are followed to improve the performance of the metallic NCs in a biological set-up, either by tailoring the metal NCs with surface ligands such as proteins,[67] thiols,[68] polymers,[69] imaging agents, anticancer drugs, physiotherapy agents or by immobilizing these metal NCs with a variety of inorganic nanostructures.[55,70,71] For examples, when metallic NPs are functionalized with proteins and peptides , some of the functional groups, such as carboxyl, thiol and amino groups, act as reducing agents or served as protecting ligands/capping agents for the metal NCs. Therefore, metallic NCs are considered as a budding nanomaterial in developing cancer nanomedicine.

1.5.1. Strategies for fabrication of Nanoclusters

Basically, “top-down” and “bottom-up” strategies are followed to fabricate nanoclusters. In “top-down” approach, materials are etched down from bulk to nano scale and usually using a ligand as stabilizer (e.g. thiol compound), already prepared

nanoparticles are scraped down into nanoclusters. This is also known as chemical etching method. There are two approaches for etching the nanoparticles. In one, with the help of a ligand, first the atoms are detached from the surface of nanoparticles and then nanoclusters are formed through atom-atom interactions.[53,72] In the other, ligands are used to etch the nanoparticles stepwise till the NCs of appropriate sizes are produced.[73]

On the other hand, in "bottom-up" method, materials are assembled from atom to cluster in presence of a ligand or template, which consequently helps to stabilize the prepared NCs. Chemical reduction, photoreduction, microwave-assisted synthesis, sonochemical synthesis and electrochemical synthesis are few examples of bottom-up method.[53]

(a) Chemical Reduction Method

It is the most widely used method where reducing agents are used to fabricate the nanoclusters. Besides, some templates and/or protecting ligands are also used in the chemical reduction process. Small molecules, containing free thiol (-SH) groups such as dihydrolipoic acid (DHLA),[74] glutathione (GSH),[75] 3-mercaptopropionic acid,[76] phenylethylthiolate,[77] *etc*. are commonly used ligands for metallic nanoclusters synthesis. Some other small molecules such as phosphines and alkynyl are also used as stabilizing agent to prepare NCs.[78] Besides the small molecules, some macromolecules like dendrimers (polyamidoamine, poly propylene imine),[79,80] polymers (poly methacrylic acid, polyethylene imine, chitosan, etc.),[76,79,80] biomolecules like protein, peptide, and DNA oligonucleotides[81] are also utilized as a template to synthesize NCs[82] which also act as reducing agent and help to stabilize them.[66,83] Among the proteins, bovine serum albumin (BSA)[21,84] is the most extensively used protein template for metallic NCs synthesis. Selection of protecting ligand or template is an important step in fabrication of NCs as it can affect the surface properties of NCs which is the main objective of their use in biomedicine.

(b) Photoreduction Method

The NCs are also fabricated by photoreduction method using microgel,[85] hydrogel,[86]

polymers,[87] and small molecules (D-penicillium, L-penicillium)[88] as template where metal ions are successfully converted into metal atoms by the irradiation of UV rays.

(c) Electrochemical Method

In electrochemical method, metal ions generated from the anode are reduced into metal atoms at the cathode. These metal atoms are then assembled into NCs in the presence of a ligand. Controlling the voltage, amount of stabilizers and electrolytes, it is easy to manipulate the size of NCs.[89]

(d) Sonochemical Method

High intensity ultrasound is used to sonicate a liquid to produce acoustic cavitations, which resulted in formation of HO_2•, H•, OH•, free electrons. These highly reactive species reduce the metal ions into metal atoms.[90]

(e) Microwave Assisted Method

Microwave irradiation assisted brisk and uniform heating in a solution produces uniform and monodispersable NCs.[91]

1.5.2. Copper Nanoclusters

Compared to other metallic NCs such as Ag NCs and Au NCs, Cu NCs are considered safe and eco-friendly as copper is a trace element in the human body. Highly fluorescent quality of the Cu NCs impart them photo- as well as chemical- stability. This promising ultra-small nanocluster has been explored recently for various multidisciplinary applications[74,75] because of its natural abundance, inexpensive, superior optical and catalytic property, tunable luminescence property, high quantum yield, good atomic precision, solubility, easy accessibility from commercial resources and above all effortless functionalization.[92] Out of all other, the catalytic and optical properties (UV-Vis absorption and fluorescence) of copper nanoclusters have been explored most in recent years.[93]

1.5.2.1. Synthesis of Copper Nanoclusters

Wet chemistry synthesis is the most commonly used approach to fabricate Cu NCs where copper ions are reduced to form copper atoms in aqueous medium. Finally these copper atoms aggregate to form Cu NCs, when associated with a pertinent template/ligand, stabilizer and/or reducing agent.[65,92] Development of Cu NCs can be achieved by template-assisted method, ligand-assisted method, electrochemical method and etching method. Copper ions first bind with the specific point of the template and then are reduced to copper atoms by reducing agents followed by cluster formation on the template. Selection of suitable protecting ligand or template is an important step of highly luminescent, stable Cu NC synthesis as it helps to overcome the intrinsic tendency of Cu NC to get oxidized in presence of oxygen.[65,75]

1.5.2.2. Applications of Metallic Nanoclusters (Cu NC)

Luminous metal NCs have been widely applied as fluorescent probe for bio-sensing ranging from *in-vitro* biological analysis to *in-vivo* targeting and bio-imaging. Currently, Cu NCs have been extensively used in cancer theranostics in addition to their wide application as catalysts, biosensors, bio-imaging and light emitting devices. Few of them are exemplified below.

(a) Biological analysis as sensors

The fluorescent Cu NCs have been used as optical probes for the detection of various objects such as metal ions (Hg^{2+}, Pb^{2+}, Cu^{2+}, Fe^{3+}, Cr(VI) and Cr^{3+}),[94-100] anions,[101] small molecules (ATP, cysteine, glutathione, homocysteine)[102-104], protein,[105] nucleic acid[21,94] and solution pH[21] utilizing the fluorescence quenching or enhancing property of metal ions and also by fluorescence turn-on method. Report of an enzyme-free platform, accomplished by smart combination of hybridization chain reaction and Cu NC for selective and quantitative detection of cancer cells and microRNAs is noted.[10,106] Detection of enzyme with the help of a luminescent Cu NC bio-probe is also reported.[10,107] A new amplified chemiluminescence system is stated using protein stabilized bimetal zinc/copper NCs for sensitive and selective detection of H_2O_2 in environmental samples.[94,108] A schematic, illustrating the applications of Cu NC in

biological analysis are exemplified in **Figure 1.5.**

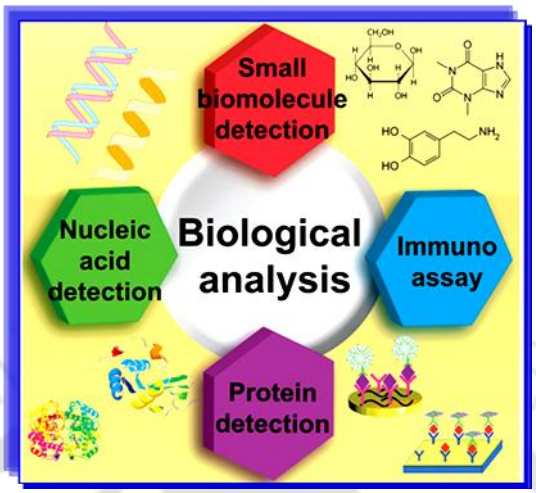

Figure 1.5 Schematic showing the biological analysis applications of Cu NC. [Reprinted with permission from **reference 10.** Copyright 2015, Royal Society of Chemistry].

(b) Bio- labeling and imaging

Recently, highly fluorescent Cu NCs have gained much attention for biolabeling and bioimaging applications because of their ultrafine size, superior biocompatibility and nontoxicity. Development of the *in vivo* imaging probes offer significant precision to diagnostics through detection and monitoring of bio-molecules in living systems.[10] Cu NCs have been efficiently employed for imaging living cells as well as for labelling the cervical cancer cells (HeLa).[94,109] BSA stabilized Cu NCs are reported to be very suitable for cellular imaging.[21,94] BSA-Cu NCs are used as a probe for real-time cellular imaging and the *in-vivo* cellular uptake by CAL-27 cells.[10,21,104] Transferrin (Trf) functionalized Cu NCs are also reported for targeted bioimaging of cancer cells.[94,110] PET radionuclide, copper-64 (^{64}Cu) is expedient as a positron emission tomography (PET) imaging agent because of its decay characteristics and is used as a tool for *in vivo* targeted radiotherapy of cancer.[53] It was introduced by a chelator-free doping method, and also played the role of energy donor besides PET imaging source.

(c) Catalyst

The electrocatalytic activity towards the oxygen reduction reaction (ORR) by copper nanoclusters demonstrated high catalytic activity for the electro-reduction of oxygen,[93]

which suggests potential utility of Cu NC as a platinum-free electrocatalysts for fuel cells.

(d) Cu NC based electrochemical sensors

Copper nanoclusters exhibit high electrocatalytic activities and using this principle various electrochemical biosensors are devised for non enzymatic detection of miRNA,[111] and glucose.[112]

(e) Therapeutic Applications

Metal nanoclusters have promising potentials in imaging-guided cancer therapies because of their brilliant optical properties. Gene therapy using metal nanoclusters, also have great potentials against some morbid diseases like malignancy and genetic disorders.[10,113] And metal nanocluster-based hybrid nanocomposites have been effectively applied for that.[114] Metal nanoclusters are investigated for immunotherapy through development of an effective vaccine which can produce strong $CD8^+$ T cell mediated immunity[115] against diseases like viral infections, cancer, and neurological disorders. They are also extensively used to inhibit the growth of pathogenic microbes. Cu NCs are widely used for annihilation of different microbes like *S.aureus*, *E.coli*, *K.pneumonae*, *B.cereus*, *C.albicans* etc. including methicillin resistant *S.aureus* (MRSA). Insulin directed metal nanoclusters have excellent potential in treatment of diabetes mellitus with a versatile utility of fluorescence imaging, x-ray computed tomography (CT) and *in vivo* blood glucose regulation.[116] Metal nanoclusters are also applied for screening of drugs like ibuprofen, warfarin, phenytoin, sulphanamide etc.[117]

(f) Theranostic Applications

Cancer being a leading cause of death creates a huge burden on society. Conventional therapeutic modalities which include surgery, chemotherapy, radiotherapy, antibody-blocking therapy, or a combination of these therapies most of the time associated with treatment failure rate. Common causes of therapeutic failure are late diagnosis, severe adverse effects and development of drug resistance by the conventional chemotherapeutic agents, and rapid degradation leading to decrease bioavailability. Therefore an improved diagnostic and therapeutic approach with minimal side-effects

is required to deal with this burning health problem. A promising trend in this direction is theranostics, which is a novel revolutionary therapeutic approach in cancer therapy allowing synchronized diagnosis and treatment and aims to eliminate multi-step procedures. It offers various advantages like improved diagnosis, targeted delivery of drugs, minimal adverse effects to normal tissues resulting in maximum efficacy, controlled release of drugs, improved pharmacokinetics etc.[118,119] As metal NCs exhibit multifaceted properties like tunable luminescence, biocompatibility, high quantum yield and ease of conjugation, they are considered as superior theranostic platform. They are believed to offer enhanced therapeutic effect because of their better renal clearance, minimal adverse reactions and less possibility of development of drug resistance.[53] Through a smart combination approach, an extremely potent and customized theranostic agent can be accomplished by exploiting the luminescence and optical properties of the metal for imaging and cancer therapy, respectively.[10,83] Moreover, multiple therapeutic/diagnostic agents can be loaded to attain better results. In recent times, a new approach for improved cancer therapy with nanocluster is the development of nanocarrier incorporating a carrier, biological payload and surface modifier.

Various theranostic platforms such as protein nanocarriers, liposome nanocarriers, inorganic nanocarriers, polymer nanocarriers and inorganic/organic hybrid nanocarriers have been developed so far for cancer treatment. Among these, protein carriers have been proved better because of their biodegradability, biocompatibility and low toxicity. Moreover, abundance of various reactive groups (-COOH, $-NH_2$, -OH etc.) help to embellish them with functional groups for different purposes.[119]

Bovine serum albumin (BSA) is extensively used for cancer theranostics because of its low cost, abundance of hydrophobic binding sites and thus serves as a natural carrier for numerous hydrophobic agents. Moreover it has 76% sequence homology with human serum albumin (HSA). Albumin-based nanocarriers could be fabricated utilizing albumin as a scaffold, template, or stabilizer, and then functionalizing with polymers, drugs, and/or contrast agents with the help of covalent and non-covalent bond. It is possible to incorporate various therapeutic drugs into a

single theranostic nanoplatform through smart designing to attain synergistic effect.[119] Various drugs like paclitaxel, doxorubicin, cisplatin, daunorubicin, cytarabine, vincristine, asparaginase, 5-fluorouracil etc. have been used for nanocarrier formulation.[74,76] Recently, a range of nonsteroidal anti-inflammatory drugs (NSAIDs), are investigated for cancer therapy because of their propensity to alter the tumor microenvironment. They are also found to increase apoptosis and decrease migration of tumor cells. Therefore, they are approved by the FDA (Food and Drug Administration) for cancer therapy or prevention regimens[120] and they can be considered as effective adjuvant to the conventional chemotherapeutic agents.[121] Several clinical trials conducted with ibuprofen, a frequently used NSAID, have revealed that it can reduce the incidence and mortality from cancer.[120] Reports of fabrication of albumin nanoparticles with successful loading of ibuprofen in the core of the nanoparticles through hydrophobic and electrostatic interactions as well as BSA gelation raised the hope of utilization of ibuprofen as a future theranostic platform for cancer treatment.[122] Schematic, representing the formulations of protein based nanocarrier as cancer theranostic platforms are illustrated in **Figure 1.6.**

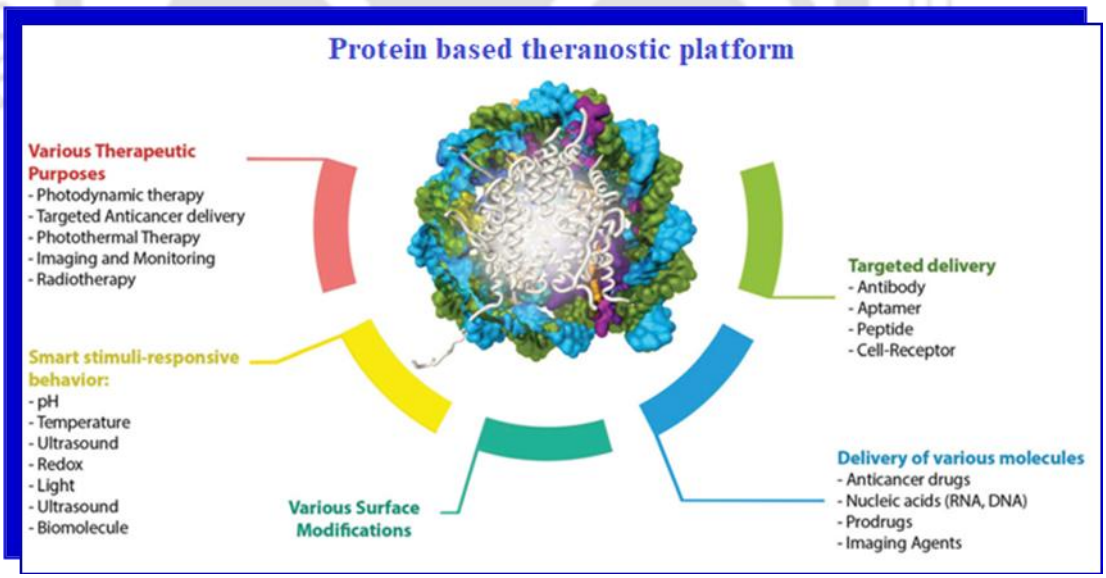

Figure 1.6. Schematic of engineering of protein-based nanoformulations as cancer theranostic platforms. [Reprinted with permission from **reference 118**. Copyright 2017, Royal Society of Chemistry].

1.6. Nanocomposites

In a broad sense, composite signifies particles made of two or more different materials which results in assimilation of multi-components in a single particle with novel properties.[123] A nanocomposite is a composite material, where one component must have at least one dimension in nanoscale range (10^{-9} m). Nanocomposites have acquired significant popularity in the field of nanoscale research considering their design uniqueness and distinctive qualities.[124] Depending on their matrix materials, they can be categorized in three different classes. (1) Metal matrix nanocomposites, e.g. Fe/MgO, Cu/Al_2O_3, Fe-Cr/Al_2O_3, Ni/Al_2O_3, Co/Cr, etc., (2) Ceramic matrix Nanocomposites, e.g. Al_2O_3/SiO_2, Ni/SiO_2, Al_2O_3/SiC etc., (3) Polymer matrix Nanocomposites e.g. polyester/TiO_2, thermoplastic/thermoset polymer/layered silicates, polymer/CNT etc.[124] Common methods for metal matrix nanocomposites preparation are spray pyrolysis, vapour techniques like physical vapor deposition (PVD) and chemical vapor deposition (CVD), electrodeposition, liquid metal infiltration, rapid solidification and chemical methods like colloidal and sol-gel processes.[124] Both metal and ceramic nanocomposites have an excellent industrial emergence specially in aerospace, electronic and military,[125] while polymer nanocomposites have a major impact in electronics,[126] optics,[127] sensors[128] etc. Each class of the nanocomposites has its own merits and demerits. Nanocomposites acquire distinctive properties because of their small size, large surface area, and the interactions of phases at their interfaces.[129] The properties of the nanocomposites are highly structure size and component dependent. Therefore, selection of materials with enhanced performance is an important aspect while engineering a nanocomposite as it connects with the properties of the materials selected for a specific application.

Combining a magnetic nanomaterial with a semiconductor or a noble metal results in a nanocomposite material with superior magneto-optical properties as they retain both the optical and magnetic properties of the individual components. Therefore they can be considered for potential applications in biological fields that rely on both the magnetic and optical responses.[123] Recent developments in the area of materials science have enabled the facile synthesis of Iron oxide nanoparticles (IONPs) offering

easy tuning of surface properties and surface functionalization with desired biomolecules. Such developments have enabled IONPs to be easily accommodated in nanocomposite platform or devices.

1.7. Key areas and scopes

Reviewing the literatures in the field of synthesis of metallic nanomaterials and their applications as theranostics and antimicrobial agents, mainly following three potential research scopes were identified:

- Developing newer metal nanomaterials using novel biotemplate for luminescence based theranostics, thereby reducing the adverse effects of the chemotherapeutic agents for reduction of mortality rate of cancer.
- Designing theranostic nanomaterials for combating multidrug resistant microbes.
- Developing nanomaterials for point of care uses.

1.8. Salient features and significance of the present study

The salient features and significance of the present study are summarized below:

- A rapid and facile method of synthesis of luminescent copper nanoclusters (Cu NCs) has been developed using protein BSA as template. The nanocarrier is biocompatible for application in cancer therapy.
- Luminescent drug (Ibuprofen) encapsulated composite nanoparticles (BSA-Cu-Ibf) were developed for combination therapy.
- The role of Ibuprofen and Cu NC in DNA damage and HDAC inhibition resulting in cell death was demonstrated both *in vitro* and *in vivo.*
- A novel bimetallic, recyclable nanocomposite on the surface of sand has been formulated for annihilation of multidrug resistant clinical isolates, isolated from different biological samples.
- The recyclable nanocomposite was utilized for point-of- use water purification with the ability to remove pathogenic bacteria and harmful metals.
- Development of a facile bimetallic dressing materials in dual forms (powder and nanocomposite embedded cotton patch) for assisting wound healing

observed in animal model (rats) with infected diabetic wound.

1.9. References:

1. Qu, X.; Li, Y.; Li, L.; Wang, Y.; Liang, J.; Liang, J. *Journal of Nanomaterials*. **2015**, 23 pages.
2. Dreaden, E. C.; Alkilany, A. M.; Huang, X. C.; Murphy, J.; El-Sayed, M. A. *Chemical Society Reviews*, **2012**, *41* (7), 2740–2779.
3. Zhang, L.; Webster, T. J. *Nano Today*, **2009**, 4, 66-80.
4. Roco, M. C. *Current Opinion in Biotechnology*, **2003**, 14:337–346.
5. Sapsford, K. E.; Algar, W. R.; Berti, L.; Gemmill, K. B.; Casey, B. J.; Oh, E.; Stewart, M. H.; Medintz, I. L. *Chem. Rev.* **2013**, *113* (3), 1904–2074.
6. Ealias, A. M. and Saravanakumar M P. *Materials Science and Engineering*, **2017**, 263, 032019.
7. Yan, Q-L.; Gozin, M.; Zhao, F-Q.; Cohen, A. and Pang, S-P. Nanoscale, **2016**, *8*, 4799–4851.
8. Li, Y.; Wang, Y.; Huang, G. and Gao, J. *Chem. Rev*. **2018**, 118, 5359−5391.
9. Jiang, S.; Win, K. Y.; Liu, S.; Teng, C. P.; Zheng, Y.; Han, M.-Y. *Nanoscale*. **2013**, *5* (8), 3127.
10. Tao, Y.; Li, M.; Ren, J.; Qu, X. *Chem. Soc. Rev.***2015**, *44*, 8636–8663.
11. Machado S, Pacheco J G, Nouws H P A, Albergaria J T and Delerue-Matos C. *Sci. Total Environ.* **2015**, *533***,** 76–81.
12. James K. Carrow, Akhilesh K. Gaharwar. *Macromol. Chem. Phys.* **2015**, *216*, 248−264
13. Ayuk, E. L.; Ugwu M. O.; Samuel A.B. *Chemistry Research Journal*, **2017**, 2(5):97-123.
14. Tiwari, D K.; Behari, J. and Sen, P. *World Applied Sciences Journal*, **2008**, *3* (3): 417-433.
15. Falagan-Lotsch, P.; Grzincic, E. M.; & Murphy, C. J. *Bioconjugate Chemistry*, **2017**, *28*(1), 135–152.
16. Bhaviripudi, S.; Mile, E.; Iii, S A S.; Zare, A T.; Dresselhaus, M S.; Belcher, A M.;

and Kong, J. *Catalysts.* **2007**, 1516–7.

17. Gawande, M. B.; Goswami, A.; Felpin, F.-X.; Asefa, T.; Huang, X.; Silva, R.; Varma, R. S. *Chemical Reviews,* **2016**, *116* (6), 3722–3811.
18. Salavati-niasari, M.; Davar, F.; and Mir, N. *Polyhedron,* **2008**, *27*, 3514–8.
19. Tamilvanan, A.; Balamurugan, K.; Ponappa, K.; & Kumar, B. M. *International Journal of Nanoscience,* **2014**, *13* (02), 1430001.
20. Manimaran, R.; Palaniradja, K.; Alagumurthi, N.; Sendhilnathan, S. and Hussain, J. *Appl. Nanosci*. **2013**, *4*, 163.
21. Wang, C.; Wang, C.; Xu, L.; Cheng, H.; Lin,Q.; Jhang, C. *Nanoscale* **2014**, *6*, 1775–1781.
22. Jiang, J.; Kim, S.-H.; Piao, L. *Nanoscale*, **2015**, *7*, 8299−8303.
23. Shelke, S. N.; Bankar, S. R.; Mhaske, G. R.; Kadam, S. S.; Murade, D. K.; et.al. *ACS Sustainable Chem. Eng*. **2014**, *2*, 1699−1706.
24. Scotti, N.; Dangate, M.; Gervasini, A.; Evangelisti, C.; Ravasio, N.; Zaccheria, F. *ACS Catal.* **2014**, *4*, 2818−2826.
25. Shim, I. W.; Noh, W. T.; Kwon, J.; Cho, J. Y.; Kim, K. S.; Kang, D. H. *Bull. Korean Chem. Soc.* **2002**, *23*, 563−566.
26. Vallabani, N. V. S.; & Singh, S. *3 Biotech,* **2018**, *8*(6), 279.
27. Gupta, AK.; Gupta, M. *Biomaterials,* **2005**, *26*(18), 3995–4021.
28. Gupta, AK.; Naregalkar, RR.; Vaidya, VD.; Gupta, M. *Nanomedicine (Lond)* **2007**, *2*(1), 23 – 39.
29. Ansari, S. A. M. K.; Ficiarà, E.; Ruffinatti, F. Al.; Stura, I.; Argenziano, M.; et.al. *Materials,* **2019**, *12*, 465.
30. Kharisov, B. I.; Dias, H. V. R.; Kharissova, O.V.; Vazquez, Y. P.; Gomez, I. RSC Adv. **2014**, *4*, 45354–45381.
31. Ali, A.; Zafar, H.; Zia, M.; Ul Haq, I.; Phull, A.R.; Ali, J.S.; Hussain, A. *Nanotechnol. Sci. Appl.* **2016**, *9*, 49–67.
32. Laurent, S.; Forge, D.; Port, M.; et al. *Chem Rev*. **2008**, *108*(6), 2064–2110.
33. Cuenya, BR. *Thin Solid Films*, **2010**, *518*(12), 3127–3150.
34. Narayanan, KB.; Sakthivel, N. *Adv Colloid Interface Sci*. **2010**, *156*(1–2), 1–13.
35. Xuan, Y. and Li, Q. *Int. J. Heat and Fluid Flow*, **2000**, *21*, 58

36. Huang, T.-K.; Lin, K.-W.; Tung, S.-P.; Cheng, T.-M.; Chang, I.; Hsieh, Y.-Z.; Lee, C.-Y. and Chiu, H.-T. *J. Electroanal. Chem*. **2009**, *636*, 123.

37. Lu, L.; Shen, Y.; Chen, X.; Qian, L. and Lu, K. *Science*, **2004**, *304*, 422.

38. Kantam, M. L.; Jaya, V. S.; Lakshmi, M. J.; Reddy, B. R.; Choudary, B. and Bhargava, S. *Catal. Commun*. **2007**, *8*, 1963.

39. Khan, N. T. and Jameel, N. *Acta Scientific Pharmaceutical Sciences*, **2018**, *2* (12), 41-43.

40. Rafique, M.; Shaikh, A. J.; Rasheed, R.; Tahir, M. B.; Bakhat, H. F.; Rafique, M. S.; & Rabbani, F. *Nano*, **2017**, *12*(04), 1750043.

41. Ruparelia, J. P.; Chatterjee, A. K.; Duttagupta S. P.; and Mukherji, S. *Acta Biomater*. **2008**, *4*, 707.

42. Mudur, G. *BMJ*, **2003**, *326*(7402), 1284.

43. Morones, J. R.; Elechiguerra, J. L.; Camacho, A. et al., *Nanotechnology*, **2005**, *16* (10), 2346– 2353.

44. Dankovich, T. A.; & Smith, J. A. *Water Research*, **2014**, *63*, 245–251.

45. Borkow, G. and Gabbay, *J. Curr. Chem. Biol*. **2009**, *3*, 272.

46. Gurtner, GC.; Werner, S.; Barrandon, Y.; Longaker, M.T. *Nature*. **2008**, *15* (453), 314–321.

47. Harding, K. G.; Morris, H. L.; Patel, G. K. *BMJ* **2002**, *324*, 160–163.

48. Shaw, J. E.; Sicree, R. A.; Zimmet, P. Z. *Diabetes Research and Clinical Practice*, **2010**, *87*(1), 4–14.

49. Chattopadhyay, S.; Raines, R. T. *Biopolymers.* **2014**, *101* (8), 821–833.

50. Hu, M. S.; Maan, Z. N.; Wu, J. C.; Rennert, R. C.; Hong, W. X. et al. *Ann. Biomed. Eng*. **2014**, *42* (7), 1494–1507.

51. Mody, V.; Siwale, R.; Singh, A.; Mody, H. *Journal of Pharmacy and Bioallied Sciences*, **2010**, *2*(4), 282.

52. Xu, P.; Zeng, G. M.; Huang, D. L.; Feng, C. L.; Hu, S.; Zhao, M. H.; Liu, Z. F. *Science of The Total Environment*, **2012**, *424*, 1–10.

53. Zhang, Q.; Yang, M.; Zhu, Ye.; and Mao, C. *Curr Med Chem*. **2018**, *25*(12): 1379–1396.

54. Shang, L; Stockmar, F; Azadfar N; Nienhaus, GU, *PubMed* **2013**, 52, (42), 11154–11157.

55. Song, X. R.; Goswami, N.; Yang, H.H.; and Xie, J. *Analyst*, **2016**, 141, 3126.

56. Jin, R. *Nanoscale*, **2015**, 7, 1549.

57. Desireddy, A.; Conn, B. E.; Guo, J.; Yoon, B.; Barnett, R. N.; Monahan, B. M.; Kirschbaum, K.; Griffith, W. P.; Whetten, R. L.; Landman U. and Bigioni, T. P. *Nature*, **2013**,*501*, 399.

58. Li G; Jin R. *Accounts of chemical research*, **2013**, *46*, (8), 1749–1758.

59. Zhang L; Zhu J; Guo S; Li T; Li J; Wang E, *Journal of the American Chemical Society*, **2013**, *135*, (7), 2403–2406.

60. Xu J-J; Zhao W-W; Song S; Fan C; Chen H-Y. *Chemical Society Reviews*, **2014**, *43*, (5), 1601–1611.

61. Li S; Cao W; Kumar A; Jin S; Zhao Y; Zhang C; Zou G; Wang PC; Li F; Liang X-J. *New Journal of Chemistry*, **2014**, *38*, (4), 1546–1550.

62. Choi H; Chen Y-S; Stamplecoskie KG; Kamat PV. *J. Phys. Chem*. **2014**, *6*, (1), 217–223.

63. Zhang X-D; Wu D; Shen X; Liu P-X; Fan F-Y; Fan S-J, *Biomaterials*, **2012**, *33* (18), 4628–4638.

64. Luo, Z.; Zheng, K. and Xie, J. *Chem. Commun*., **2014**, *50*, 5143.

65. Wang, Z., Chen, B., & Rogach, A. L. *Nanoscale Horizons.* **2017**, *2*(3), 135–146.

66. Goswami, N.; Zheng, K.; Xie, J. *Nanoscale* **2014**, *6* (22), 13328–13347.

67. Deng H-H; Wang F-F; Shi X-Q; Peng H-P; Liu AL; Xia X-H; Chen W. *Biosensors and Bioelectronics*, **2016**, *83*, 1–8.

68. Shu T; Su L; Wang J; Lu X; Liang F; Li C-Z; Zhang X. *Anal Chem.* **2016**, *88*(11), 6071-7.

69. Wu X; Zhang Z; Li J; You H; Li Y; Chen L. *Sensors and Actuators B: Chemical*, **2015**, *211*, 507–514.

70. Tay, C. Y.; Yu, Y.; Setyawati, M. I.; Xie J. and Leong,D. T. *Nano Res.*, **2014**, *7*, 805.

71. Yuan, X.; Goswami, N.; Mathews, I.; Yu Y.; and Xie, J. *Nano Res*., **2015**, *8*, 3488.

72. Zhang, C; Sun, X; Li, J; Liu, Y-N. *Nanoscale*, **2013**, J, (14), 6261–6264.

73. Habeeb Muhammed MA; Ramesh S; Sinha SS; Pal, SK; Pradeep, T. *Nano Research*, **2008,** *1*, (4), 333–340.
74. Ghosh, R.; Goswami, U.; Ghosh, S. S.; Paul, A.; Chattopadhyay, A. *ACS Appl. Mater. Interfaces.* **2015**, *7*, 209−222.
75. Das, N. K.; Ghosh, S.; Priya, A.; Datta, S.; Mukherjee, S. *J. Phys. Chem. C* **2015**, *119*, 24657−24664.
76. Sahoo, A. K.; Banerjee, S.; Ghosh, S. S.; Chattopadhyay, A. *ACS Appl. Mater. Interfaces*, **2014**, *6*, 712−724.
77. Lee, D.; Donkers, R. L.; Wang, G.; Harper, A. S.; Murray, R. W.; Hill, C.; Carolina, N. *J. Am. Chem. Soc.* **2004**, 126, 6193-6199.
78. Wan X-K; Tang Q; Yuan S-F; Jiang D.-e.; Wang QM. *Journal of the American Chemical Society*, **2015**, *137*, (2), 652–655.
79. Díez, I.; Pusa, M.; Kulmala, S.; Jiang, H.; Walther, A.; Goldmann, A. S.; Müller, A. H. E.; Ikkala, O.; Ras, R. H. A. *Angew. Chem. Int. Ed*. **2009**, *48*, 2122–2125.
80. Duan, H.; Nie, S. *J. Am. Chem. Soc.* **2007**, *129*, 2412–2413.
81. Petty, JT; Zheng, J; Hud, NV; Dickson, RM. *Journal of the American Chemical Society*, **2004**, *126*, (16), 5207–5212.
82. Online, V. A.; Feng, J.; Huang, H.; Zhou, D.; Cai, L.; Tu, Q.; Wang, A. *J. Mater. Chem. C*, **2013,** *1*, 4720–4725.
83. Yu, Y.; Mok, B. Y. L.; Loh, X. J.; Tan, Y. N. *Adv. Healthcare Mater.* **2016**, *5*, 1844 –1859.
84. Gu, X. Le; Benjamin, H.; Jung, G.; Hollemeyer, K.; Trouillet, V.; Schneider, M. J. *Phys.Chem. C* **2011**, *115*, 10955–10963.
85. Zhang, J; Xu, S; Kumacheva, E. *Advanced Materials*, **2005**, *17* (19), 2336–2340.
86. Roy, S; Banerjee, A. *Soft Matter*, **2011**, *7* (11), 5300–5308.
87. Diez, I; Kanyuk, MI; Demchenko, AP; Walther, A; Jiang, H; Ikkala, O; Ras, RH. *Nanoscale*, **2012**, *4* (15), 4434–4437.
88. Liu, Y-F; Wang, G-Q; Zhao, J-B; Jiang, L; Fang, S-M; Sun, Y-A, *Colloids and Surfaces A:Physicochemical and Engineering Aspects*, **2013**, *426*, 12–17.
89. Vilar-Vidal, N; Blanco, MC; López-Quintela, MA; Rivas, J; Serra, C. *J. Phys. Chem.C*, **2010**, *114* (38), 15924–15930.

90. Ciawi, E; Rae, J; Ashokkumar, M; Grieser, F. *J. Phys. Chem.B*, **2006**, *110* (27), 13656–13660.

91. Liu, S; Lu, F; Zhu J-J. *ChemComm*, **2011**, *47* (9), 2661–2663.

92. Guo, Y.; Cao, F.; Lei, X.; Mang, L.; Cheng, S. Song, J. *Nanoscale*, **2016**, *8*, 4852–4863.

93. YiZhong, L.U.; WenTao, W.; Wei, C. *Chin Sci Bull*, **2012**, *57*: 41-47.

94. Hu, X., Liu, T., Zhuang, Y., Wang, W., Li, Y., Fan, W., & Huang, Y. *TrAC*, **2016**, *77*, *66–75.*

95. Yang, X.; Feng, Y.; Zhu, S.S.; Luo, Y.W.; Zhuo, Y.; Dou, Y. *Anal. Chim. Acta*, **2014**, *847*, 49-54.

96. Goswami, N.; Giri, A.; Bootharaju, M. S.; Xavier, P.L.; Pradeep, T.; Pal, S.K. *Anal. Chem.* **2011**, *83*, 9676-9680.

97. Gui, R.; Sun, J.; Cao, X.; Wang, Y.; Jin, H. *RSC Adv*. **2014,** 4, 29083-29088.

98. Feng, J.; Ju, Y.; Liu, J.; Zhang, H.; Chen, X. *Anal. Chim. Acta*, 2015**,** *854*, 153-160.

99. Cui, M.; Song, G.; Wang, C.; Song, Q. *Microchim. Acta*, **2015,** *182*, 1371-1377.

100. Singh, A.; Kaur, S.; Kaur, A.; Aree, T.; Kaur, N.; Singh, N.; Bakshi, M.S. *ACS Sustainable Chem. Eng.* **2014,** *2*, 982–990.

101. Lin, Y.J.; Chen, P.C.; Yuan, Z.; Ma, J.Y.; Chang, H.T. *Chem. Commun*. **2015,** *51*, 11983-11986.

102. Zhou, Z.X.; Du, Y.; Dong, S.J. *Anal. Chem*. **2011,** *83*, 5122-5127.

103. Hu, Y.; Wu, Y.; Chen, T.; Chu, X.; Yu, R. *Anal. Methods*, **2013,** *5*, 3577-3581.

104. Li, J.; Zhu, J-J.; Xu, Kai. *TrAC*, **2014,** *58*, 90–98.

105. Zhang, L.; Zhao, J.; Duan, M.; Zhang, H.; Jiang, J.; Yu, R. *Anal. Chem*. **2013,** *85*, 3797- 3801.

106. Zhang, Y.; Chen, Z.; Tao, Y.; Wang, Z.; Ren J.; Qu, X. *Chem. Commun*., **2015**, *51*, 11496.

107. Qing, Z.; Qing, T.; Mao, Z.; He, X.; Wang, K.; Zou, Z.; Shi H. and He, D. *Chem. Commun.*, **2014**, *50*, 12746.

108. Chen, H.; Lin, L.; Li, H.; Li, J.; Lin, J.M. *ACS Nano*, **2015**, *9*, 2173-2183.

109. Ghosh, R.; Sahoo, A.K.; Ghosh, S.S.; Paul, A.; Chattopadhyay, A. *ACS Appl. Mater. Interfaces* **2014**, *6*, 3822-3828.

110. Zhao, T.; He, X.W.; Li, W.Y.; Zhang, Y.K. J. *Mater. Chem. B*, 2015**,** *3*, 2388-2394.

111. Wang, Z.; Si, L.; Bao, J.; Dai, Z. *Chem. Commun.* **2015,** *51*, 6305-6307.

112. Kang, X.; Mai, Z.; Zou, X.; Cai, P.; Mo, J. *Anal. Biochem*. **2007**, *363*, 143-150.

113. Yin, L.; Song, Z.; Kim, K. H.; Zheng, N.; Gabrielson, N. P.; and Cheng, J. *Adv. Mater.*, **2013**, *25*, 3063.

114. Tian, H.; Guo, Z.; Chen, J.; Lin, L.; Xia, J.; Dong, X.; and Chen, X. *Adv. Healthcare Mater*., **2012**, *1*, 337.

115. Tao, Y.; Zhang, Y.; Ju, E.; Ren H.; and Ren, J. *Nanoscale*, **2015**, *7*, 12419.

116. Liu, C.-L.; Wu, H.-T.; Hsiao, Y.-H.; Lai, C.-W.; Shih, C.-W.; Peng, Y.-K.; Tang, K.-C.; Chang, H.-W.; Chien, Y.-C.; Hsiao, J.-K.; Cheng, J.-T.; and Chou, P.-T. *Angew. Chem., Int. Ed*., **2011**, *50*, 7056.

117. Yu, Y.; New, S. Y.; Xie, J.; Su, X. and Tan, Y. N. *ChemCommun*., **2014**, *50*, 13805.

118. Zangabad, P. S.; Karimi, M.; Mehdizadeh, F.; Malekzad, H.; Ghasemi, A.; Bahrami, S.; Zare, H. Moghoofei, M.; Hekmatmaneshk, A. Hamblin, M. R. Nanoscale, **2017**, *9*, 1356–1392.

119. Gou, Y.; Miao, D.; Zhou, M.; Wang, L.; Zhou, H.; & Su, G. *Front. in Pharmacol.* **2018**, *9*, 421.

120. Rayburn, E. R.; Ezell, S. J. and Zhang, R. *Mol Cell Pharmacol*. **2009**; 1(1), 29–43.

121. Jana, N. R. *Cell. Mol.Life Sci.*, **2008**, *65*(9), 1295–1301.

122. Li, J., & Yao, P. *Langmuir*, **2009**, *25*(11), 6385–6391.

123. Lin, X.-M.; Samia, A.C.S. *J. Magn. Magn. Mater*, **2006**, *305*(1), 100–109.

124. Camargo, P.H.C.; Satyanarayana, K.G.; Wypych, F. *Materials Research*, **2009**, *12* (1), 1-39.

125. Voevodin, A.A.; Zabinski, J.S. *Composites Science and Technology*. **2005**, *65*(5), 741-748.

126. Vassilliou, J.K.; Ziebarth, R.P.; Disalvo, F.J. *Chemistry of Materials*. **1990**, *2*(6), 738-741.

127. Beecroft, L.L.; Ober, C.K. *Chemistry of Materials*. **1997**, *9*(6), 1302-1307.

128. Cão, G.; Garcia, MF.; Aleala, M.; Burgess, LF.; Mallouk, TE. *J. Am. Chem. Soc.*

1992, *114*(19), 7574-7575.

129. Hussain, D.S.; Shah, M.A.; Sheikh, N.A.; Butt, M.M. *Characterization and Application of Nanomaterials*, **2019**, *2*.

CHAPTER-2

Integration of Nonsteroidal Anti-Inflammatory Drug with Luminescent Copper for *in vivo* Cancer Therapy in Mouse Model

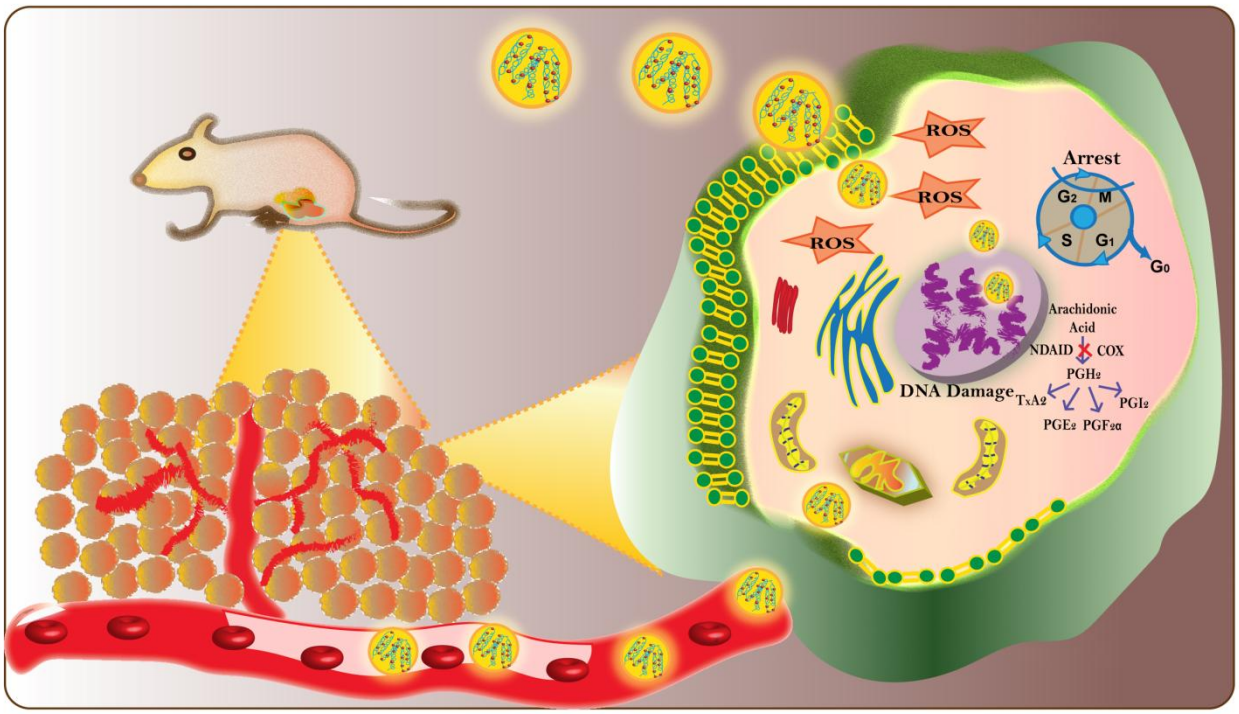

In Chapter 2, a facile and novel method for formulation of a protein (BSA) directed water soluble, stable and luminescent copper nanocluster (BSA-Cu NCs) customized ibuprofen nanodrug (BSA-Cu NC-Ibf) has been reported for *in vivo* cancer therapy. The as-synthesized nanodrug was found to be effective against human cervical (HeLa) cells and also illustrated significant chemotherapeutic efficacy on DLA mice model.

CHAPTER -2

2.1. Introduction

It has been already established that inflammation induces carcinogenesis, plays a role in the progression and metastasis of numerous cancers as both inflammation and cancer expresses similar type of phenotypes.[1] Various cancer cells express pro-inflammatory molecules like cytokines and chemokines and their receptors. These inflammatory mediators have a substantial role on angiogenesis, cell migration, and metastasis.[2,3] Inflammation may also help in strategic genetic mutations and provide a suitable environment to nurture cancer growth. Statistics says, prostatitis can increase prostate cancer risk by 14% [4-6], ulcerative colitis can increase risk of colorectal cancer by 25% [7,8] and there is 10-20 fold increase risk of pancreatic cancer in pancreatitis.[9-11] So inflammation has now become a target for cancer treatment because of its pro-tumor effects. Prostaglandin is the key regulatory molecule for inflammation and mitogenesis. Cyclooxygenase 2 (COX-2), the enzyme for prostaglandin biosynthesis is the most frequently evaluated anticancer anti-inflammatory target.[12]

Various anti-inflammatory agents, including the nonsteroidal anti-inflammatory drugs (NSAIDs), are investigated for cancer therapy and prevention. They modify the tumor microenvironment and thus decrease migration of tumor cells, increase apoptosis and effective adjuvants for conventional chemotherapeutic agents.[13-15] According to different epidemiological studies, incidence of breast, colorectal, and lung cancer is decreased with the use of nonsteroidal anti-inflammatory drugs.[16] Numerous clinical trials have revealed that, ibuprofen; a NSAID reduces the incidence and mortality from cancer. They are also approved by the FDA (Food and Drug Administration) for cancer therapy or prevention regimens.[12]

There are many reports regarding the mechanism of anti-cancer activity of NSAIDs. They suggested that it is not only due to inhibition of cyclooxygenases, but may also involve decrease expression of various NF-kB targets, cell adhesion

molecules, growth factors, and anti-apoptotic proteins.[17,18] NF-kB is a protein that controls transcription of DNA and cytokine production. Incorrect regulation of NF-κB can cause cancer, inflammatory and autoimmune diseases. [19] It is also reported that, NSAIDs can inhibit expression of drug resistance proteins and thus increase uptake and improve retention of chemotherapeutic agents by tumor cells.[20,21] As NSAID alone is not sufficient for complete eradication of cancer cells, combination therapy is suggested. A number of clinical trials suggest that the combined use of anti-inflammatory agents with conventional chemotherapeutic agents may give satisfactory results. [12]

But increased risk of developing gastrointestinal (GI) ulceration restricts their use, especially for cancer prevention. However, compared to the adverse effects associated with the various chemotherapeutic agents due to their non-specific distribution, toxicity associated with NSAIDs is very nominal. Reports of reduced toxicity of the conventional chemotherapeutic agents with administration of NSAIDs are also available.[22-24]

Different modifications of ibuprofen have been tried and tested to overcome the adverse effect. However most of these modifications failed to achieve the targeted goal due to simultaneous reduction of anti-inflammation or anticancer activity compared to parent compound. [25-28]

Much emphasis is given on investigating new combinations and less work has been carried out by incorporating it with nanomaterials for its application. Herein, we formulated a novel copper nanocluster (Cu NC) customized ibuprofen nanocarrier, thus repositioning NSAIDs for cancer therapy and performed an *in vivo* study in animal model. Nanomaterials can play a significant role in delivery of drugs and have several advantages over the conventional chemotherapy. They can improve solubility of hydrophobic drugs, improve bioavailability, minimize non-specific uptake, reduce adverse effects, improve cellular penetration, and help in cancer targeting.[29-31] Bioavailability and the anticancer activity of NSAIDs can be improved only by decreasing the particle size to nanoscale level with the help of nanotechnology. Different techniques have been developed for nano-formulation of NSAIDs[32-36] which are less toxic, easy to synthesize and also cost effective.[37] Discovering additional

utilities of the already existed drugs through a method of drug repositioning is an alternative approach to traditional drug discovery system. And lately, drug repositioning of NSAIDs through nanotechnology offers tremendous possibilities in the field of cancer therapy.[38]

Herein, a nanodrug formulation containing BSA-Cu NC and hydrophobic NSAID-ibuprofen referred here as BSA-CuNC-Ibf has been reported. The nanodrug was tested for its anti cancerous efficacy by *in vivo* animal study using Dalton's lymphoma ascites (DLA) cells for developing T-cell peritoneal lymphoma that mimics human lymphoma on Swiss albino mice.

2.2. Outline of the Present Work

A facile, novel process of fabrication of a luminescent bovine serum albumin (BSA)-copper nanocluster (BSA-CuNC) customized ibuprofen nanodrug (BSA-CuNC-Ibf), encapsulating the ibuprofen was developed. Non steroidal anti-inflammatory drug, Ibuprofen was used as the model drug. The formation of BSA-Cu NCs initiated by encapsulation of the Cu ions within the protein moiety followed by gradual reduction of the Cu ions by certain amino acid residues like tyrosine and tryptophan at alkaline pH resulting in formation of BSA-Cu NCs within the protein template. Heat treatment and lowering the pH, fitted the ibuprofen in the centre by hydrogen bonding, hydrophobic and electrostatic interactions and resulted in formation of nanoparticles. The nanodrug (BSA-CuNC-Ibf) thus formed was characterized by transmission electron microscopy (TEM), dynamic and static light scattering (DLS) and zeta potential. The spherical shaped nanodurg have a hydrodynamic diameter of about 100.4 ± 28.9 nm. The encapsulation efficiency was found to be 94% which corresponds to 1880 µg/mL of ibuprofen in the BSA-CuNC-Ibf nanodrug. The as synthesized BSA-CuNC-Ibf exhibited cytotoxicity on both human cervical cancer cells (HeLa) and human lung cancer cells (A549). The present nanodrug when explored for its tumour preventive role on Daltons lymphoma ascites (DLA) bearing Swiss albino mice, exemplified sizeable inhibition of tumour growth by reactive oxygen species mediated apoptosis and also by modulating prostaglandin (PGE_2) level. It also inhibited metastasis of the cancer cells, thus enhance the life expectancy of mice.

2.3. Experimental Section

2.3.1. Materials

All reagents were utilized as received without any purification. The sources for the nanodrug (BSA-CuNC-Ibf) were bovine serum albumin (BSA), copper II sulphate pentahydrate ($CuSO_4.5H_2O$), sodium hydroxide (NaOH) and 80% hydrazine hydrate procured from Merck Specialties Private Limited, India. For all the experiments, Milli-Q grade water with resistivity 18.2 MΩ cm, was used. The model drug, ibuprofen (4-Isobutyl-α-methyl-phenylacetic acid, 99%, $C_{13}H_{18}O_2$) was purchased from Thermo Fisher Scientific India Pvt. Ltd., Mumbai, India. Two different cell lines, human cervical carcinoma (HeLa) and human lung cancer (A549) were obtained from National Centre for cell Sciences (NCCS), Pune, India. The 2,7-dichlorofluoresceindiacetate (DCFH-DA) dye used for FACS analysis was obtained from Sigma-Aldrich, USA. To perform the animal experiments, Swiss albino mice (male) weighing 22−25 g were procured from Chakraborty enterprise (1443/PO/b/11/CPCSEA), Kolkata and housed at Central Animal Facility (CAF) of Institute of Advanced Study in Science and Technology (IASST), Guwahati, Assam.

2.3.2. Formulation of Copper Nanocluster on protein template (BSA-CuNCs)

BSA-Cu NCs were synthesized by following a well established protocol[39,40] where in 100 mg of bovine serum albumin (BSA), (0.1M) aqueous solution of copper sulphate ($CuSO_4$) was added under vigorous magnetic stirring at room temperature. Then freshly prepared NaOH (1M) solution was added drop wise till the color turned purple, pursued by slow injection of N_2H_4 (1 mL). The color of the medium turned bright yellow ensuring the synthesis of Cu NCs. After synthesis, BSA-CuNCs were stored at 4 °C for further experiments.

2.3.3. Formulation of Copper Ibuprofen (BSA-CuNC-Ibf) nanodrug

For the formulation of the nanodrug composite (BSA-CuNC-Ibf), 8 mg ibuprofen was added to a diluted aqueous dispersion (2 mL BSA-Cu NCs + 2 mL Milli-Q grade water) of the as-synthesized BSA-Cu NCs, under constant magnetic stirring and pH was adjusted to 7 with the help of acetic acid. For the development of nanocarrier,

acetic acid was added drop wise into the above mixture till the reaction mixture turned turbid. During the process moderate heat (60 °C) was applied. The as synthesized BSA-CuNC-Ibf was then collected following centrifugation at 6000 rpm for 10 min at room temperature. The pellets thus obtained after discarding the supernatant were re-dispersed in 4 mL of Milli-Q water for further use. The method for repositioning of ibuprofen and thus formulation of the nanodrug was a modified version of the methods previously adopted.[41]

2.4. Characterization

2.4.1. Fluorescence and UV-Visible Spectra Measurements

Fluorescence spectrum was verified in HORIBA Jobin Yvon FluoroMax-4 spectrofluorimeter and UV-vis spectrum was recorded using Perkin Elmer Lamda 25 UV-vis spectrophotometer.

2.4.2. Encapsulation Efficiency

For this, first the UV absorbance (222 nm)[42] of only ibuprofen, used for the development of BSA-CuNC-Ibf nanodrug, was measured. Following this, the synthesized BSA-CuNC-Ibf was centrifuged at 6000 rpm for 10 min and the UV absorbance of the supernatant was measured. Thus, the encapsulation efficiency (E.E) was calculated with the following formula:

$$E.E = \frac{\text{Ibf}\,i - \text{Ibf}\,f}{\text{Ibf}\,i} \qquad (2.1)$$

Where Ibf *i* corresponds to UV absorbance of control Ibf that was used in BSA-CuNC-Ibf synthesis and Ibf *f* refers to the absorbance of Ibf in the supernatant that was produced after centrifugation of BSA-CuNC-Ibf.

2.4.3. Transmission Electron Microscopy (TEM) Analysis

To probe the external morphology and particle size of the BSA-CuNCs and the as-synthesized BSA-CuNC-Ibf, TEM analysis were performed (JEOL, JEM 2100 TEM; Peabody, MA, USA) at maximum accelerating voltage of 200 kV. For analysis, BSA-CuNCs were diluted (10 µL of BSA-Cu NCs were added in 190 µL of Milli-Q water)

and drop-cast on copper grid whereas for BSA-CuNC-Ibf, 1 mL of the prepared BSA-CuNC-Ibf was centrifuged at 6000 rpm for 10 min followed by re-dispersion of the pellets in 1 mL of Milli-Q water and subsequently 20 μL of which was diluted in 180 μL of water. Finally, 8 μL from the above dispersion was drop-cast on copper-coated TEM grid and kept for drying for 6 h at room temperature followed by analysis.

2.4.4. Dynamic Light Scattering Based Measurements

The change in dynamic light scattering (DLS) along with the net surface charge (zeta potential) of the BSA-CuNC-Ibf was measured using Malvern Zeta Size Nano ZS-90 instrument. For this, 100 μL of the dispersion was diluted with 900 μL of Milli-Q water and then hydrodynamic size and surface charge of the BSA-CuNCs before and after Ibf binding were measured at 25 °C in triplicate with a fixed run time of 11 s with scattering angle set at 90°. For data analysis, Malvern DTS 5.10 software was used.

2.4.5. *In Vitro* Experiments (Mammalian Cell Culture)

In Vitro experiments were carried out in Human cervical cancer cell line (HeLa) and adenocarcinomic human alveolar basal epithelial cells (A549) which were procured from National Centre for Cell Sciences, Pune. Both the cell lines were grown in Dulbecco's modified Eagle's medium (DMEM) supplemented with glucose (10%), penicillin (10000 units) and streptomycin (10 mg/mL). The cells were cultured and maintained under humidified atmosphere in a CO_2 incubator with 5% carbon dioxide.

2.4.6. Confocal Laser Scanning Microscopy

To confirm the uptake of BSA-CuNC-Ibf on HeLa cell lines confocal laser scanning microscope study was carried out. For this, a total of 5×10^3 cells were placed over a cover slip separately and incubated keeping them in a 35 mm culture plate in a CO_2 incubator for 24 h. Then the cells were treated with BSA-CuNC-Ibf and after 3 h of treatment, washed with PBS followed by fixing with 4% formaldehyde. Thereafter, the coverslips containing the treated cells were placed upside down on a glass slide, and the sides were sealed. Simultaneously, control cells (without any treatment) were also checked. The prepared samples were observed under LSM 880 microscope at λ_{ex} 524 nm and λ_{em} 625 nm.

2.4.7. Cell Viability Assay

The MTT (3-4,5-dimethylthiazolyl-2)-2,5-diphenyltetrazolium bromide) assay was carried out for two different cell lines Hela and A-549 for 24 h in triplicates. For the treatment, different concentrations of BSA-Cu NCs (1.33-10 µg/mL), IBF (0.09-0.46 mg/mL) and BSA-Cu NC-Ibf (7.52 - 37.6µg/mL w.r.t. Ibf) were given in 10×10^3 cells seeded in each well of a 96-well culture. After 24 h of treatment MTT was added which results in purple colour formazon production which corresponds to the number of viable cells having absorbance at 655 nm. The cell viability following the various treatments was calculated using the following equation.

$$\%\ \text{of cell viability} = \frac{(A550-A655)\text{Sample}}{(A550-A655)\text{Control}}\ X\ 100 \qquad (2.2)$$

2.4.8. FACS Analysis for Reactive Oxygen Species Generation

Cell permeable fluorescent and chemiluminescent 2′-7′-Dichlorodihydrofluorescein diacetate (DCFH-DA) probe was used to measure the reactive oxygen species (ROS) generated by the cancer cells. The DCFH-DA, which is non-fluorescent, converted to Dichlorofluorescin (DCFH) by cellular esterases and is later oxidized into green fluorescent (λex=488 nm and λem=530 nm) 2', 7' –dichlorofluorescein (DCF) by ROS. The experiment was instigated with seeding of 10×10^3 cells in each well of a 96-well culture plate. After overnight incubation, cells were treated with BSA-Cu NCs (3.3µg/mL which is the final amount of copper present in the nanodrug), Ibf (37.6 µg/mL) and of BSA-CuNC-Ibf nanodrug (with 37.6 µg/mL of Ibf and 3.3 µg/ml of Cu) Following 3 h of treatment, DCFH-DA (10 µM) dye was added and kept for 30 min at 37 °C. Simultaneously, a batch of control was also maintained. The cells were then treated with trypsin to dissociate the adherent cells from the plate and re-dispersed in Dulbecco's Modified Eagle Medium (DMEM) and analyzed in, FITC channel (530/30nm, green emission) of a flow cytometer (CytoFLEX, Beckman Coulter).

2.4.9. Cell Cycle Analysis

Cell cycle analysis was done using DNA binding dye, propidium iodide (PI). For this, 10×10^3 cells/well were plated in a 96 well culture plate and incubated overnight. Cells

were then treated with BSA-Cu NCs, Ibf and BSA-CuNC-Ibf nanodrug. After 24 h of treatment, cells were trypsinized and then collected to centrifuge at 650 rcf for 6 min, followed by fixing of the cells by chilled 70% ethanol (1 mL) under constant vortexing. Cells were again centrifuged after keeping them at -20 °C for 1 h and the pellets were re-dispersed in PBS followed by incubation at 37 °C, in 0.4 mg/mL RNase solution for 1 h. Then, propidium iodide (10 μg/mL) was added and kept in dark for 30 min. The cells were then analyzed at 488 nm excitation wavelength in PE-A channel (band-pass filter, 585/42 nm) of flow cytometer (CytoFLEX flow cytometer, Beckman Coulter) and the emission was recorded. ModFit LT software 5.0 was used for analyzing the data.

2.4.10. *In Vivo* Animal Study

In vivo animal experiment was carried out with adult male Swiss albino mice weighing 22− 25 g at Central Animal Facility, Institute of Advanced Study in Science and Technology (IASST), Guwahati, Assam. All experiments were done as per standard protocols of the Institutional Animal Ethics Committee, IASST (IASST/IAEC/2016−17/ 2301), following the guidelines of the Committee for the Purpose of Control and Supervision of Experiments on Animals (CPCSEA), Government of India. The mice were housed in polypropylene cages in a 12 h−12 h light−dark environment with cage temperature around 22 °C and 60−70% humidity. Before experiments mice were kept under close observation to acclimatize for a week, with a standard diet and water (Rodent pellet and water ad libitum).

2.4.11. Growth of *in Vivo* Tumor

As soon as the mice were ready for the experiment, tumor was induced by injecting 1 x 10^6 (0.2 mL) viable Dalton's ascites lymphoma (DLA) cells through intraperitoneal (I.P.) route. The index of the tumor growth was increased body weight as well as abnormal abdominal distension, visible in 8−10 days after induction.

2.4.12. Animal Study Design

For the tumor progression, DLA cells (0.2 mL of 1×10^6 cells/ mice) were injected intraperitoneally on day 0 and drug treatment was started simultaneously at an interval of 48 h for 16 days. Total 45 mice were taken for the experiment and divided into 5 groups as follows with 9 mice in each group.

Group 1: Normal mice (Negative control)

Group 2: Mice with DLA tumor + No drug treatment (Positive control).

Group 3: DLA-bearing mice +0.2 mL of BSA-CuNCs for 16 days.

Group 4: DLA-bearing mice + Ibf (2 mg/kg, I.P.) for 16 days.

Group 5: DLA-bearing mice + BSA-CuNC-Ibf (2 mg/kg, I.P.) for 16 days.
Doses were decided on basis of the cell viability studies.

2.4.13. Effect of Treatment on Tumor Growth

Effect of treatment on tumor growth was determined by measuring the body weight. The body weight changes were recorded on day 0, 8 and 16, and at the end of the treatment (16 day). Cells from all the groups were collected to determine the cell viability. At day 16, three mice from each group were sacrificed by decapitation to collect the blood, liver, and kidney for hematological, biochemical, serological and histopathological analysis. The remaining mice were kept under observation till 31 days for determination of percentile increase in life span (% ILS) and mean survival time (MST).

2.4.14. Haematological profiling

After the treatment period, blood from various treatment groups was collected, in Ethylene diamine tetra acetic acid (EDTA) vacutainer to examine different hematological parameters. Then red blood cells (RBC), white blood cells (WBC) and haemoglobin (Hb) levels were estimated using fully automated haematology analyser (Coulter LH750 Analyzer, Beckman Coulter, US). Results were expressed in mean ± S.D.

2.4.15. Biochemical Parameters

A part of blood was also collected in gel vacutainer (without anticoagulant) and allowed to clot. After 30 mins, centrifuged at 3000 rpm for 5 min at room temperature and levels of Aspartate Transaminase (AST), Alanine Transaminase (ALT), Alkaline Phosphatase (ALP), albumin, urea and creatinine were measured with the supernatant (serum). All the biochemical tests were done using fully automated chemical analyzer (Dimension RXL Max, Siemens, Germany).

2.4.16. Determination of Percentage Increase in Life Span (% ILS) and Mean Survival Time (MST)

After sacrificing three mice (post treatment, i.e. on 16th day) from each group, remaining mice were kept under observation to determine the effect of drug treatment on mortality rate of the cancer (DLA) mice. Kaplan meier curve was established to represent the death of mice on respective days. % ILS and MST were calculated using the following equation, respectively:

$$\text{Increase in life span (ILS)}\% = \left(\frac{\text{Mean survival time of treated groups}}{\text{Mean survival time of untreated groups}} - 1\right) \text{x } 100 \quad (2.3)$$

$$\text{Mean survival time} = \frac{(\text{First death} + \text{Last death})}{2} \quad (2.4)$$

2.4.17. Biochemical Testing and Cell Cytology of the Ascitic Fluid

At the end of the treatment period i.e. on 16th day of treatment, peritoneal fluid was collected from the mice of all the studied groups for estimation of total protein, sugar, total cell count, differential count along with cytological examination under microscope. Biochemical parameters like total protein and sugar was estimated with the help of fully automated chemical analyzer (Dimension RXL Max, Siemens, Germany). Total WBC count of the peritoneal fluid was estimated using fully automated haematology analyser (Coulter LH750 Analyzer, Beckman Coulter, US). Then thin smear of the fluid of each group was made in clean glass slide and then stained with Leishman stain, dried and observed under oil emersion objective of binocular

microscope (Olympus, CH 20i) to see the differential count. Next to study the cell cytology, smears of the respective ascitic fluid was stained with Giemsa stain, dried and observed under both 40x and oil immersion objective of binocular microscope (Olympus, CH 20i).

2.4.18. Quantitative Analysis of Prostaglandins in Blood and Peritoneal Fluid

Research established that, besides oxidative stress mediated apoptosis, NSAIDs also inhibit cyclooxygenase 1 and 2 (COX-1 and COX-2) activity leading to down regulation of the synthesis of prostaglandins, the primary mediators of inflammation.[43,44] Cyclooxygenase converts arachidonic acid to prostaglandins (PGs) and thromboxane A2. Arachidonic acid is first converted to prostaglandin H2 (PGH2) followed by immediate conversion to prostaglandin E2 (PGE2). PGE2 can induce vascular endothelial growth factor (VEGF) production which is the key mediator of angiogenesis in cancer.[15] As prostaglandin is considered to have a strategic role in cancer progression through inflammation, blood and peritoneal fluid from the all the treatment groups were collected on day 16, post treatment for prostaglandin estimation. The blood was centrifuged at 1500 rpm at 4 ºC for 5 min and the serum was collected. Then prostaglandin level was determined by Abcam's Prostaglandin E2 (PGE_2) ELISA (Enzyme Linked Immunosorbent Assay) kit. According to data supplied by the manufacturer, minimum detectable dose of PGE2 using ELISA kit was found to be 13.4 pg/mL. This was determined by the average optical density of the 0 pg/mL standard and comparing to the average optical density for standard 7. The detection limit was determined as the concentration of PGE2 measured at two standard deviations from the zero along the standard curve. The intra and inter-assay precision was expressed in coefficient of variation (CV%) and proclaimed to be between 5.8 – 17.5 % and 3.0- 5.1 %, respectively. Assay specificity was calculated to be 100 %.

2.4.19. Statistical Analysis

Statistical analysis was done using two way ANOVA, where statistical significance is denoted by '*' ($p < 0.05$), '**' ($p < 0.005$), '$$$' and '***' ($p < 0.001$) and '****' ($p<0.0001$). For standard statistical analysis, Graph Pad Prism 6 software was used

and Kaplein–Meier method was followed for survival study.

2.4.20. Histopathology Assessment

The histopathology assessment was performed in order to see the metastasis of the tumor cells. Liver and kidneys were collected on day 16, after treatment. Then fixed using 10% formalin, and embedded in paraffin for preservation. Hematoxylin and eosin (H&E) staining were done to investigate microscopically the migration of tumor cells. Photographs were taken from different areas of each section.

2.5. Results and Discussions

Formulation of protein (BSA) directed water soluble, stable and luminescent nanocluster (BSA-Cu NCs) was accomplished in aqueous solution at ambient temperature using hydrazine (N_2H_4) as the reducing agent. (Refer to Experimental section for details). For the formulation of the nanodrug (BSA-CuNC-Ibf) ibuprofen was added to diluted (1:1) as-synthesized BSA-Cu NCs. (Refer to Experimental Section for details). Here, BSA was selected as the model protein because, 17 intra chain disulfide bonds and 1 free thiol group of BSA could provide steric protection and thus stabilize the cluster.[33] Besides, albumin has the ability to bind reversibly with any hydrophobic molecule and thus transport and release at the cell surface.[6,8,9] The schematic representation of the nanodrug synthesis with its chemotherapeutic effect in DLA mice model has been illustrated in **Figure 2.1**.

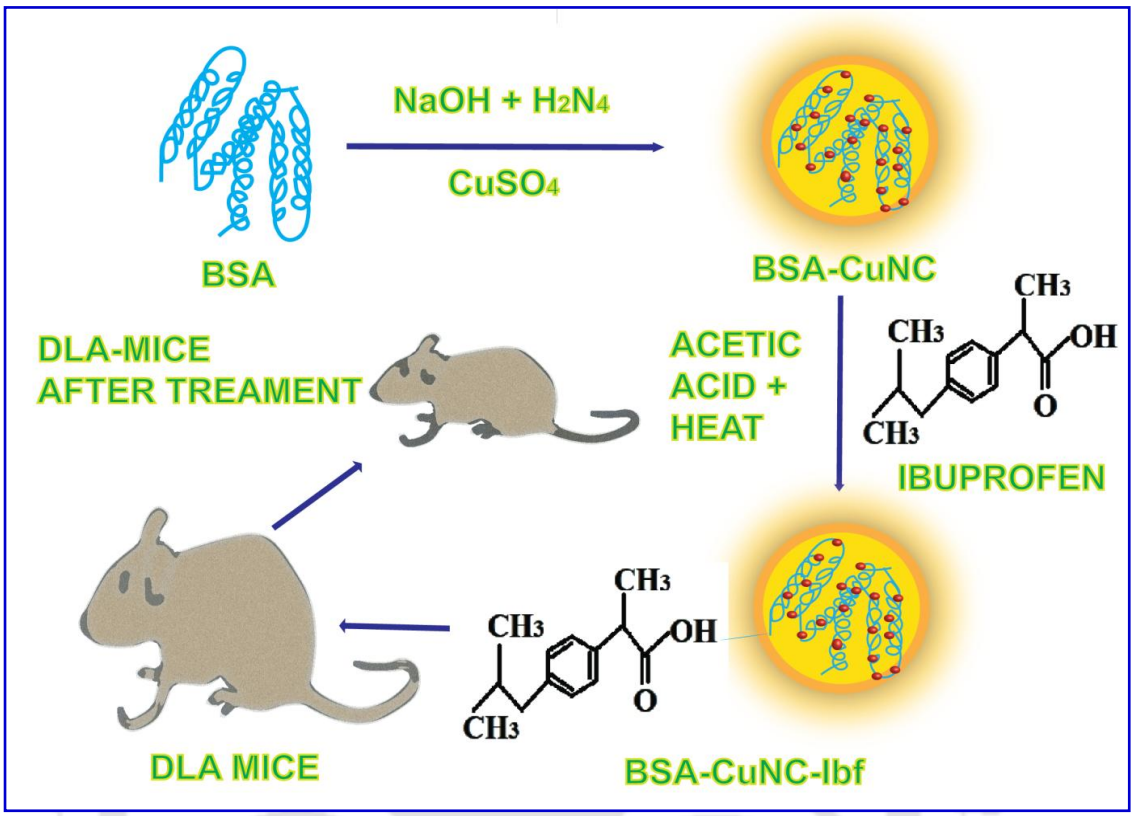

Figure 2.1. Schematic diagram of nanodrug formulation by integration of NSAIDs (Ibuprofen) with Cu NCs and their application in animal model for cancer therapy.

Thus, BSA-Cu NCs formed were validated from TEM image (**Figure 2.2a**). The Cu NCs of the size 4.29 ± 2.22 nm in the BSA-Cu NCs were observed in the TEM image (**Figure 2.2b,**). At the same time from UV spectroscopy data, absence of absorbance peak of copper nanoparticles (**Figure 2.2c**) confirmed the formation of luminescent Cu NCs **(inset of Figure 2.2c).**

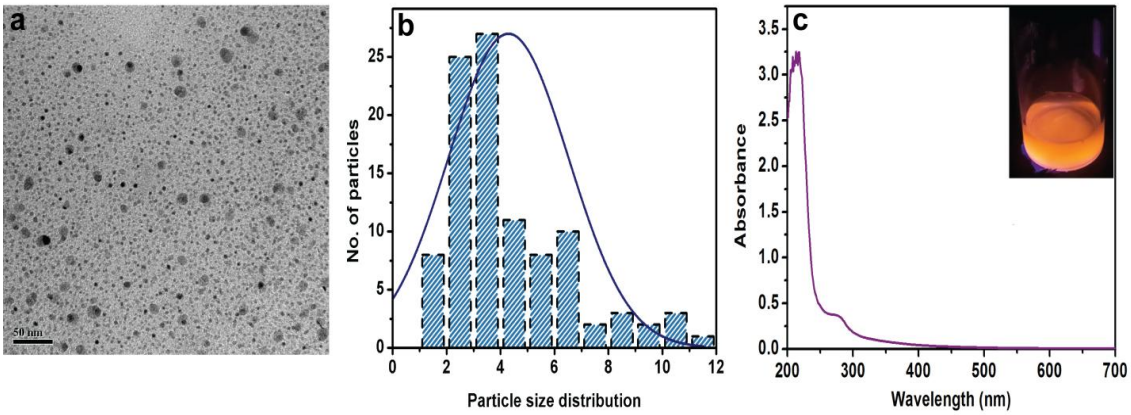

Figure 2.2. (a) TEM image of BSA-Cu NCs (scale bar 50 nm), (b) Histogram showing size distribution of BSA-Cu NCs, obtained from panel a and (c) UV absorbance of BSA-Cu NCs (λem= 222 nm) with bright yellow fluorescence (inset Figure c).

After synthesis of BSA-Cu NCs, a hydrophobic drug, ibuprofen was taken where both albumin of BSA-Cu NCs and the ibuprofen possibly self-assembled to form nanoparticles encapsulating the hydrophobic drugs in aqueous solution. Moreover, the heat induced gelation of albumin involved unfolding of it, followed by fixing of ibuprofen in the core by inter protein interactions like hydrogen bonding, disulfide-sulfydryl interchange reactions, hydrophobic and electrostatic interactions, which helped in formation of the nanoparticles. The formation of nanoparticles were confirmed by TEM analysis where the as-synthesized BSA-CuNC-Ibf NPs revealed spherical nature as observed in TEM image, insert is the magnified image **Figure 2.3a.** The nanoparticles in TEM images exhibited a narrow size distribution. The average particle size of the BSA-Cu NC-Ibf nanodrug was calculated from about 100 particles in TEM images using ImageJ software and found to be of 100.4 ± 28.9 nm. The histogram plot of the as-synthesized BSA-Cu NC-Ibf nanodrug was shown in **Figure 2.3b**. While no characteristic SAED pattern for Cu metal was noticed that confirmed formation of the nanoclusters (**Figure 2.3c**). The as-synthesized BSA-Cu NC-Ibf displayed bright red emission at 625 nm (**Figure 2.3d)** with bright yellow fluorescence (**inset Figure 2.3d**).

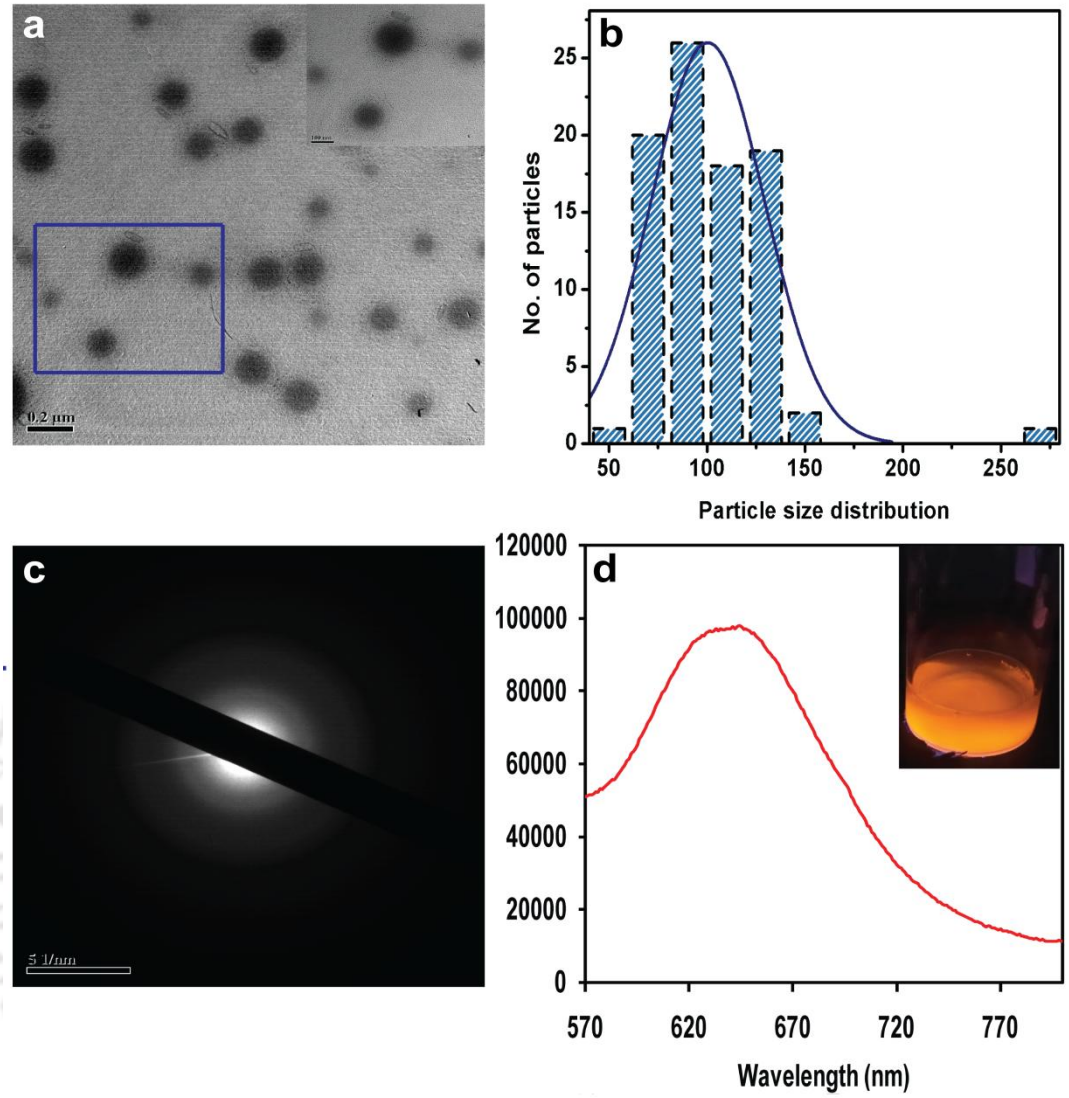

Figure 2.3. (a) TEM image of as-synthesized BSA-Cu NC-Ibf , inset is the magnified view of the TEM image (b) Histogram showing size distribution of BSA-Cu NC-Ibf, obtained from panel a, (c) Featureless SAED pattern obtained from image in (a) and (d) Photoluminescence spectra (λex= 222 nm) of BSA-Cu NC-Ibf (red).

To find out the amount of ibuprofen encapsulated within the nanodrug, the encapsulation efficiency was calculated and was found to be 94% of ibuprofen. This binding % corresponds to 1880 µg/mL of ibuprofen in the BSA-CuNC-Ibf nanodrug along with 165 µg/mL of Cu. Further, the findings of the TEM analysis were substantiated by measuring the change in dynamic light scattering, from where the particle size of the nanodrug composite was calculated as 125± 2.65 nm **(Figure 2.4a).** The diameters of the nanoparticles in TEM images were smaller than the

diameter determined by DLS which may be due to a hydration layer surrounding the NPs core as DLS provides the data in the liquid medium, whereas TEM showed the images of dried particles. Later on**,** to understand the mechanism of nanoparticles synthesis, DLS based zeta potential measurements were performed. The zeta potential data revealed a negative charge of -18.1± 6.0 mV for the as-synthesized BSA-Cu NCs **(Figure 2.4b)**. After the formation of nanodrug composite (BSA-CuNC-Ibf), the net surface charge was found to be -9.26 ± 0.52 mV. This shifting in zeta potential from -18.1 to -9.26 on addition of ibuprofen, (**Figure 2.4c**) suggested that the electrostatic mode of interaction between them definitely played a role in formation of the nanodrug (BSA-CuNC-Ibf). Moreover, hydrogen bond, disulfide-sulfydryl interchain reactions and hydrophobic interactions may also help in the formation of the nanoparticles. Accomplishment with the nanoparticles size criteria is important as particles of <200 nm have enhanced permeability and retention effect (EPR) necessary for effective drug delivery.[24]

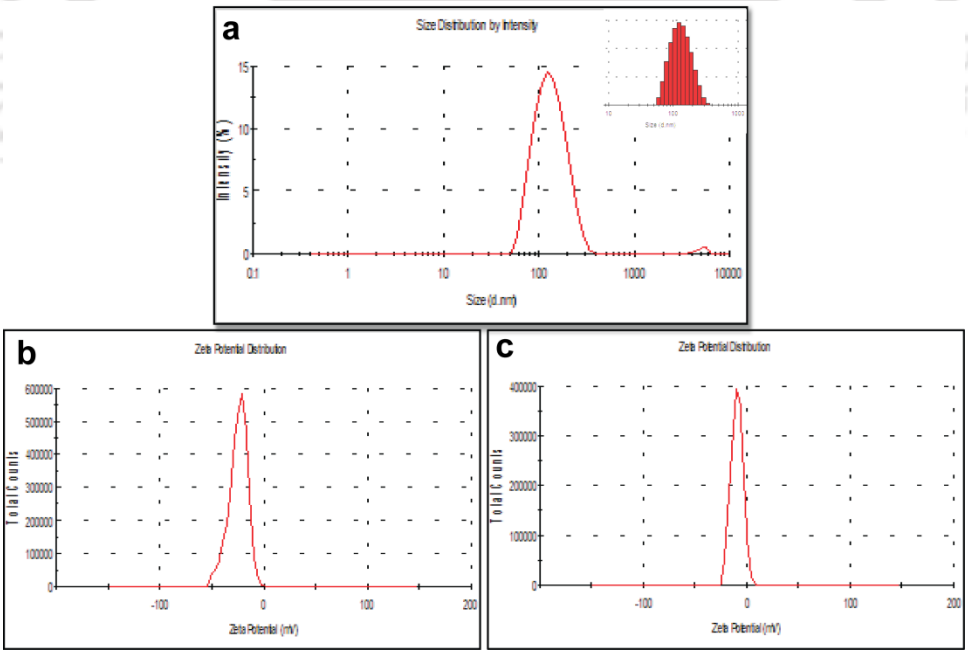

Figure 2.4. (a) DLS results representing the hydrodynamic size of as-synthesized BSA-CuNC-Ibf-nanodrug, inset is the histogram representing the distribution of size, (b) Zeta potential of BSA-Cu NCs and (c) Zeta potential of BSA-Cu NC-Ibf nanodrug.

.

Next, to check the uptake of the BSA-Cu NC-ibf-nanodrug, high resolution confocal microscopy studies were carried out. It has been found that HeLa cells after 4 h of treatment with BSA-CuNC-Ibf revealed bright red luminescence in the cytoplasm indicating the uptake of the nanodrug inside the cells (**Figure 2.5b,c**) and was substantiated with depth projection study (**Figure 2.5d**) which confirmed the uptake of nanodrug.

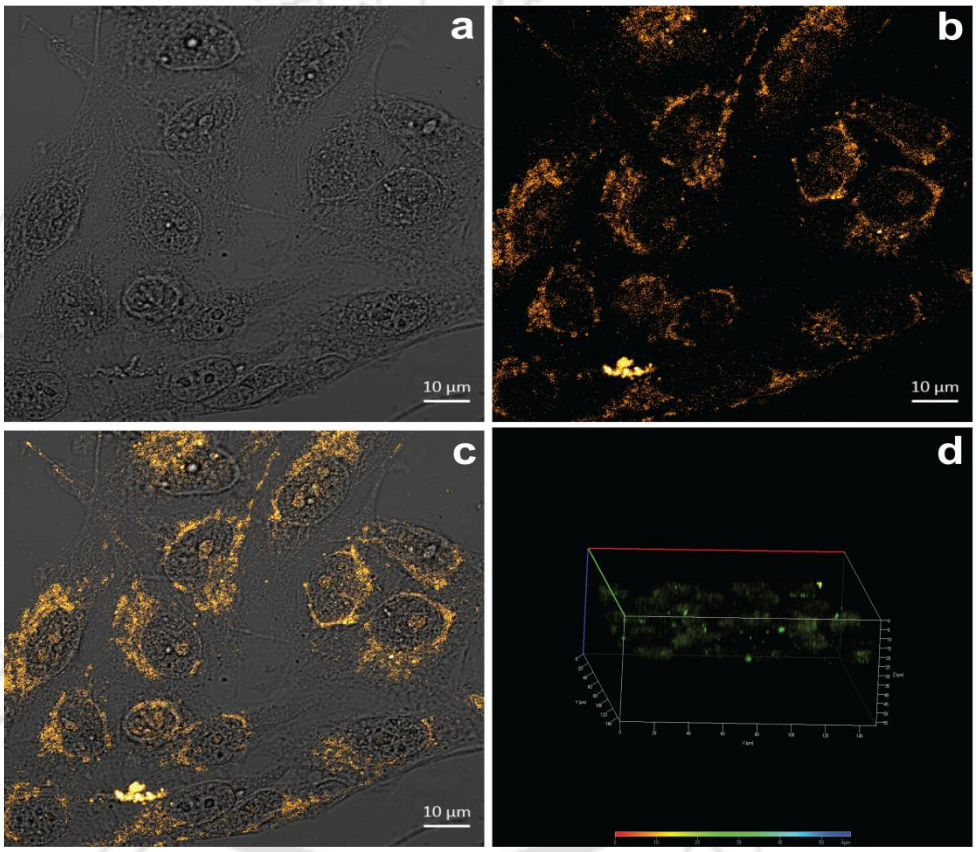

Figure 2.5. (a) Bright field confocal images of HeLa cell treated with BSA-CuNC-Ibf for 4 h. (b) fluorescence image of the HeLa cells showing distinct yellow emission of BSA-CuNC-Ibf, (c) Merged image of both (a) and (b); (d) Z-stack projection of the cell imaged in (a) confirming the uptake of the NPs. (False color was chosen to match with the luminescence color of BSA-CuNC-Ibf).

To assess the therapeutic efficacy of the nanodrug, MTT-based cell viability test was done in two cell lines (HeLa and A549). The cells of both the cell lines were incubated at different concentrations of BSA-Cu NCs, ibuprofen, and BSA-CuNC−Ibf nanodrug for 24 h at 37 °C. The BSA-CuNC-Ibf nanodrug, following synthesis has 165

µg/mL of Cu and 1880 µg/mL of Ibf into it. To carry out cytotoxic assay various concentration of Cu NC-Ibf Nanodrug (7.52 - 37.6 µg/mL w.r.t. Ibf) were tested in Hela cells. It was revealed that at highest concentration of Ibf in Cu NC-Ibf-Nanodrug (37.6 µg/mL) along with Cu (3.3 µg/mL), 45% of cells remain viable. Interestingly, Ibf alone at this particular concentration (37.6µg/mL) have a viability of 78.53% (**Figure 2.6a**). Similarly, Cu individually at concentration of (3.3 µg/mL) has viability of 79.24 % (**Figure 2.6d**). Thus individually at the above particular concentrations, Ibf and Cu did not have much activity. For reference the cytotoxic activities of Ibf and Cu NCs have been tested separately and it was observed that Ibf and Cu NC individually was capable of showing 45% cell viability on HeLa cells, at a concentration of 0.46 mg/mL and 10 µg/mL, respectively (**Figure 2.6e and f**). Hence, looking at the anti-cell proliferative effect of Ibf when incorporated in BSA-Cu NCs as evidenced by considerable reduction of cell viability compared to free drug molecule (Ibf), synergistic mode of therapeutic efficacy could be concluded. To prove this combination index (CI)-isobologram equation of Chou-Talalay was followed for quantitative determination of additive (CI = 1, in the isobologram plot), synergism (CI < 1) or antagonism (CI > 1) effect of the nanodrug. All calculations were done using CalcuSyn software (Biosoft, Version 2.1). The isobologram plot of MTT data (**Figure 2.6a**) was calculated and the results confirmed synergistic mode of drug interaction as all the data points except of concentration 7.52 µg/mL (w.r.t to Ibf) were below the line of additivity and thus synergy (**Figure 2.6b**). The calculated combination index (CI) values were found to be < 1 in 4 data points (15.04 – 37.6 µg/mL) and hence synergistic and were tabulated (**Table 2.1**). At the same time efficacy of the nanodrug was also checked in adenocarcinomic human alveolar basal epithelial (A549) cells and was found to have viability of 65% at Ibf and Cu concentration of 37.66 and 3.3 µg/mL, respectively of the nanodrug **(Figure 2.6c).** Thus, Cu NC-Ibf nanodrug has better activity for Hela cells.

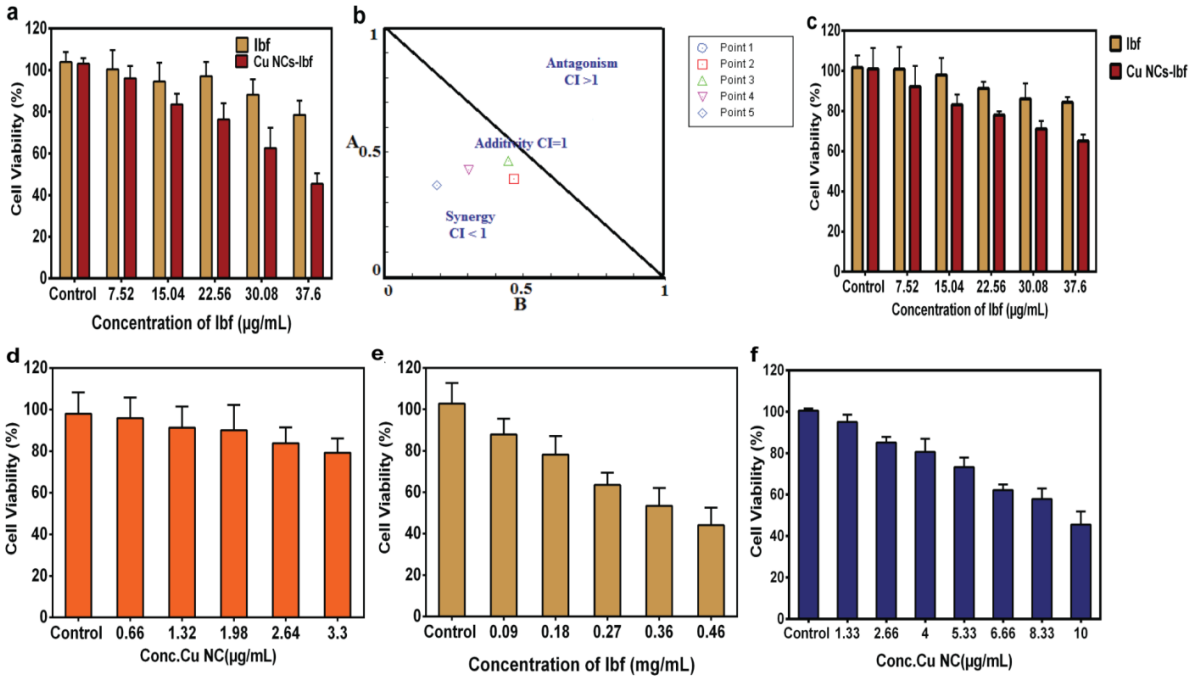

Figure 2.6. (a) Cell viability based on MTT assay after 48 h of treatment with varying concentrations of Ibf and BSA-CuNC−Ibf NPs in HeLa cells. The experiments were carried out in triplicate and are represented as the mean ± SD, (b) Isobologram analysis showing all points below additive line indicating synergistic effect, (c) Cell viability based on MTT assay after 48 h of treatment with varying concentrations of Ibf and BSA-Cu NC−Ibf NPs in A549 cells, (d) Cell viability based on MTT assay after 48 h of treatment with varying concentrations of Cu NC, (e) Cell viability based on MTT assay after 48 h of treatment with varying concentrations of Ibf, (f) Cell viability based on MTT assay after 48 h of treatment with varying concentrations of Cu NC in HeLa cells.

Table 2.1. Calculated combination index (CI) values.

Dose of Ibf	Dose of Cu	Effect %	CI < 1
7.52	0.66	0.96	1.65809
15.04	1.32	0.83	0.85788
22.56	1.98	0.76	0.91265
30.08	2.64	0.62	0.73397
37.6	3.3	0.45	0.55621

Thereafter, FACS based analysis of the nanodrug (BSA-CuNC−Ibf) treated samples were carried out to shed light on the mechanism of cell death exerted by the nanodrug. First, production of the reactive oxygen species (ROS) was measured using cell permeable 2′,7′-dichlorodihydrofluorescin diacetate (DCFH-DA) chemiluminescent probes to measure the redox state of the cell. The non-fluorescent DCFH-DA is de-esterified intracellularly and oxidized to highly fluorescent (green) 2′,7′-dichlorofluorescein (DCF) in the presence of ROS. There was a shift in fluorescence intensity in the nanodrug (BSA-Cu NC−Ibf) treated cells, which signified the amount of intracellular ROS production (**Figure 2.7a**). Control Cu NCs also generated ROS (**Figure 2.7b).** On the contrary, Ibuprofen generated less ROS compared to BSA-CuNC-Ibf nanodrug as observed in (**Figure 2.7b**). Further, on cell cycle analysis, arrest of G2/M phase was observed upon treatment with BSA-CuNC-Ibf nanodrug, whereas there was no significant change in the G2/M population in the cells which were treated with only Ibuprofen. There was also an increase in the G2/M population in the cells which were treated with only Cu NCs, but less as compared with the BSA-CuNC-Ibf treated group (**Figure 2.7c**).

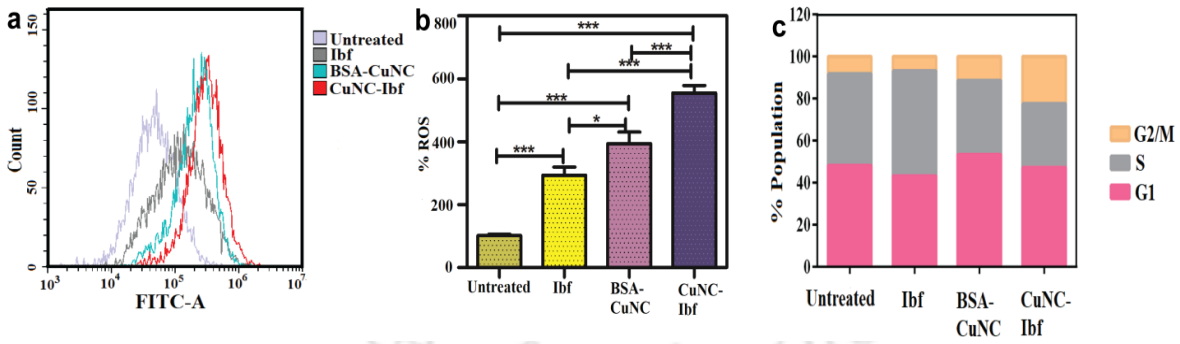

2.7. (a) Images of ROS generation by different treated cells, (b) % of relative ROS generation, (c) Cell cycle analysis.

Ultimately, the *in vivo* efficacy of the nanodrug (BSA-Cu NC−Ibf) was explored in DLA bearing adult male Swiss albino mice. Total 45 mice were included in the experiment and tumor was induced by subcutaneous inoculation of DLA cells in total 36 animals dividing them in 4 groups (n = 9). One group was assigned as positive

control i.e. mice bearing DLA tumor without any treatment followed by groups treated with BSA-Cu NCs (2 mg/kg), free Ibf (2 mg/kg), and BSA-CuNC-Ibf nanodrug (2 mg/kg). Subsequently, the nonlethal dose (2 mg/kg) of BSA-CuNC, free Ibf and BSA-CuNC-Ibf was injected into the peritoneal cavity of the mice of the respective groups at scheduled intervals for 16 days as illustrated in the experimental Section. Detail study plan was narrated in **Figure 2.8a.** Tumor growth was monitored by measuring the body weight on day 0, 8 and 16. Tumor size was considerably increased in the positive control group (i.e. group of mice bearing DLA without receiving any treatment). In all other treated groups increase in tumor size was observed to be less compared to the positive control group. In fact, at the end of the treatment period, among all treatment regimes, the BSA-CuNC-Ibf nanodrug displayed the maximum potential in tumor regression with body weight increase of about only 6.4 ± 1.6g compared to 14.57 ± 2.0g in the positive control group (**Figure 2.8b**). Refer **Table 2.2** for details. After 16 days of treatment period, three mice from each group were sacrificed by decapitation to collect cells, blood, ascitic fluid and organs like liver and kidney for cell viability assessment along with biochemical, hematological, cytological, serological and histopathological analysis. The remaining mice were observed for up to 31 days to estimate the percentage increase in life span (% ILS) and mean survival time (MST). The superior chemo prophylactic efficacy of BSA-CuNC-Ibf nanodrug has noticeable effect on the increased life span of DLA mice as compared to other treated groups. As evident from (**Figure 2.8c**), all mice from the positive control, BSA-Cu NCs and Ibf treated groups died by 19 days of the experiment. But interestingly, the anti-cancer efficacy of BSA-CuNC-Ibf nanodrug reduced DLA cells and hence, the mice survived till 31 days of the study.

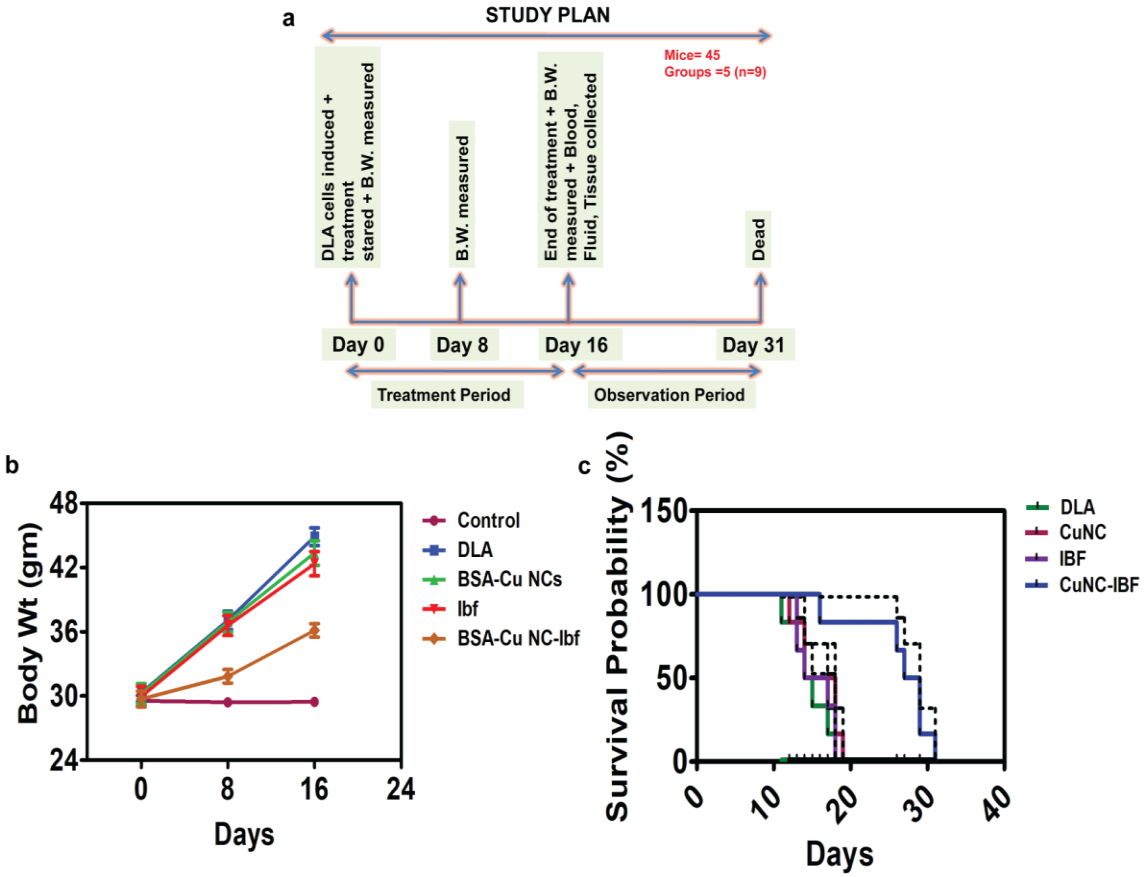

Figure 2.8. (a) Schematic of the study plan, (b) changes in the body weight of the mice after treatment with BSA-Cu NCs, Ibf, and BSA-CuNC-Ibf nanodrug, respectively, along with control till 16 days of treatment. (c) Survival probability of DLA induced mice monitored up to 31 days after treatment with BSA-Cu NCs, Ibf, and BSA-CuNC-Ibf nanodrugas represented by Kaplan−Meir curve.

Table 2.2. Effect of drug treatment on body weight changes and cell viability assay in DLA mice.

Groups	Treatment regime	Increment in body weight (gm)		Viable cell count (10^5 cells/mL)
		Day 8	Day 16	
Group 1	Normal mice (Control)	-0.13 ± 1.0	-0.1 ± 0.9	
Group 2	DLA + No drug treatment	6.75 ± 2.0 $^{\$\$\$}$	14.57 ± 2.0 $^{\$\$\$}$	38.9 ± 0.28
Group 3	DLA + BSA-Cu NCs	6.65 ± 2.3	12.43 ± 2.5*	39.83 ± 2.07
Group 4	DLA + Ibf	6.7 ± 2.2	13.15 ± 2.5	38.27 ± 0.85
Group 5	DLA + BSA-CuNC-Ibf	2.1 ± 1.6***	6.4 ± 1.6***	26.96 ± 4.09

Results of the hematological parameters of the blood of all the groups showed leucocytosis (increased WBC count, **Figure 2.9b**) and anemia (decreased Hb level, **Figure 2.9c**) along with decreased RBC (**Figure 2.9a**) and platelet counts (**Figure 2.9d**) except the BSA-Cu NC-Ibf treated group (**Table 2.3**) where almost normal picture was noticed.

Table 2.3. Effect of drug treatment on hemopoietic system represented by the following hematological parameters.

Groups	Treatment regime	RBC (million/cmm)	WBC Cell/cmm	Hb (g/dL)	Platelet count (lacs/cmm)
Group 1	Normal mice (Control)	5.16 ± 0.2	9466 ± 665	12.1 ± 0.35	3.04 ± 0.51
Group 2	DLA + No drug treatment	2.63 ± 0.46$^{\$\$\$}$	18600 ± 600$^{\$\$\$}$	7.0 ± 0.21$^{\$\$\$}$	0.81 ± 0.16$^{\$\$\$}$
Group 3	DLA + BSA-Cu NCs	3.09 ± 0.18	17300 ± 360***	9.2 ± 0.38***	1.06 ± 0.12
Group 4	DLA + Ibf	3.23 ± 0.45	17000 ± 200***	9.0 ± 0.75***	0.99 ± 0.11
Group 5	DLA + BSA-CuNC-Ibf	4.42 ± 0.41***	11500 ± 500***	11.1 ± 0.61***	1.34 ± 0.13

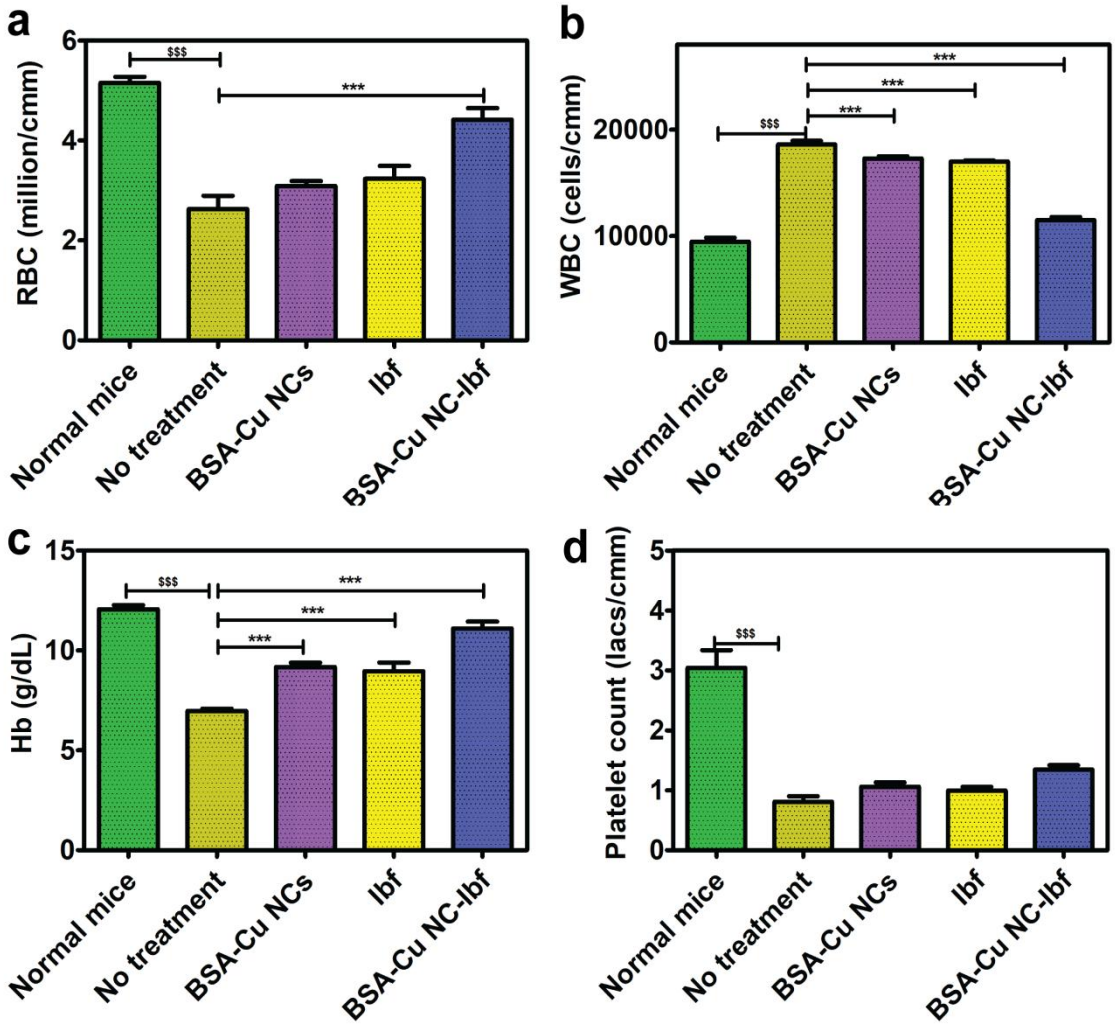

Figure 2.9. Graphical presentation showing effect of drug treatment on hemopoietic system where (a) represents results of RBC, (b) WBC, (c) Hb and (d) results of platelet count. Abbreviations used were, RBC- red blood cells, WBC- white blood cells, Hb- hemoglobin and cmm- cubic milli meter of blood.

Further, to evaluate the hepatotoxic and nephrotoxic possibility of the drug used for the study, liver functions tests (LFT) and renal function tests (RFT) were performed. DLA induction in mice without any treatment (i.e. in positive control group) significantly raised all the liver enzymes (AST, ALT and ALP; **Figure 2.10a,** along with reduction of albumin (Alb; **Figure 2.10b**) level compared to those of treated groups (**Table 2.4).** Though Ibf and BSA-Cu NCs administration showed noticeable variations, but the BSA-CuNC-Ibf treatment showed highly significant ($p < 0.001$) decline of all the liver enzymes with significant increase in albumin level, in close

proximity to normal. That revealed that DLA tumor has deleterious effect on liver but with treatment it was found to be resolved and the resolving capacity of the BSA-CuNC-Ibf nanodrug was found to be more pronounced. RFT (urea and creatinine) results did not show any abnormality in any of the studied groups suggesting no effect of either of the DLA tumour and the nanodrug on the kidney functions (**Figure 2.10c and d**). Refer **Table 2.5** for details.

Table 2.4. Effect of drug treatment on biochemical parameters to check functioning of liver.

Groups	**Treatment regime**	**AST (IU/L)**	**ALT (IU/L)**	**ALP (IU/L)**	**Albumin (g/dL)**
Group 1	Normal mice	31.3 ± 4.12	43.3 ± 5.86	111.3 ± 7.51	3.01 ± 0.25
Group 2	DLA + No drug treatment	90.7 ± 9.02$^{\$\$\$}$	90.7 ± 5.13$^{\$\$\$}$	212.3 ± 9.5$^{\$\$\$}$	1.53 ± 0.4$^{\$\$\$}$
Group 3	DLA + BSA-Cu NCs	79.3 ± 2.52	80.7 ± 5.03	194 ± 6.56**	2.33 ± 0.35*
Group 4	DLA + Ibf	75 ± 3**	75.7 ± 5.86*	182.3 ± 7.09***	2.4 ± 0.44*
Group 5	DLA + BSA-CuNC-Ibf	41.7 ± 4.73***	50.7 ± 4.51***	120.3 ± 4.04***	2.77 ± 0.32**

Table 2.5. Results of renal function tests, following drug treatment.

Sl. No.	**Treatment regime**	**Urea (mg/dL)**	**Creatinine (mg/dL)**
Group 1	Normal mice	13 ± 2.89	0.47 ± 0.15
Group 2	DLA + No drug treatment	14.3 ± 1.53	0.6 ± 0.1
Group 3	DLA + BSA-Cu NCs	13.3 ± 2.08	0.53 ± 0.15
Group 4	DLA + Ibf	14 ± 2	0.67 ± 0.12
Group 5	DLA + BSA-CuNC-Ibf	13.7 ± 0.58	0.47 ± 0.11

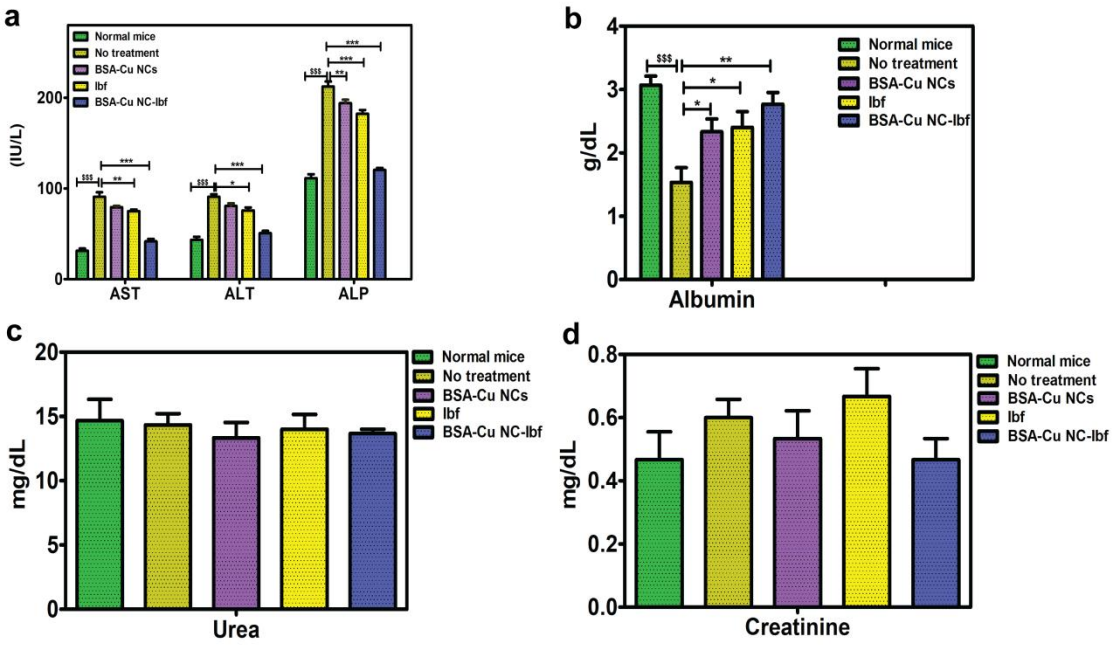

Figure 2.10. Graphical presentation showing effect of drug treatment on biochemical parameters to check functioning of liver and kidney where (a) represents results of liver enzymes, (b) albumin, (c) urea and (d) results of creatinine. Abbreviations used were, AST- aspartate transaminase, ALT- alanine transaminase and ALP- alkaline phosphatase.

Peritoneal fluid, which was collected at the end of the treatment period for biochemical and cell count analysis, revealed statistically significant difference in the total protein and sugar value between the treated and untreated groups. It was observed from **Table 2.6 and Figure 2.11a**, that though there was drop in the total protein level in the BSA-Cu NCs and Ibf treated groups, but it was much more pronounced in case of BSA-CuNC-Ibf treated group. Leakage of the protein rich fluid from the tumour cells was the cause of increased concentration of protein in the peritoneal fluid. Another biochemical parameter, sugar level in the ascitic fluid, revealed undetectable amount in the untreated DLA mice (**Table 2.6** and **Figure 2.11b,**). On the contrary, it was found to be significantly increased in all the treated groups which helped to elucidate that overgrown malignant cells in the ascitic fluid of the untreated DLA mice thrived on sugar for their survival and decrease in number of malignant cells resulted in rise in sugar level in the treated groups. It was observed that, the increase in sugar level was more pronounced in the BSA-CuNC-Ibf treated group.

Table 2.6. Results of biochemical tests of ascitic fluid following treatment.

Groups	Treatment regime	Total protein (g/dL)	Sugar (mg/dL)
Group 2	DLA + No drug treatment	2.3 ± 0.2	0
Group 3	DLA + BSA-Cu NCs	1.73 ± 0.35*	2 ± 0.1***
Group 4	DLA + Ibf	1.4 ± 0.3***	2.2 ± 0.2***
Group 5	DLA + BSA-CuNC-Ibf	0.7 ± 0.1***	4.3 ± 0.42***

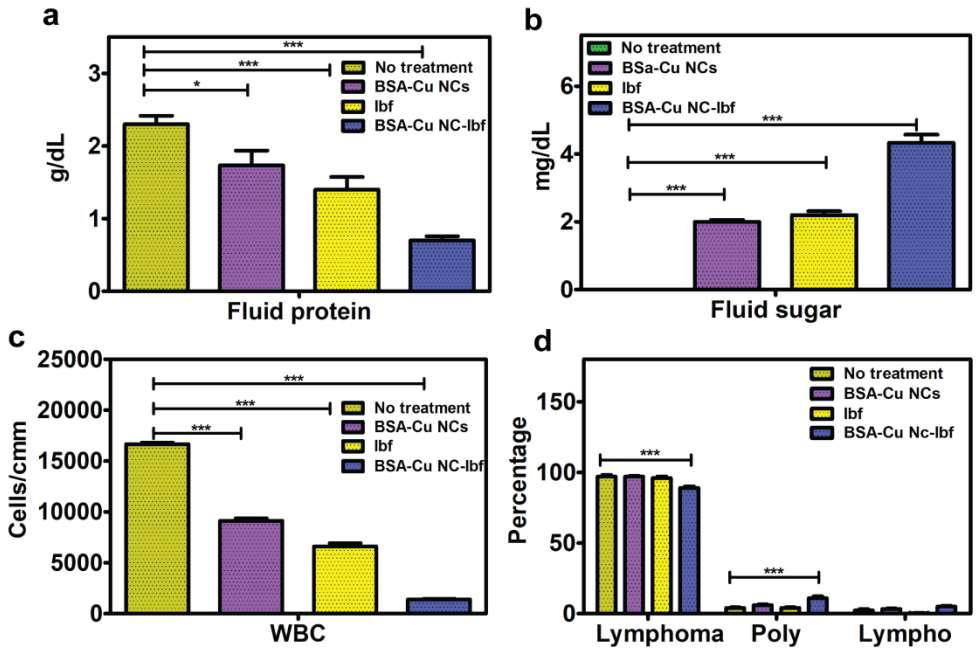

Figure 2.11. Graphical presentation showing examination results of ascetic fluid where (a) represents results of total protein, (b) sugar, (c) WBC and (d) results of differential count. The abbreviations used were, WBC- white blood cells, Lymphoma- lymphoma cells, Poly- polymorphonuclear cells and Lympho- lymphocytes.

This observation was later substantiated by the results of the cell count analysis of the ascitic fluid. The observed increased number of total WBC count in the positive control group was found to be reduced in all the treated groups and the drop in cell count was more distinct in the BSA-CuNC-Ibf treated group (**Table 2.7 and Figure 2.11c**) which also indirectly explained the increment rise in sugar level as well as

gradual decrease in protein level in the BSA-Cu NCs, Ibf and BSA-CuNC-Ibf treated groups. On examining the differential cell count it was observed that more than 95% of the cells were lymphoma cells in the untreated group (positive control) and groups treated with BSA-Cu NCs and only Ibf. Whereas, the percentage of lymphoma cells in the ascitic fluid of the mice treated with BSA-CuNC-Ibf was found to be significantly reduced to 89% (**Table 2.7 and Figure 2.11d**).

Table 2.7. Results of cell count analysis of ascitic fluid following treatment.

Groups	**Treatment regime**	**WBC**	**Lymphoma cells**	**Poly**	**Lympho**
Group 2	DLA + No drug treatment	16660 ± 286	97 ± 2	1 ± 0.6	2 ± 1.5
Group 3	DLA + BSA-Cu NCs	9133 ± 403***	97 ± 1	3 ± 2	3 ± 0.6
Group 4	DLA + Ibf	6620 ± 530***	96 ± 2	4 ± 1	0.3 ± 0.6
Group 5	DLA + BSA-CuNC-Ibf	1398 ± 99***	89 ± 2***	7 ± 2***	5 ± 1

Next, Giemsa stained smears of the peritoneal fluid collected from all the studied groups were examined under 40X and oil immersion objectives of binocular microscope. Photographs of the Giemsa stained smears of the fluids of all the studied groups are illustrated in **Figure 2.12**. It was observed that, under 40X and oil immersion objective, heavy cellularity in the untreated DLA mice compared to treated groups. In the BSA-CuNC-Ibf treated group, smear showed grossly reduced number of cells which confirmed effective antimitotic role of the nanodrug.

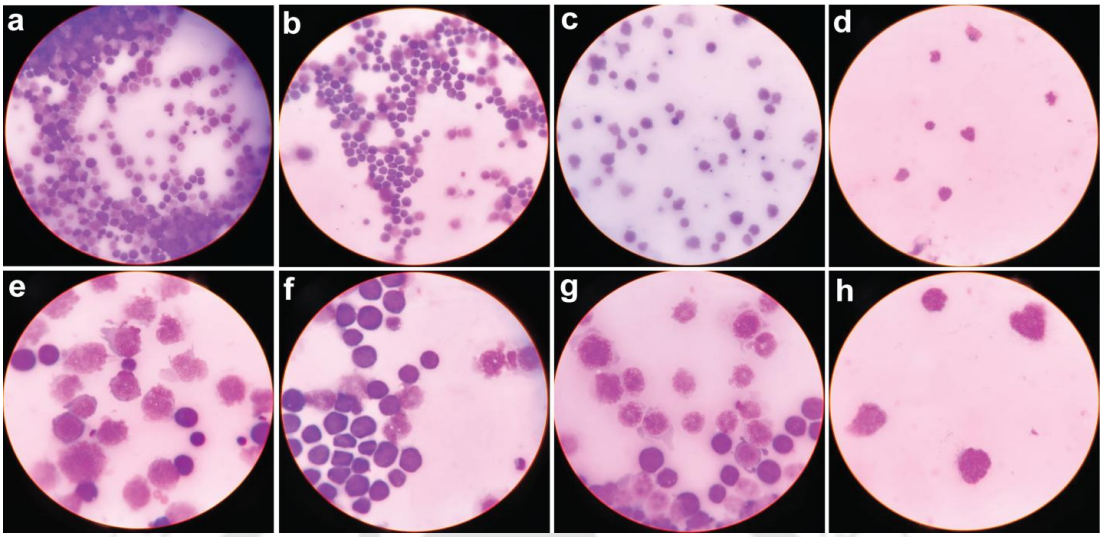

Figure 2.12. Photographs of Giemsa stained smear of ascetic fluid of different study groups taken under 40X (a-d) and Oil Immersion (e-f) objective of microscope where a and e represents fluid of untreated DLA mice , b and f- DLA mice treated with BSA-Cu NCs, c and g- DLA mice treated with Ibf and d and h- DLA mice treated with BSA-CuNC-Ibf.

It is worth mentioning here that, the link between NSAIDs and cancer is observed in the view of inhibition of cyclooxygenase (COX) thus decreasing prostaglandin synthesis, which is responsible for tumorogenesis.[45] Moreover, overexpression of COX in some of cancers causing angiogenesis which in turn plays a crucial role in tumour invasion and metastasis, make NSAIDs a potential candidate for cancer research as they are regular use COX inhibitors.[46,47] Furthermore, PGE2 is a product of COX activity and it has been reported to be elevated in cancer cells causing cancer cell proliferation and invasion,[48,49] so it was decided to measure the PGE2 level in both blood and ascitic fluid to access the role of ibuprofen in cancer therapeutics through COX dependent pathway.

It was observed that, PGE2 level of blood from the untreated group showed a statistically significant rise than that of the normal mice. Interestingly, there was a significant drop in the PGE2 level after treatment with BSA-Cu NCs, Ibf and BSA-CuNC-Ibf, which was evident in case of both blood and ascitic fluid (**Figure 2.13b**). The PGE2 level of both blood and ascitic fluid of BSA-CuNC-Ibf group was even less

than that of PGE2 level of BSA-Cu NCs and Ibf treated groups. The results established the COX dependent mode of action of ibuprofen and better results in BSA-CuNC-Ibf treated groups may be due to the synergistic action of BSA-Cu NCs and Ibf. Refer to **Table 2.8** for details.

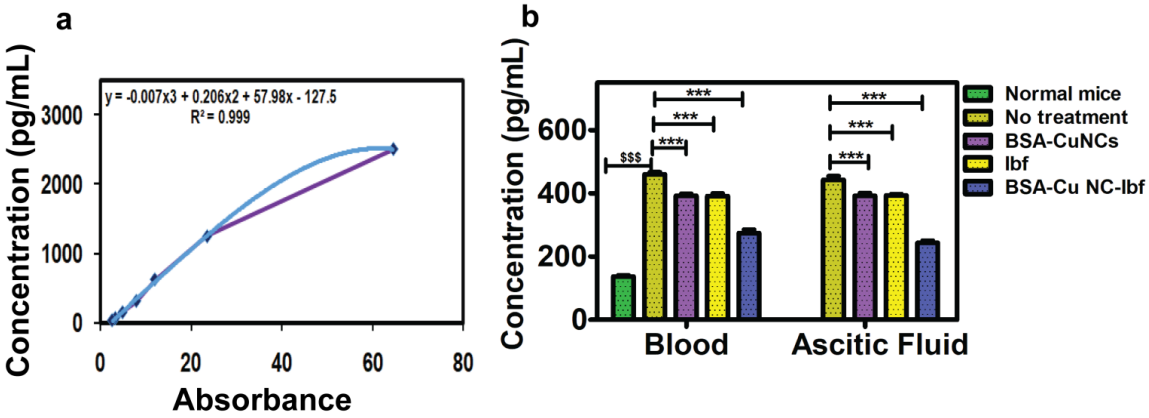

Figure 2.13. (a) Standard graph of PGE2 (b) estimated PGE2 level in blood and ascetic fluid of different study groups.

Table 2.8. Results of PGE2 of both serum and ascitic fluid following treatment.

Sl.No.	Treatment regime	Serum (pg/mL)	Ascitic Fluid (pg/mL)
Group 1	Normal mice (Control)	$136.77 \pm 7.55^{\$\$\$}$	
Group 2	DLA + No drug treatment	$460.47 \pm 11.81^{***}$	$442.77 \pm 21.15^{***}$
Group 3	DLA + BSA-Cu NCs	$392.2 \pm 11.3^{***}$	$392.37 \pm 14.9^{***}$
Group 4	DLA + Ibf	$391.87 \pm 13.3^{***}$	$393.7 \pm 6.71^{***}$
Group 5	DLA + BSA-CuNC-Ibf	$274.33 \pm 19.25^{***}$	$243.63 \pm 11.86^{***}$

Finally, to examine tumor metastasis, liver and kidney tissue sections were examined microscopically. Histopathological examination of liver tissue sections of DLA mice (**Figure 2.14b**) showed expanded portal tract due to infiltration of lymphocytes may be due to tumor migration to liver cells. Hepatocytes are unremarkable and liver sinusoids were dilated. Sections from the other groups were

free from lymphocytic infiltration except the DLA mice treated with BSA-Cu NCs, where very few lymphocytic infiltrations in portal tract were noticed (**Figure 2.14c**). Sections from the kidney (**Figure 2.14f-j**) did not show any tumor cell metastasis except features of acute tubular necrosis in the form of pyknotic nuclei of tubules, intensely eosinophilic cytoplasm and sloughing out epithelial cells at some places, which is a regular phenomenon in postmortem cases due to acute ischemia of renal artery before death.

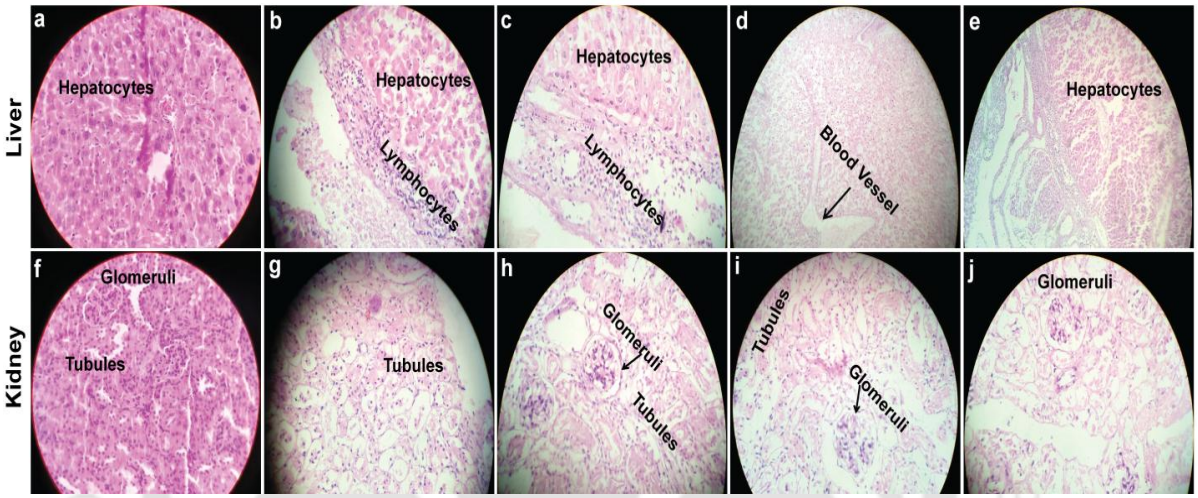

Figure 2.14. Histopathological images of liver (a−e) and kidney (f−j), stained with hematoxylin and eosin where part (a and f) represents negative control (normal mice), (b and g) DLA mice without treatment (c and h) DLA mice treated with BSA-Cu NCs, (d and i) DLA mice treated with Ibf, (e and j) DLA mice treated with BSA-CuNC-Ibf. The organs were collected on day 16 after treatment.

2.6. Conclusion

Herein, a novel method of aqueous synthesis of a novel nanodrug in the form of BSA-CuNC-Ibf has been reported. The as-synthesized nanodrug were found to be effective against human cervical (HeLa) and human lung cancer (A549) cells with 45 % cell viability against HeLa and 65 % cell viability against A549 cells with 37.66 µg/mL (w.r.t. Ibf) of the nanodrug. Moreover, the work also described chemotherapeutic efficacy and the significance of synergistic activity of BSA-Cu NCs and Ibf in the formulated nanodrug when tested on DLA mice model. A non chemotherapeutic agent

(Ibuprofen) can be converted into a potent chemotherapeutic agent by combining it with different nanoplatforms. This can significantly reduce the adverse effects of conventional drug regime and bring down the mortality rate of cancer. Thus the results of the combination therapy of the current study bring new hope in cancer theranostics.

2.7. References

1. Arias, J. I.; Aller, M. A.; Arias, J. *Mol. Cancer*, **2007**, *6*, 1–10.
2. Coussens, L. M.; Werb, Z. *Nature*, **2002,** *420*, 860-867.
3. Lu,Y.; Cai, Z.; Galson, D.L.; Xiao,G.; Liu,Y.; George, D.E.; Melhem, M. F.; Yao, Z. Zhang, J. Prostate, **2006**, *66*,1311–1318.
4. Rothman, I.; Stanford, J.L.; Kuniyuri, A.; Berger, R.E. *Urology*, **2004**, *64* (5), 876 880.
5. Nelson, W.G.; DeMarzo, A.M.; DeWeese, T.L.; Isaacs, W.B. *J. Urol.* **2004**, *172* (5 II), S6–S12.
6. Rosenblatt, K. A.; Wicklund, K. G.; Stanford, J. L. *Am. J. Epidemiol.* **2001**, *153* (12), 1152– 1158.
7. Adelstein, P. *Cancer*, **1979**, *43*, 2553-2557.
8. Loftus, E.V. *Gastroenterol. Clin. North Am.* **2006**, *35* (3), 517–531.
9. Farrow, B.; Sugiyama, Y.; Chen, A.; Uffort, E.; Nealon, W.; Mark, E. B. *Ann. Surg.* **2004**, *239* (6), 763–771.
10. Otsuki, M. *J. Gastroenterol.* **2003**, *38* (4), 315–326.
11. Ammann, R. W.; Akovbiantz, A.; Largiader, F.; Schueler, G. *Gastroenterology*, **1984**, *86*, 820–828.
12. Rayburn, E.R.; Ezell, S. J.; Zhang, R. *Mol Cell Pharmacol.* **2009**, *1* (1), 29-43.
13. Zlotnik, A. *Contrib Microbiol*, **2006**, *13*, 191–199.
14. Jana, N. R. *Cell. Mol. Life Sci.* **2008**, *65* (9), 1295–1301.
15. de Groot, D. J. A.; de Vries, E. G. E.; Groen, H. J. M.; de Jong, S. *Crit. Rev. Oncol. Hematol*,.**2007**, *61* (1), 52–69.
16. Arun, B.; Goss, P. *Semin. Oncol.* **2004**, *31* (2), 22–29.
17. Stark, L. A.; Din, F. V. N.; Zwacka, R. M.; Dunlop, M. G. *FASEB J.* **2002**, *15* (7), 1273–1275.

18. Loveridge, C. J.; MacDonald, A. D. H.; Thoms, H. C.; Dunlop, M. G.; Stark, L. A. *Oncogene*, **2008**, *27* (18), 2648–2655.
19. Perkins, N. D. *Nat. Rev. Mol. Cell Biol.* **2007**, *8* (1), 49–62.
20. O'Connor, R.; O'Leary, M.; Ballot, J.; Collins, C. D.; Kinsella, P.; Mager, D. E.; Arnold, R. D.; O'Driscoll, L.; Larkin, A.; Kennedy, S.; et al. *Cancer Chemother. Pharmacol.* **2007**, *59* (1), 79–87.
21. Zrieki, A.; Farinotti, R.; Buyse, M. *Pharm. Res.* **2008**, *25* (9), 1991–2001.
22. Albouy, B.; Tourani, J. M.; Allain, P.; Rolland, F.; Staerman, F.; Eschwege, P.; Pfister, C. *BJU Int.* **2007**, *100* (4), 770–774.
23. Javle, M. M.; Cao, S.; Durrani, F. A.; Pendyala, L.; Lawrence, D. D.; Smith, P. F.; Creaven, P. J.; Noel, D. C.; Iyer, R. V.; Rustum, Y. M. *Clin. Cancer Res.* **2007**, *13* (3), 965–971.
24. Fabi, A.; Metro, G.; Papaldo, P.; Mottolese, M.; Melucci, E.; Carlini, P.; Sperduti, I.; Russillo, M.; Gelibter, A.; Ferretti, G.; et al. *Cancer Chemother. Pharmacol.* **2008**, *62* (4), 717–725.
25. Ouyang, N.; Ji, P.; Williams, J. L. *Int. J. Oncol.* **2013**, *42* (2), 643–650.
26. Johnson, C.C.; Hayes, R. B.; Schoen, R. E.; Gunter, M. J.; Huang, W-Y. *Am. J. Gastroenterol.* **2010**, *105* (12), 2646–2655.
27. Harris, R. E.; Beebe-Donk, J.; Alshafie, G. A. *BMC Cancer* **2008**, *8*, 237.
28. Harris, R. E.; Beebe-Donk, J.; Doss, H.; Burr Doss, D. *Oncol. Rep.* **2005**, *13* (4), 559–583.
29. Davis, M. E.; Chen, Z.; Shin, D. M. *Nat. Rev. Drug Discov.* **2008**, *7* (9), 771–782.
30. Nguyen, K. T. *J. Nanomed. Nanotechnol.* **2011**, *02* (05).
31. Kumar, R. *J. Nanomed. Nanotechnol.* **2016**, *7* (4).
32. Sondhi, S. M.; Rani, R.; Singh, J.; Roy, P.; Agrawal, S. K.; Saxena, A. K. *Bioorganic Med. Chem. Lett.* **2010**, *20* (7), 2306–2310.
33. Suri, S. S.; Fenniri, H.; Singh, B. *Journal of Occupational Medicine and Toxicology*, **2007**, *2*, 16.
34. Verma, S.; Gokhale, R.; Burgess, D. J. *Int. J. Pharm.* **2009**, *380* (1–2), 216–222.

35. Kumar, R.; Siril, P.F.; Soni, P. *Propellants Explos. Pyrotech*. **2014**, 39, 383 – 389.

36. Kumar, R.; Siril, P. F. *RSC Adv.* **2014**, *4* (89), 48101–48108.

37. Vainio, H.; Morgan, G. *Scand. J. Gastroenterol.* **1998**, *33* (8), 785–789.

38. Ashburn, T. T.; Thor, K. B. *Nat. Rev. Drug Discov.* **2004**, *3* (8), 673–683.

39. Wang, C.; Wang, C.; Xu, L.; Cheng, H.; Lin, Q.; Zhang, C. *Nanoscale*, **2014**, *6* (3), 1775–1781.

40. Yu, Y.; New, S. Y.; Xie, J.; Su, X.; Tan, Y. N. *Chem. Commun.* **2014**, *50* (89), 13805–13808.

41. Li, J.; Yao, P. *Langmuir*, **2009**, *25* (11), 6385–6391.

42. Yu-Bin, J.; Xin, L. I.; Guo-Song, X.; Qin-Bing, X. *IOP Conf. Ser. Earth Environ. Sci.* **2017**, *100* (1), 012048.

43. Kawamori, T.; Rao, C. V.; Seibert, K.; Reddy, B. S. *Cancer Res.* **1998**, *58* (3), 409–412.

44. Sun, Y.; Rowehl, L. M.; Huang, L.; Mackenzie, G. G.; Vrankova, K.; Komninou, D.; Rigas, B. *Breast Cancer Res.* **2012**, *14* (1), 1–12.

45. Wong, R. S. Y. *Adv. Pharmacol. Sci.* **2019**, 1–10.

46. Kulkarni, S.; Rader, J. S.; Zhang, F.; Liapis, H.; Koki, A. T.; Masferrer, J. L.; Subbaramaiah, K.; Dannenberg, A. J. *Clin. Cancer Res.* **2001**, *7* (2), 429–434.

47. Leahy, K. M.; Ornberg, R. L.; Wang, Y.; Zweifel, B. S.; Koki, A. T.; Masferrer, J. L. *Cancer Res.* **2002**, *62* (3), 625–631.

48. Roberts, H. R.; Smartt, H. J. M.; Greenhough, A.; Moore, A. E.; Williams, A. C.; Paraskeva, C. *Carcinogenesis* **2011**, *32* (11), 1741–1747.

49. Ke, J.; Yang, Y.; Che, Q.; Jiang, F.; Wang, H.; Chen, Z.; Zhu, M.; Tong, H.; Zhang, H.; Yan, X.; et al. *Tumor Biol.* **2016**, *37* (9), 12203–12211.

CHAPTER-3

Bimetallic Fe–Cu Nanocomposites on Sand Particles for the Inactivation of Clinical Isolates

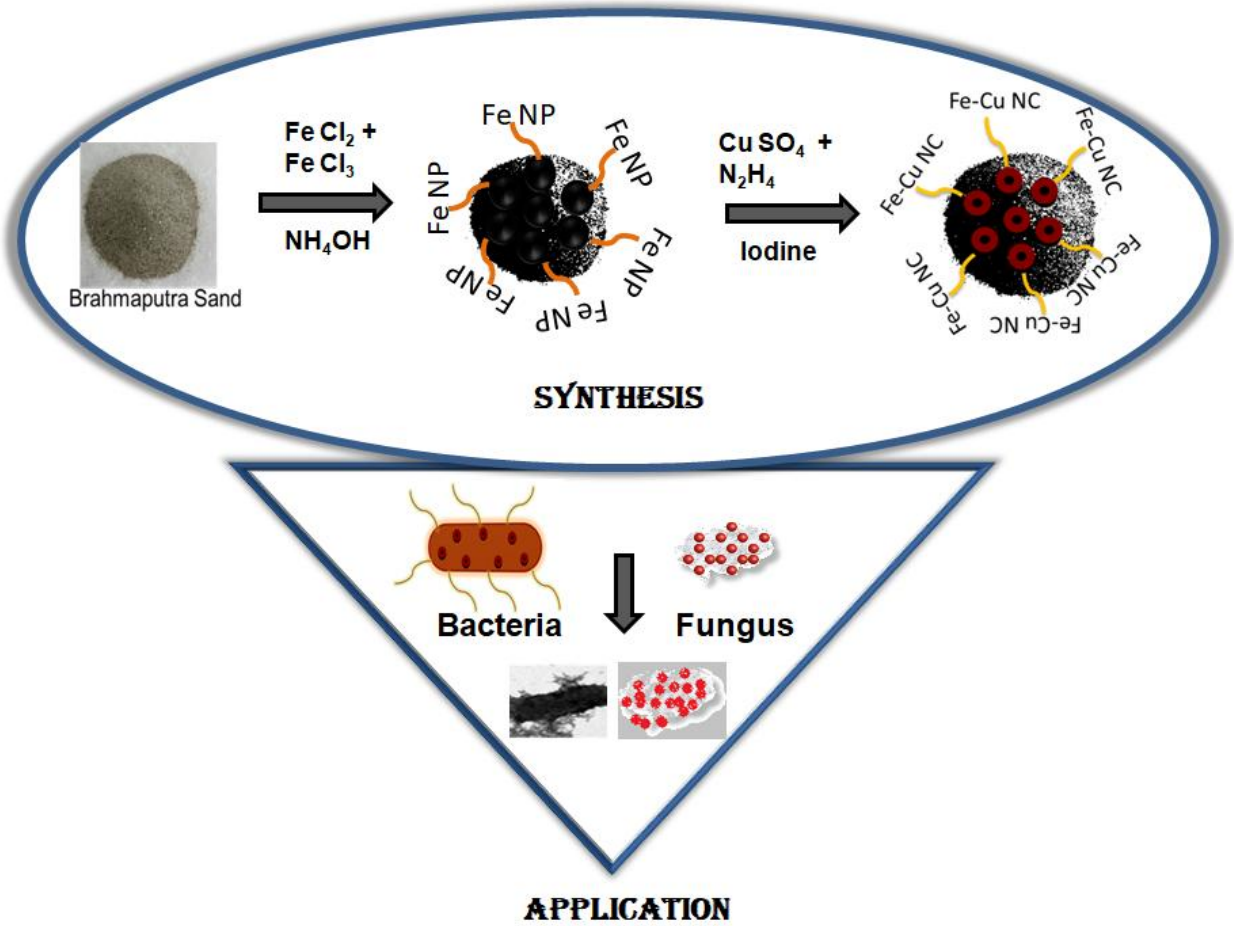

In Chapter 3, facile synthesis of iodine stabilized bimetallic Fe-Cu-nanocomposites on surface of the *Brahmaputra* River (in India) bank sand, under normal atmospheric conditions has been reported. To ensure its broad spectrum antimicrobial activity, the compound was tested on various clinical isolates collected from real biological samples like blood, pus and urine.

Indian Patent Application No. 201831016639 dated May 2, 2018
https://pubs.acs.org. DOI: 10.1021/acsabm.8b00572

CHAPTER -3

3.1. Introduction

A major proportion of the health hazards in developing countries like India are due to different types of clinical isolates (pathogens)[1] and they are also considered as the foremost cause of global morbidity and mortality. Perpetual increase in the development of multidrug resistance among the clinical isolates further intricate the problem.[2] Non-judicious use of conventional broad-spectrum antibiotics has led to generation of new strains of pathogens with increasing levels of antibiotic resistance thereby contributing to the ensuing threat to the public health.[3] Therefore, antibiotic resistance is one of the most imperative issues in public health globally. In order to alleviate this problem there have been various efforts from different scientific fields. In this milieu, invention of new bactericidal agents, which may also be used as a tool to evade multidrug resistance (MDR) mechanisms has become an essential objective in materials science.[4,5]

With the advent of nanotechnology, different strategies have been emerged to develop novel nanostructures with flexible antimicrobial properties. Amongst the wide range of nanostructures, special attention has been aimed at nanoparticles because of their various properties like ease of synthesis, biocompatibility and modulated release, make them a favorable tool to combat different pathogenic clinical isolates.[2] The large surface area to volume ratio of the nanoparticles make possible to interact more closely with microbial membranes. Moreover, easy surface functionalization of the NPs help to bring a paradigm shift in management of multi drug resistant clinical isolates.[3,6-8] The demand of NPs as an antimicrobial agent is enhanced because of their ability to overcome the multidrug resistance mechanisms.[2] There are several means by virtue of which NPs have been reported to act as an antimicrobial agent such as, interacting with the bacterial cell wall directly, generating reactive oxygen species, interacting with bacterial DNA and proteins, elevating host immune response, resisting the biofilm

formation etc. As their mechanism of action is absolutely different to that of the conventional antibiotics, they are found to be effective against MDR bacteria.[2,3]

Recently, various metallic nanoparticles have been studied extensively in this regard and have received remarkable global focus as an innovative tool for combating the high rates of antimicrobial resistance.[3] The effectiveness of Ag NPs as bactericidal agent is well-known and silver containing products are also commercially available. There is strong evidence that it is linked with cationic release and hence the potential risk of cytotoxicity and genotoxicity in human cells cannot be ignored.[9-10] Copper can be seen as a better candidate on the merit of its affordability, availability and properties similar to that of other metallic NPs. It is also a natural constituent of living tissues and human body can resist copper toxicity to some extent.[11,12] In addition to that, it has also been approved by EPA (US Environmental Protection Agency).[13] At the same time, Cu NPs are known to have bactericidal effects against various strains of microbes including methicillin resistant *Staphylococcus aureus*.[14-16]

There are several reports describing the mechanism of antimicrobial properties of CuNPs. For example, there is a suggestion of reaction of copper with the -SH groups of amino acid, leading to inactivation of the cell proteins and thus cell death.[16] Further there are reports where copper ions leached from the nanoparticles were anticipated to have role in antimicrobial activity.[14,17] In addition, the reactivity of the NPs due to their dimensions assist in close interaction with the microbial surface.[18] It has been reported that there is production of hydroxyl radicals, which bind with DNA molecules and lead to distortion of the helical structure and also denature the vital proteins by binding with the sulfhydryl amino and carboxyl groups of amino acids.[19] The NPs affect the membrane integrity by inactivating the cell membrane proteins and also interrupt the biochemical processes of the bacterial cells.[19] On the contrary, reports showing the role of Cu NPs instead of copper ions for contact killing of microbes have also been published.[18,20] Thus contact of the Cu NPs to the microbial cell wall leads to cell wall disruption and leakage of the cellular proteins and other intracellular constituents and ultimately leading to cell death.[20,21] Research explaining bacterial inactivation due to oligodynamic effect brought about by the diffusion of copper ions into the bacteria through the porins is also available.[22]

Synthesis of stable metallic Cu-NPs is a real challenge as they undergo rapid oxidation and aggregation in air or aqueous media.[23] Such problems can be prevailed by using various protecting agents and ligands but possibilities of limiting the catalytic activity of Cu NPs cannot be ignored as most of active sites of the Cu NPs are blocked by the protecting agents.[23] Different studies are reported on preparing stable Cu NPs by anchoring them on supports like iron oxides, SiO_2 and polymers.[24-27] Preparation of Cu NPs by anchoring them on support materials may bring alterations in final material's physicochemical properties as these support materials may also confer their own properties and thus resulting in a more effective product. Therefore, selection of an appropriate support material is a crucial step as doing this, it is possible to fabricate a novel Cu NP suitable for selected application.

On the basis of the findings of different studies, fabrication of a new nanocomposite, blending different ingredients that retain all the properties of its components, was initiated. Herein, synthesis of iodine stabilized bimetallic Fe-Cu-nanocomposites on surface of the *Brahmaputra* river bank sand under normal atmospheric conditions has been reported. Enhanced bactericidal activity with the use of bimetallic nanoparticles have been reported to provide better efficacy than the constituent ingredients.[28] Also, it has been reported that compared to single nanoparticle, low concentration of bimetallic nanoparticles can exhibit better bactericidal and antimycotic activity against multidrug-resistant bacteria and fungi.[29] It has also been proposed that reactivity of the matrix metal can be enhanced by addition of a second metal.[30] The purpose of selecting iron and copper here was that both are constituent elements of human body and comparatively safe to be used. They are also easily available and affordable and like Cu NPs, Fe NPs are also known for their antimicrobial properties.[31] Moreover, Fe NPs are used to add magnetic properties to other engineered particles for easy separation of biological products using an external magnetic field.[32,33] The use of an inert scalar substance such as sand combined with bimetallic Fe-Cu-nanocomposites offers a cost effective method for further applications besides its antimicrobial role. Herein, *Brahmaputra* river bank sand was used in synthesizing the nanocomposites as it is well known for its silty and fine nature and it is easily available as well.

So, the present invention is aimed at preparation of potent, stable, reusable and cost effective nanocomposites exhibiting a strong antimicrobial activity against a wide range of microbes' viz.multidrug resistant bacteria and fungus. To ensure its broad spectrum bactericidal role, it was tested on various clinical isolates collected from different patients' coming for treatment to Guwahati Neurological Research Centre (GNRC) Medical Hospital, Guwahati. Various biological specimens like urine, blood and pus were tested for isolation of microbes.

3.2. Outline of the Present Work

Herein a bimetallic Fe−Cu nanocomposite with an average size of 26.4 ± 4.7 nm were prepared on the surface of fine sand particles by modified coprecipitation and the chemical reduction method and were applied as an *in vitro* broad spectrum antimicrobial agent. The size of the nanocomposites could be further tuned to 11.8 ± 1.6 nm when prepared after ball milling the sand particles, keeping the antimicrobial property intact. The results showed that the chemical nature and morphology of the nanocomposites had a great effect on both Gram-positive and Gram-negative bacteria with a minimum inhibitory concentration of 10.6 μg/mL and 13.8 μg/mL of copper, whereas the minimum bactericidal concentration was found to be 15.9 μg/mL and 21.2 μg/mL. The nanocomposites exhibited antimicrobial activity against multidrug-resistant bacteria as well as fungus isolated from different human biological samples like blood, urine, pus, and wound swabs.

3.3. Experimental Section

3.3.1. Materials

The *Brahmaputra* river bank sand was collected and washed several times alternately with hydrochloric acid and Milli-Q grade water and then dried before use. The sources for iron-copper-nanocomposites were ferrous chloride (extra pure hydrate) from Loba Chemie, ferric chloride anhydrous and copper II sulphate pentahydrate (CuSO4.5H2O) along with 25% ammonia solution and 80% hydrazine hydrate obtained from Merck. Iodine was purchased from Sigma Aldrich chemical Pvt. Ltd., Kolkata, India. All

reagents were used as received without further purification. Milli-Q grade (resistivity 18.2 MΩcm-1) water was used in all experiments.

3.3.2. Bacterial Strains and Media

Different species of microorganisms used in the experiments were isolated from various patients' samples collected from patients attending Guwahati Neurological Research Center (GNRC) Medical Outdoor Clinic (North Guwahati, India) or admitted there for treatment after taking written consent from them. The media used for growth of these microorganisms were cysteine lactose electrolyte deficient CLED) agar, nutrient agar, Muller Hinton agar (MHA) and MHA with 2% glucose and 0.5 mg/L methylene blue dye for fungus, purchased from Himedia, Mumbai, India. Further, GFP-expressing recombinant *E. coli* (MTCC 433 Strain) and *Bacillus Cereus* (MTCC 1305) grown in nutrient agar (Himedia, Mumbai, India) were also used in the experiments.

3.3.3. Preparation of Fe-Cu-Nanocomposites on Sand

The Fe-Cu-nanocomposites on sand was prepared by two steps procedure of co-precipitation and chemical reduction method under normal atmospheric conditions. Briefly, in 50 mL of Milli-Q grade water, 150 mg of Brahmaputra river bank sand, 1.0 g of $FeCl_2$ and 1.5 g of $FeCl_3$ were added in a conical flask and left under constant magnetic stirring with moderate heating (60°C) for 4-5 min. Then 6 mL of (25%) ammonium hydroxide (NH_4OH) was added. Color of the solution turned black indicating formation of iron oxide NPs on the surface of sand in the medium. Into this medium, $CuSO_4$ pentahydrate crystals (250 mg) were added to produce bimetallic Fe-Cu-nanocomposites on sand by reduction with fresh solution of hydrazine (1mL) keeping the conditions same. 300 µL of iodine solution (0.2M) was added as a stabilizing agent as molecular iodine is known to form a film on the surface of copper and thus provides stability towards oxidation and agglomeration.[35] Then the reaction mixture was kept under stirring condition for 5 min. The flask was then removed and allowed to cool at room temperature followed by centrifugation of the reaction mixture at 6000 rpm for 5 min. The supernatant was discarded and the precipitate was washed with Milli-Q grade water several times to remove the unreacted compounds and kept

for drying in a hot air oven at 37°C. The method used here for preparing Fe-Cu-nanocomposites on sand was a modified version of the methods previously used.[21,34,35]

3.3.4. Preparation of Fe-Cu-Nanocomposites on Sand after Ball Milling of Sand

To grind sand in nanoscale level, first the sand (collected from Brahmaputra River Bank) was thoroughly washed with hydrochloric acid and Milli-Q grade water alternately for several times followed by drying in hot air oven and then subjected to ball milling on PM 100 of Retsch; 126270304 at 350 rpm for 4 h. Thereafter the grinded sand was used for synthesis of sand-Fe-Cu-nanocomposites following the same procedure as mentioned earlier.

3.4. Characterization

3.4.1. Transmission Electron Microscopy (TEM)

The external morphology study for the size, shape and structure of the Sand-Fe-Cu-nanocomposites (both prepared before and after ball milling of sand) was pursued by transmission electron microscopy (TEM; JEM 2100; Jeol, Peabody, MA, USA). For the analysis, 2 mg of prepared nanocomposites was mixed with 1 mL of distilled water along with 10 µL 0.1% acetic acid and from which 8 µL was added on carbon-coated copper grid, air dried and taken for measurements. TEM & SAED (selected area electron diffraction) images were recorded and from the corresponding particle size distribution of the TEM images, size of the nanocomposites was measured.

3.4.2. Powder X-Ray Diffraction (XRD)

Powder XRD experiments were carried out on a Bruker AXS D8 Advance X-ray diffractometer with Cu Kα1 radiation (λ = 1.54060 Å) with the instrument being operated at 40 kV and 40 mA.

3.4.3. Field Emission Scanning Electron Microscopy (FESEM)

The surface texture and morphology of Sand-Fe-Cu-nanocomposites (prepared both before and after ball-milling of sand were studied using field emission scanning electron microscope (FESEM), SIGMA-01-37, ZEISS. During FESEM analysis, the energy dispersion X-ray spectrum (EDX) was also performed. Samples were coated

with gold using sputter coater EDWARDS A652-01-903.

3.4.4. In vitro Studies of Antimicrobial Activity

The antimicrobial activity of the Sand-Fe-Cu-nanocomposites was determined by Lawn culture method. For this, the overnight grown bacterial suspension (in 5 mL peptone) of both Gram positive *Bacillus cereus* and Gram negative, GFP-expressing *Escherichia coli* were inoculated in an agar plate followed by incubation at 37 °C with the prepared nanocomposites. After 12 h of incubation, the bacterial growth was monitored visually. For determination of minimum inhibitory concentration (MIC) and minimum bactericidal concentration (MBC), first the respective strain of bacteria was allowed to grow overnight at 37 °C and from which 1 $\times 10^6$ CFU/mL of each strain was inoculated in 5 mL peptone followed by treatment with gradually increasing concentration of the composite at 37 °C for 12 h. The bacterial growth was monitored by measuring the optical density (OD) of the various treated groups of each strain - collected at different time points of 2, 4, 6, 8, 10 and 12 h- at 595 nm using a UV−visible spectrophotometer (Lambda; Perkin-Elmer, Fremont, CA, USA). Further antimicrobial property of the nanocomposites was also determined on different species of microorganisms including methicillin resistant *Staphylococcus aureus* (MRSA) and fungus (*Candida albicans*) isolated from various patients' samples collected from patients attending Guwahati Neurological Research Center (GNRC) Medical (North Guwahati) Outdoor Clinic or admitted there for treatment after taking written consent from them. Streak culture method was used for isolation of organisms in pure culture from different clinical specimens. One loop of specimen was transferred and streaked onto the surface of a well dried culture plate. Different media were used for different specimens like Cysteine Lactose Electrolyte Deficient Agar (CLED) for urine, Nutrient Agar for specimens like blood/pus/sputum etc. and for fungus Sabouraud Dextrose Agar (SDA) media. For antibiotic susceptibility test (AST), a loop of grown colony was inoculated in 5 mL of peptone and from which surface of a plate (MHA for bacteria and MHA with 2% glucose and 0.5% methylene blue for fungus) was smeared with the help of swab soaked with the respective bacterial suspensions. Thereafter, the prepared nanocomposites were applied along with conventional antibiotic disc (usually used in

Medical Microbiology Lab) over the inoculated plates with bacteria followed by overnight incubation at 37°C. Sensitivity or resistance was determined by visual observation of clear zone of inhibition for growth of bacteria around the prepared nanocomposites.

The *in vitro* antimicrobial property of the Sand-Fe-Cu-nanocomposites (synthesized after ball milling of sand) was also determined on Gram positive cocci, both methicillin sensitive (MSSA) and methicillin resistant *S. aureus* (MRSA) and Gram negative bacilli, *E. coli* and *Klebsiella pneumoniae* by Lawn culture method as described earlier. The bacteria were isolated from urine and pus of patients attending GNRC Medical, North Guwahati for treatment after getting written consent from them.

3.4.5. Fluorescence Assisted Cell Sorting (FACS)

To find out the bacterial **c**ell viability, FACS based assay was carried out using BD FACS Calibur system (BD Biosciences, San Jose, CA). To measure the disruption of cell membrane integrity, propidium iodide (PI), a DNA staining dye was used. Normal living cells, due to their intact cell membrane do not allow PI to penetrate and thus show green fluorescence (from GFP of the recombinant bacteria). On the other hand, emergence of red fluorescence indicates penetration of PI into the cell through the pores developed in the cell wall followed by binding with DNA, thus capable of producing red fluorescence in case of compromised and dead cells. For this, GFP expressing recombinant *E. coli* (MTCC 433 Strain) were treated with MIC concentration of Sand-Fe-Cu-nanocomposites, Sand-Cu-nanocomposites, Sand-Fe-nanocomposites, and 50 µL of copper solution (prepared by dissolving 250 mg $CuSO_4$ in 50 mL of Milli-Q water) for 6 h. At the same time, GFP bacteria without any treatment were also maintained. Following treatment, 100 µL (10^6 cells / mL) of bacterial cultures from each tube were taken and centrifuged for 5 min at 1000 rpm. The collected cell pellets were re-dispersed in 0.9 % NaCl and stained with 3 µL of propidium iodide (PI) for 5 min before doing the FACS analysis. In FACS, PI and GFP emissions are acquired in FL2-H (red channel) and FL1-H (green channel), respectively and accordingly bacterial cell viability assessment reveals existence of four different cell populations in response to an antimicrobial agent. The lower right (LR) quadrant

corresponds to live population (only GFP emission), upper right (UR) quadrant for compromised cell population (both GFP and PI emission), upper left (UL) for dead cells (only PI emission) and lower left (LL) represents lysed cell population (devoid of fluorescence).

3.4.6. Determination of Stability of the Nanocomposites

Stability was studied by checking the antimicrobial activity of nanocomposites at different times after preparation on *B. cereus* (MTCC 1305) and GFP expressing bacteria *E. coli* (MTCC 433 Strain).

3.4.7. Control Experiment

Control experiments for the nanocomposites treatment were conducted with (1) 50 µL of copper solution prepared by dissolving 250 mg of copper sulphate pentahydrate salt in 50 mL of Milli-Q water, (2) Sand-Fe-nanocomposites, (3) Sand-Cu-nanocomposites and (4) Sand-Fe-Cu-nanocomposites both on GPC and GNB.

3.5. Results and Discussions

Fe-Cu-nanocomposites were synthesized on the surface of the Brahmaputra river bank sand under normal atmospheric conditions. The iodine stabilized dark brown colored nanocomposites were prepared from the reaction of $FeCl_2$ and $FeCl_3$ with ammonia solution in presence of sand and then finally with $CuSO_4$ and hydrazine. The precipitate obtained was separated from the reaction mixture, washed, centrifuged and dried. The schematic representation of the Fe-Cu nanocomposite synthesis on the surface of sand with their role in annihilation of different clinical isolates has been illustrated in **Figure 3.1**.

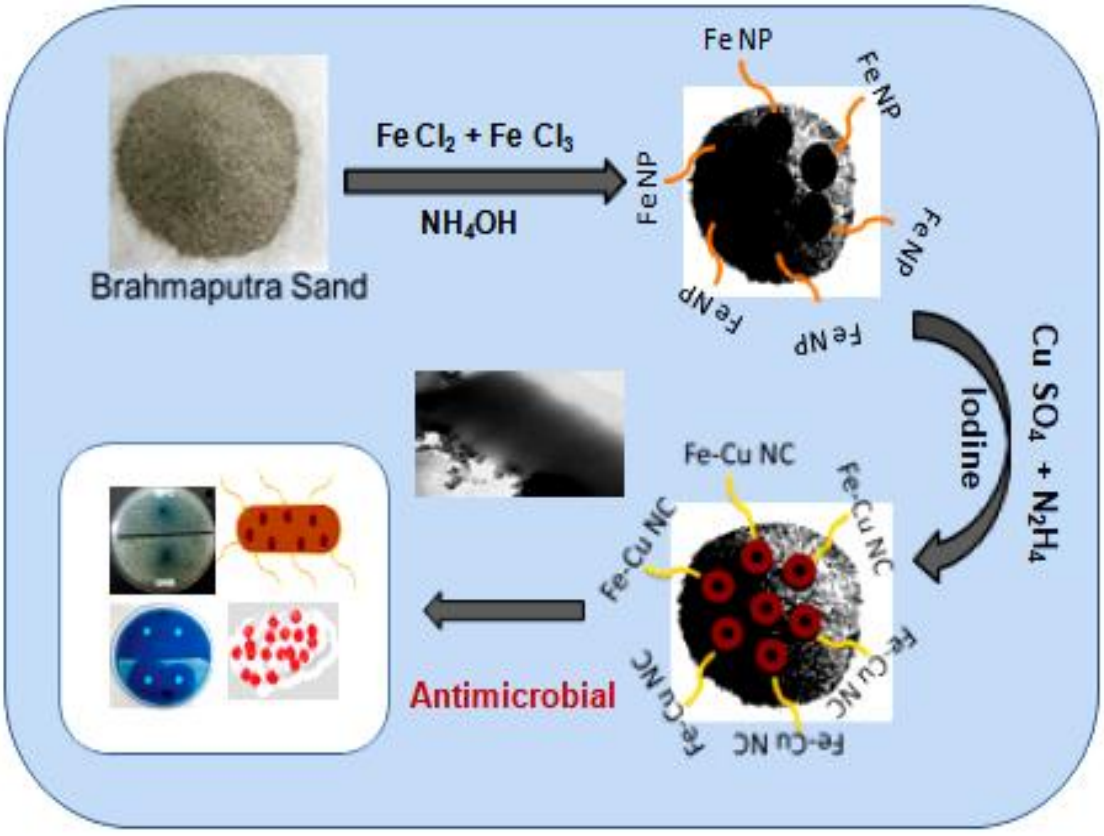

Figure 3.1. Schematic representation of Fe-Cu nanocomposite synthesized on surface of sand and their role in annihilation of clinical microbes.

Same procedures were repeated to prepare the nanocomposite after ball milling of sand. The nanocomposites prepared following ball milling of sand were of finer texture. (**Figure 3.2**)

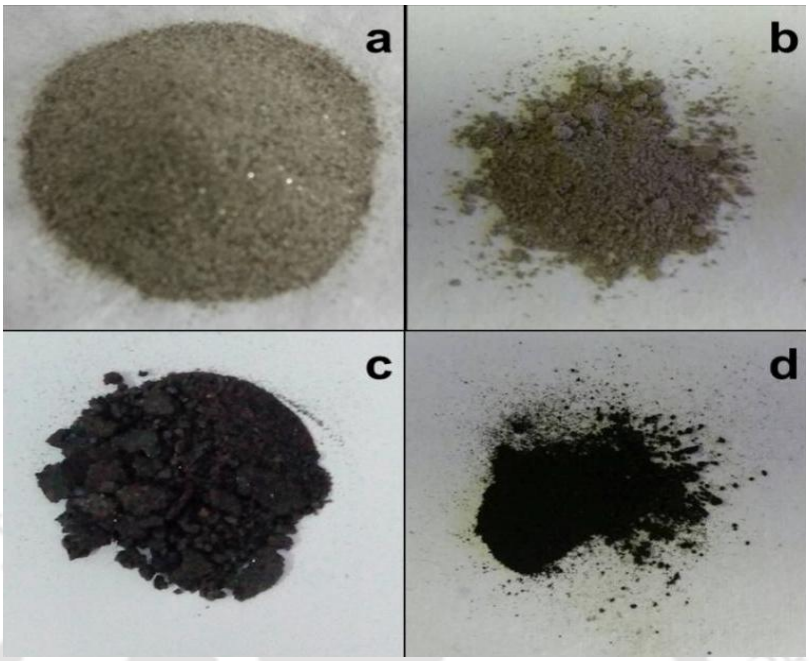

Figure 3.2. (a) Photograph of sand before and (b) after ball milling, (c) Photograph of sand−Fe−Cu nanocomposites prepared before and (d) after ball milling of sand.

Synthesis and presence of iron oxide NPs and copper oxide NPs in the nanocomposites was confirmed by TEM, which revealed formation of nanoparticles (**Figure 3.3a**). Distinct SAED patterns (**Figure 3.3b**) for iron oxide NPs and copper oxide NPs were observed with prominent rings. For Cu_2O, interplanar spacing values of 0.129 and 0.264 nm, respectively corresponding to 311 and 111 planes were observed. The values 0.200, 0.180, 0.12 and 0.109 nm, which correspond to 111, 200, 220 and 311 planes, respectively, were for Cu in cubic structures. Again, the lattice spacing of 0.211 and 0.171 nm indexed to 400 and 511 reflections were assigned for Fe_3O_4. The average particle size of the nanoparticles in the nanocomposites was found to be of 26.4 ± 4.7 nm as observed in particle size distribution histogram calculated from various images with the help of ImageJ software (**Figure 3.3c**). The TEM image of the nanocomposites prepared after ball milling of sand (**Figure 3.3d**) also confirmed the presence of iron oxide NPs and copper oxide NPs in the nanocomposites. The diffraction rings in SAED pattern (**Figure 3.3e**) with lattice spacing of 0.200(111), 0.123 (220) and 0.108 (311) were for Cu in cubic structures, whereas values of

0.128(311) and 0.196(112) nm were for Cu_2O and CuO, respectively. Again the lattice spacing of 0.301 and 0.171 nm indexed to 200 and 511 reflections were assigned to Fe_3O_4. The average particle size of the nanoparticles in the nanocomposites was found to be of 11.8 ± 1.6 nm as shown in particle size distribution graph (**Figure 3.3f**). These assignments are in agreement with the values available in literature.[36-38]

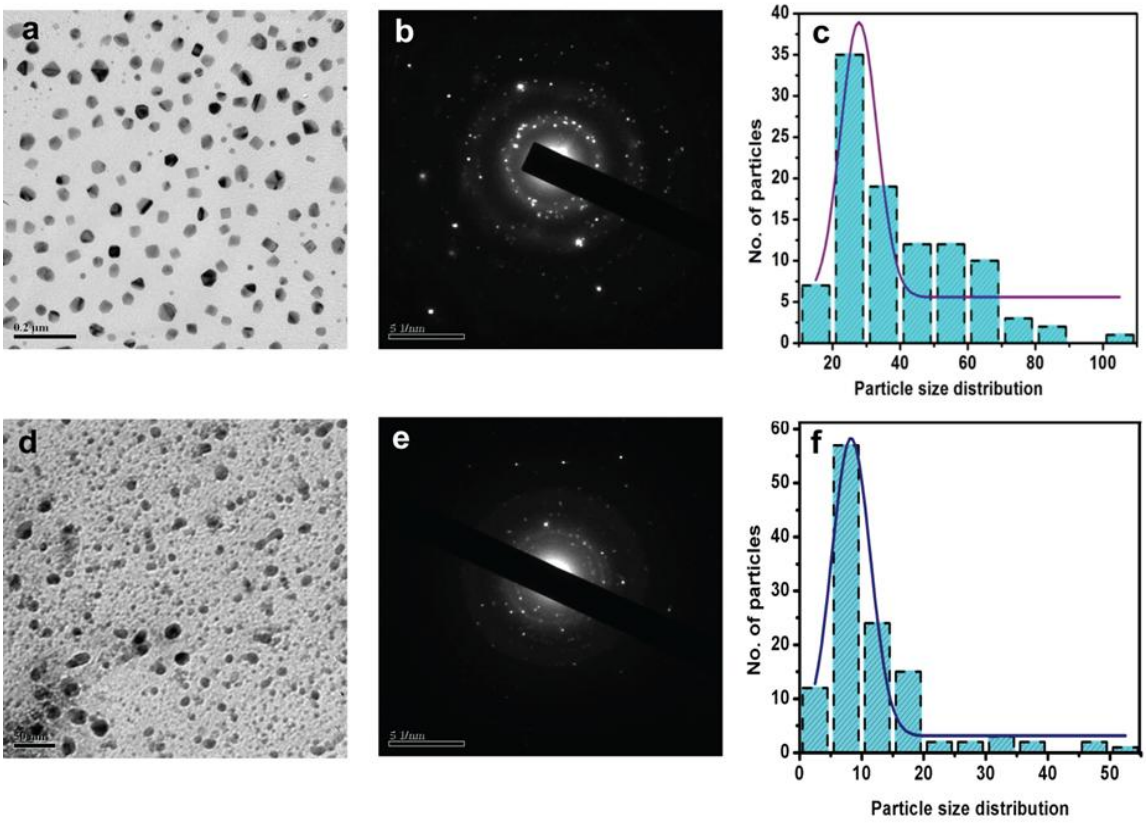

Figure 3.3. (a) TEM image of the Sand-Fe-Cu-nanocomposites prepared before ball milling of sand with (b) SAED pattern and (c) histogram showing particle size distribution, (d) TEM image of the Sand-Fe-Cu-nanocomposites prepared after ball milling of sand with (e) SAED pattern and (f) histogram showing particle size distribution.

Further, powder XRD was pursued on various samples, which also confirmed the presence Fe, Cu and sand in the prepared nanocomposites. XRD patterns of only sand (**Figure 3.4a**) showed diffractions at 2θ values of 21.0(100-Q), 25.7(002-K), 27(011-Q), 28.4 (002-A), 35.5 (201-K/131-I), 36.8 (110-Q/200-K), 39.7(131-K,111-Q),

42.8(200-Q), 46.1(201-Q), 50.5(112-Q), 55.2(204-K/240-K/022-Q), 59.96(121-Q) and 68.1(122-Q) degrees, indicating the presence of quartz(Q), kaolinite(K), illite(I) and albite(A).[39-42] The Sand-Fe-nanocomposites (**Figure 3.4b**), showed major characteristic peaks of iron oxide NPs (Fe_2O_3) at 2θ values of 33.2(104), 35.7(110), 49.49(024), 54.1(116), 62.5(214), 72.6(119) and 75.1 (220) degrees. Further, peaks at 30.2(220) and 56.9(511) indicated the formation of Fe_3O_4.[43-49] Peaks at 27.1(011), 36.5(110), 42.9(200) and 68.2(122) degrees suggested the presence of Quartz in the sample as well.[39-42] **Figure 3.4c**, corresponds to Sand-Fe-Cu-nanocomposites where peaks at 2θ values of 24.4(012), 33.12(104), 35.6(110), 39.9(006), 40.9(113), 63.9(300) and 69.2(208) degrees, confirmed the presence of iron oxide NPs (Fe_2O_3). Fe_3O_4NPs were validated by the peaks at 2θ values of 51.1(400) and 56.9(511).[43-49] At the same time, peaks for CuO and Cu_2O were observed at 2θ values of 35.6(002), 49.4 (200,) 53.9 (20-2), 61.3(113), 75.3(-222) and 30(110), 53.2(211), 61.3 (220), 72.9 (311) degrees, respectively.[50-51] Presence of quartz was confirmed by the peaks at 21.3 (100), 27.2 (011), 36.7 (110) and 59.2 (121) degrees.[39-42] Similarly, powder XRD conducted on the nanocomposites (prepared after ball milling of sand) also revealed the existence of Fe and Cu along with sand. The peaks showed in **Figure 3.4d**, with diffraction at 2θ values of 20.87(100-Q), 26.7(011-Q), 28.1 (002-A), 36.5 (110-Q/200-K), 39.4(111-Q/131-K), 42.6(200-Q), 50.15(112-Q), 55.5(204-K/240-K/022-Q), 59.96(121-Q), and 68.2(122-Q) degrees, indicated the presence of quartz(Q), kaolinite(K) and albite(A).[39-42] Following synthesis of Fe-Cu-nanocomposites on sand after ball milling (**Figure 3.4e**) XRD peaks at 2θ values of 32.48(104), 35.6(110), 39.71(006) and 72.1(119) degrees were observed, which suggested the formation of iron oxide (Fe_2O_3); and peaks for Fe_3O_4 were observed at 2θ values of 30.1(220), 51.95(400) and 57.2(511) degrees.[43-49] For CuO and Cu_2O, peaks were observed at 2θ values of 35.6(002), 36.14(11-1), 50.27(200), 53.57 (20-2) and 30.1(110), 62.72(220), 74.09 (311) degrees.[50-51] The presence of Quartz was indicated by peaks at 21.65(100), 26.75(011), 43.25(200) and 68.1(122) degrees.[39-42] Thus the TEM and XRD results confirmed the formation of iron oxide NPs and copper oxide NPs on sand. The validated nanocomposites were then tested for antimicrobial activity.

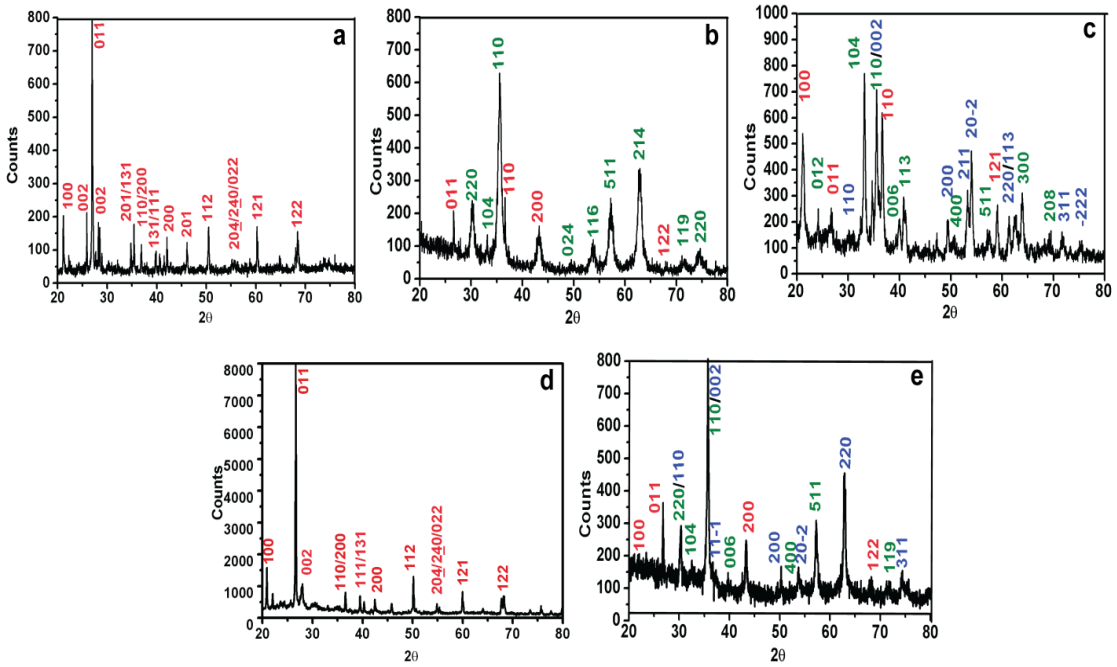

Figure 3.4. Powder XRD pattern of (a) Sand, (b) Sand-Fe-nanocomposites, (c) Sand-Fe-Cu-nanocomposites prepared before ball milling of sand and XRD pattern of (d) Sand, (e) Sand-Fe-Cu-nanocomposites prepared after ball milling of sand.

Afterwards field emission scanning electron microscopy (FESEM) was done which also supplemented the findings of TEM and XRD. The energy dispersion X-ray spectrum (EDX) was performed during FESEM analysis to see the element distribution of iron and copper on sand. As illustrated in **Figure 3.5b**, 16.3 % of copper and 37.3% of iron (in weight %) was found in Sand-Fe-Cu-nanocomposites that was prepared before ball milling of sand. The nanocomposites which were prepared after ball milling of sand contains 31.3% copper and 10.8% iron (in weight %) as shown in **Figure 3.5d**. Thus, the EDX spectrum confirmed the presence of both iron and copper on sand.

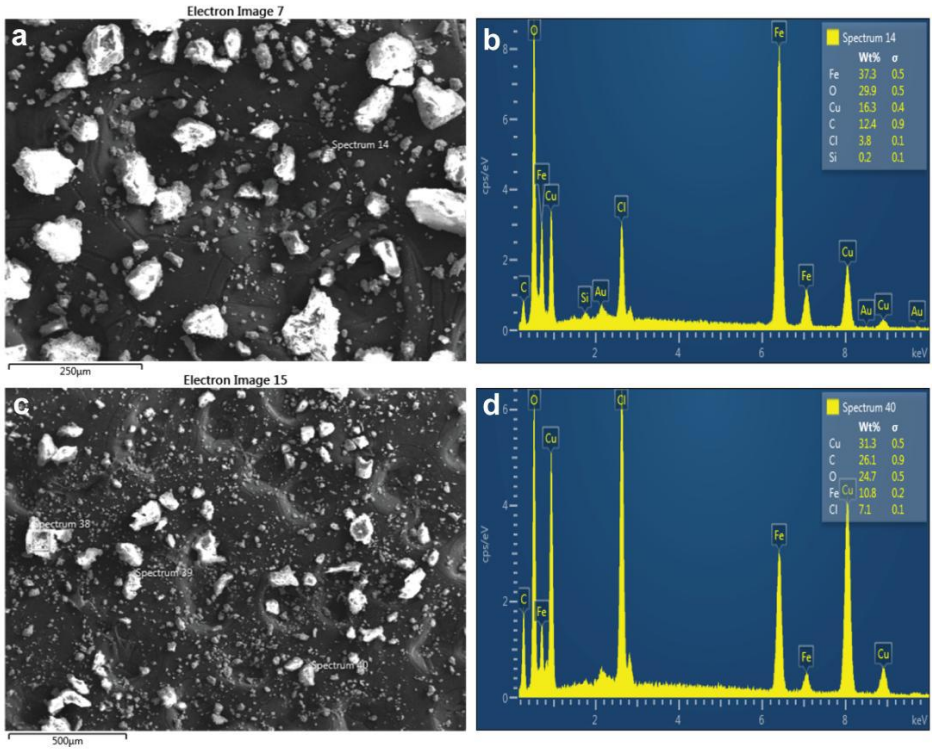

Figure 3.5. (a) FESEM image of sand−Fe−Cu nanocomposites prepared before ball milling of sand, (b) EDX showing element distribution, (c) FEFEM image of sand−Fe−Cu nanocomposites prepared after ball milling of sand and (d) EDX showing element distribution.

In vitro Studies of Antimicrobial Activity of the Sand-Fe-Cu-nanocomposites: As microorganisms are some of the predominant pollutants of water sources, therefore, development of effective treatment against microbes is of foremost interest. For this, the bactericidal activity of the as synthesized Sand-Fe-Cu-nanocomposites was determined on Gram positive *B. cereus* and Gram negative GFP-expressing *E. coli*, separately by both turbidity test and by Lawn culture method (**Figure 3.6**). Turbidity tests showed better result in Gram positive as compared to Gram negative bacteria. For determination of minimum inhibitory concentration (MIC) and minimum bactericidal concentration (MBC), 1 $\times 10^6$ CFU/mL of Gram positive as well as Gram negative bacteria were inoculated in peptone and incubated overnight at 37 °C along with the composite at varying concentrations. The minimum concentration of the composite at which microbial growth was noticeably inhibited (i.e., no visible turbidity) was considered as the MIC value. The cultures that were not turbid were re-inoculated in

peptone. The MBC of the composite was considered to be the minimum concentration of the composite that prevented growth of the bacterial cells following re-inoculation, as observed visually by the lack of turbidity (after 12 h). The MIC values were found to be 10.6 µg/mL and 13.8 µg/mL of copper for Gram positive and Gram negative bacteria, respectively, whereas MBC values were found to be 15.9 µg/mL and 21.2 µg/mL of copper for Gram positive and Gram negative bacteria, respectively.

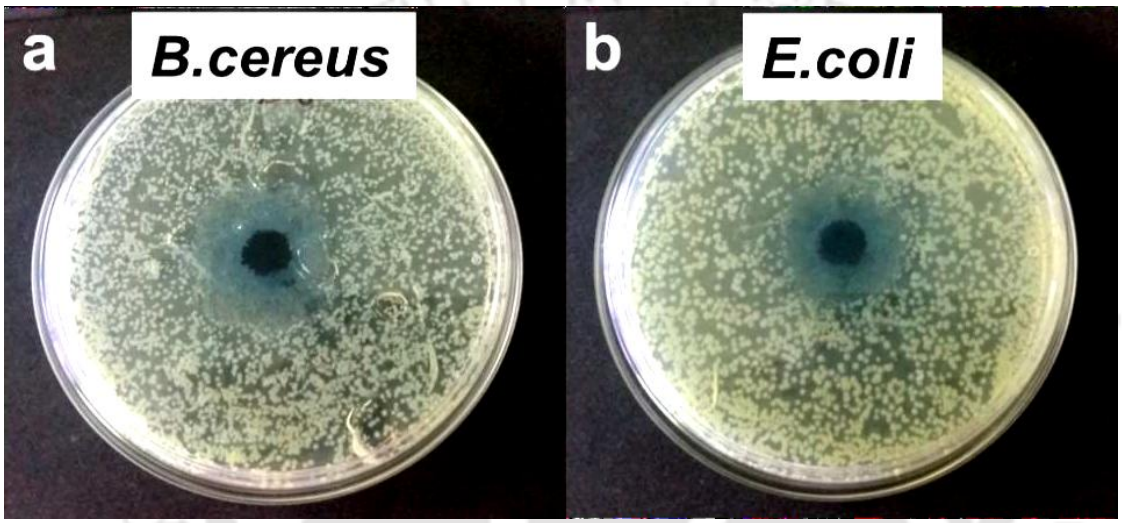

Figure 3.6. Antibacterial activity of the sand−Fe−Cu nanocomposites on Gram positive *B. cereus* (a) and Gram negative *E. coli* (b) as tested using Nutrient agar plate with the nanocomposites in the center of the plate.

Further, similar concentrations were used to find the antibacterial activity on different species of microorganisms isolated from various patients' samples collected from patients attending Guwahati Neurological Research Center (GNRC) Medical Outdoor Clinic or admitted there for treatment. For this, 15 mg of the composites for Gram Positive Cocci (GPC) and 20 mg for Gram Negative Bacilli (GNB) were used, which correspond to 15.9 µg and 21.2 µg of copper respectively along with traditionally used antibiotic discs. As is evident in **Figure 3.7 a-f**, clear zone of bacterial growth inhibition was observed around the Sand-Fe-Cu- nanocomposites along with some of the antibiotic discs in all the tested samples, the details of which

are illustrated in **Table 1**. In case of methicillin resistant *S. aureus* (MRSA), almost all the antibiotic discs were unable to arrest its growth as evident by the visible opacity around the antibiotic discs (**Figure 3.7b**). But the prepared nanocomposites were effective in arresting the growth of both methicillin sensitive and resistant strain of bacteria. Similar experiments were carried out for fungus (*Candida albicans*) also, where 20 mg of composites inhibited the growth and clear zone of inhibition was observed (**Figure 3.7g**). Thus the *in vitro* antimicrobial results supported the use of nanocomposites as a broad spectrum antimicrobial agent that can also arrest the growth of multi drug resistant strains.

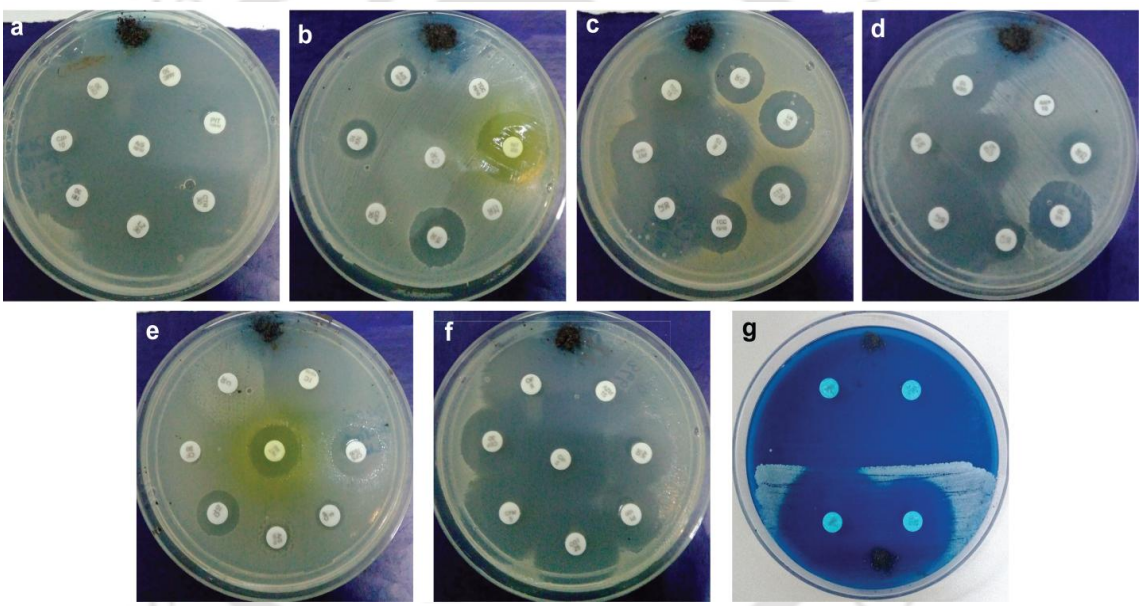

Figure 3.7. Antimicrobial activity of the nanocomposites tested on the patients' samples (mentioned on **Table 1**) along with different antibiotic discs traditionally used in medical microbiology lab where Figure (a) shows inhibition of growth of methicillin sensitive *S. aureus*, Figure (b-d) shows inhibition of growth of methicillin resistant *S. aureus* isolated from urine, blood & wound swab; Figure (e & f) shows inhibition of growth of *E. coli* & *K. pneumoniae* isolated from urine & pus, respectively; (g) Antimicrobial activity of the nanocomposites on Candida Sp. isolated from urine specimen of a patient.

Table 1. Showing the patient details with their clinical history and investigation findings, which indicated that the patients had microbial infections:

Cs No	Pt Details	Clinical History	Investigation Findings	C/S Report
a	6days M	Premature baby with hypoglycemic seizure	Blood C/S: Growth of *Staph. aureus* (MSSA)	Resistant to : Nil Sensitive to: Amp+Clav, Ampi, Ampi+Sul, Cefaclor, Cefazolin, Cephalothin, Chloram, Cipro, Clinda, Tetra, Lizolid, Netilmycin, Pip+Tazo, Teicoplanin, Tetra.
b	67yrs M	Low grade fever-5days	Urine C/S: Growth of *Staph. aureus* (MRSA)	Resistant to: Ampi, Ampi-Sul, Cefaclor, Cefazolin, Ceftriaxone, Cephalothin, Cipro, Genta, NorfloxTicar-Clav. Sensitive to: Chloram, Lizolid Nitrofurantoin, Teicoplan, Vanco.
c	28yrs M	Non healing ulcer	Wound Swab C/S: Growth of *Staph. aureus* (MRSA)	Resistant To: Chloram, Amik, Ampi+Sul, Cefoperazone+Sulb, Oflox. Sensitive to: Teicoplanin, Vanco, Erythro, Pip+Tazo, Ticarcillin, Cefotaxime, Linezolid, Tige.
d	35 M	Fever and burning micturition	Urine C/S Growth of *S.aureus* (MRSA)	Resistant to: Ampi, Ampi-Sul, Cefaclor, Cefazolin, Ceftriaxone, Cephalothin, Cipro, Ticar-Clav. Sensitive to: Chloram, Genta, Lizolid Nitrofurantoin, Teicoplan, Vanco.
e	35 yrs F	Dysuria, frequency	Urine C/S: Growth of *E.coli*	Resistant to: Ampi, Ampi-Sul, Cefaclor, Cefixime, Cefodoxime, Ceftazidime, Chloram, Cipro, Co-Tri, Norflox. Sensitive to: Amikacin, Colis, Imepenem-Cilastatin, Nitrofurantoin.
f	63yrs M	Foul smelling discharge/anus Admitted for infected fissure	TC-18700, ESR-80, RBS-524, Urea-93, Creat-3.0. Pus C/S: growth of *Klesb.Pneumoniae*	Resistant to: Ampi, Cefixime, Cefodoxime, Clindamycin. Sensitive to: Amikacin, cefoperazone. Cipro, Co-Tri, Ertapenem, Colistin, Ertapenem, Oflox.
g	23yrs F	Ureteric Colic	Urine R/E: Numerous pus cells, RBC:5-6/HPF Urine C/S: Growth of *Candida Sp.*	Sensitive to: Fluconazole, Voriconazole

Abbreviations: cfu- colony forming unit, Cs- case, Pt- patient, C/S- culture & sensitivity, UTI- urinary tract infection, Hb- haemoglobin, TRBC- total red blood cells, MSSA- methicillin sensitive *Staphylococcus aureus*, MRSA- methicillin resistant *Staphylococcus aureus*, TC- total cell count, ESR- erythrocyte sedimentation rate, RBS- random blood sugar, creat- creatinine, RBC- red blood cells, hpf- high power field.

Similarly, the antimicrobial property of the Sand-Fe-Cu-nanocomposites synthesized after ball milling of sand was determined on methicillin sensitive and methicillin resistant *S. aureus* (GPC) and Gram negative Bacilli (GNB), *E. coli* and *K. pneumoniae*. As is evident in **Figure 3.8**, the nanocomposites that was synthesized after ball milling of the sand, was also effective as an antimicrobial agent against both methicillin sensitive *S. aureus* (MSSA) as shown in **Figure 3.8a** (top) and methicillin resistant *S. aureus* (MRSA) as evident from **Figure 3.8b** (top) as well as Gram negative bacteria *E. coli* (**Figure 3.8a**- bottom) and *K. pneumoniae* (**Figure 3.8b**-bottom).

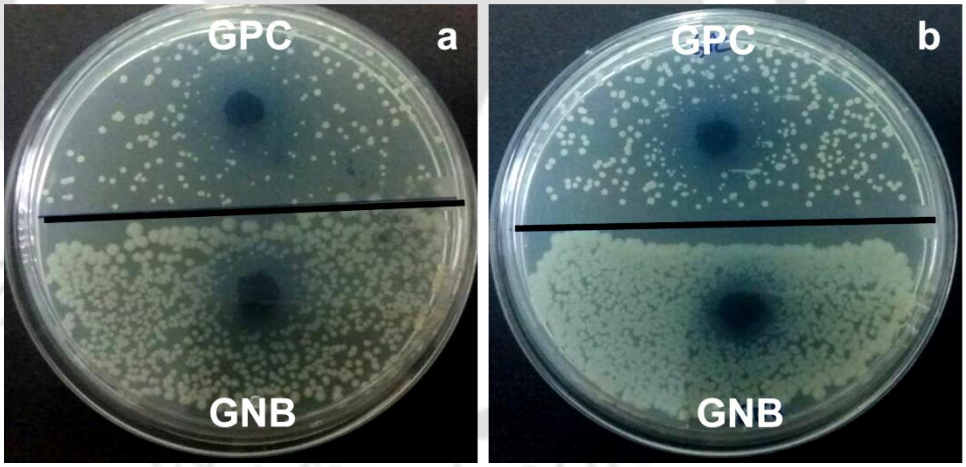

Figure 3.8. Antimicrobial activity of the nanocomposites (synthesized after ball milling of sand) tested on (a-top) Gram positive cocci- methicillin sensitive *S. aureus* (MSSA) and (a-bottom) Gram negative bacilli- (*E. coli*) (b-top), Gram positive cocci- methicillin resistant *S. aureus* (MRSA) and (b-bottom) Gram negative bacilli- *K. pneumoniae* isolated from urine and pus, respectively.

To find out the mechanism of cell death, FACS based assays of the treated samples were carried out with propidium iodide (PI) staining method. The results of the FACS analysis revealed that bacterial cells after treatment with MIC dose of

Sand-Fe-Cu-nanocomposites for 6 h, showed a gradual shift of population from viable (LR) to compromised (UR) with cell population of 28.97% and 43.58%, respectively (**Figure 3.9f**). On the other hand, population of lysed (LL) and dead cells (UL) were found to be 19.14% and 8.31%, respectively, whereas only 9.45% of lysed (LL) cells were observed in the control bacteria without any % of dead cells (UL) as depicted in **Figure 3.9b**. Parallel to this, all the samples of the control groups treated with copper solution; Sand-Fe-nanocomposites and Sand-Cu-nanocomposites were also tested for their efficacy. Interestingly, it was observed that Sand-Cu-nanocomposites treated samples also exhibited similar results, where the percentage of compromised cells (UR) were 47.26 and that of dead cells (UL) were 7.66 (**Figure 3.9e**). Copper solution and Sand-Fe-nanocomposites treated samples revealed much less % of compromised cells (UR) i.e., 7.76 and 2.8 with dead cells (UL) population of only 0.91% and 0.22%, respectively (**Figure 3.9c and 3.9d**). Results are enumerated in **Table 2**. These results indicated the probable role of CuNP as an effective antimicrobial agent with high rate of efficacy and thus can be a potent microbial exterminator.

Table 2. Percentage of total bacteria at their different viability stages, untreated and treated with different nanocomposites at concentration of MIC as measured by flow cytometry.

Different population of cells	Untreated Cells	Treated with Copper Solution	Treated with Sand-Fe-nanocomposites	Treated with Sand-Cu-nanocomposites	Treated with sand-Fe-Cu-nanocomposites
Dead cells (UL)	0%	0.91%	0.22%	7.66%	8.31%
Compromised cells (UR)	0.11%	7.76%	2.8%	47.26%	43.58%
Lysed cells (LL)	9.45%	27.85%	21.21%	12.04%	19.14%
Live cells (LR)	90.43%	63.47%	75.77%	33.04%	28.97%

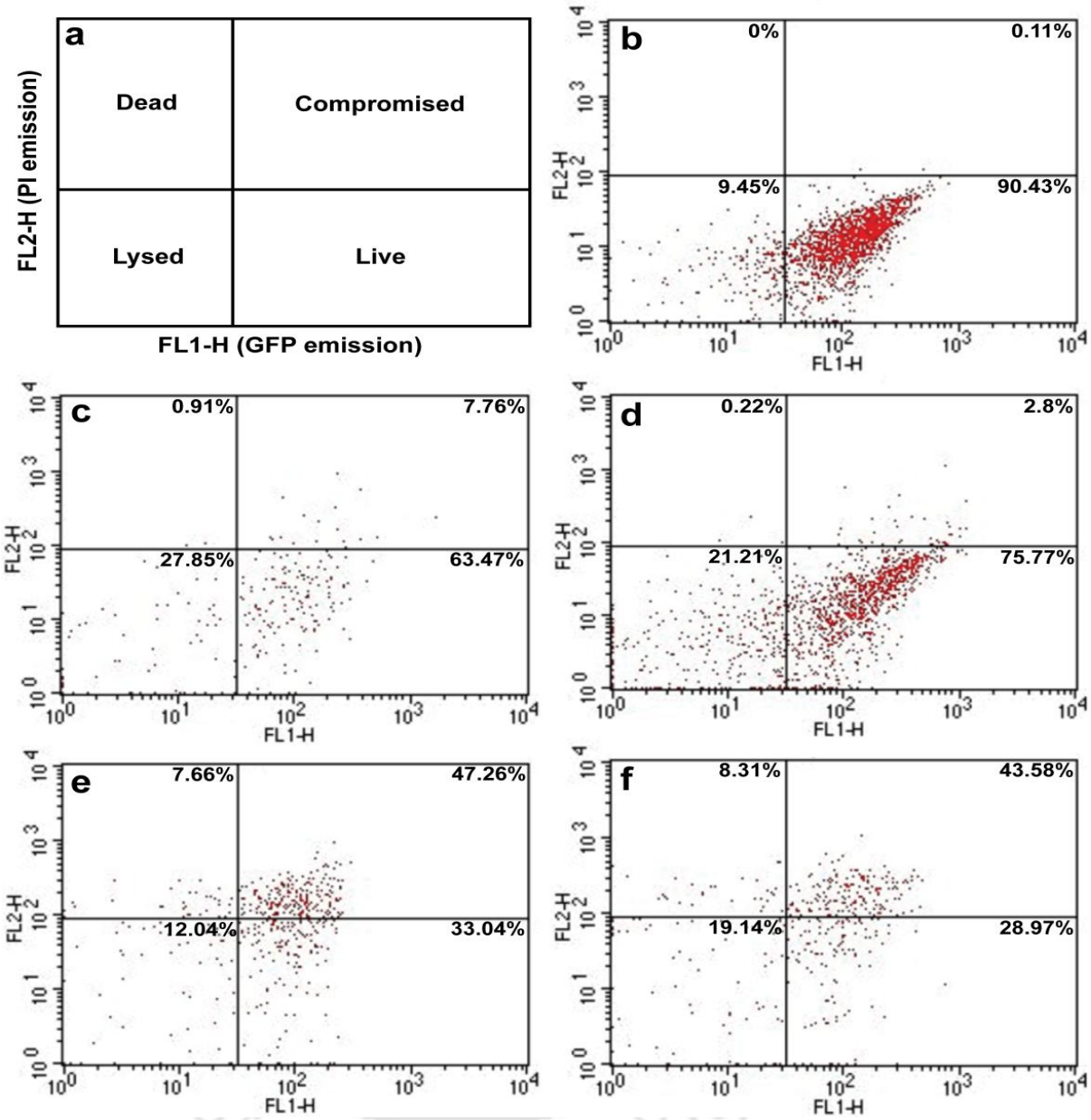

Figure 3.9. Dot plots showing populations of *E. coli* cells (GFP expressing stained with PI) at different viability stages, measured by flow cytometer. (a) Schematic representation of the dot plots showing different bacterial cell viability stages, (b) represents untreated bacterial cells (control), followed by bacterial cell populations following treatment with MIC dose of (c) copper solution, (d) Sand-Fe-nanocomposites, (e) Sand-Cu-nanocomposites and (f) Sand-Fe-Cu-nanocomposites.

Interaction of the nanocomposites with the bacterial cell wall was further examined with the help of TEM. The TEM images of the nanocomposites treated bacteria showed the attachment of the nanoparticles on the surface of bacteria (**Figure 3.10a-b**). As evident in **Figure 3.10c-d**, there were prominent penetration of particles inside the bacteria and thus it highlighted the role of composite nanoparticles in cell wall damage and eventually towards death as damaged cell wall causing leakage of intracellular proteins and other constituents leading to cell death has been already reported.[21] Whereas in case of untreated bacteria (**Figure 3.10e & f**) uniform texture with preserved morphology was noticed along with clean and clear magnified image (**Figure 3.10g**) without any embedded particles.

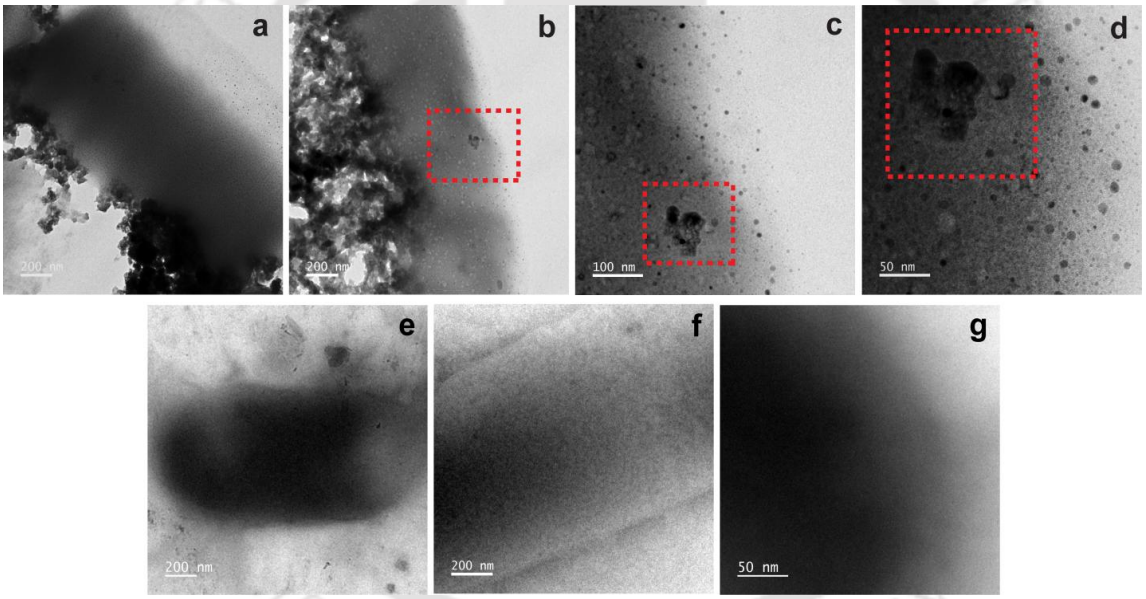

Figure 3.10. TEM image of (a-d) nanocomposites (MIC) treated bacteria and (e-g) control bacteria. Red marked portions indicate nanocomposites attachment on the bacterial cell wall.

As copper NPs are reported to be unstable and are prone to be oxidized,[23] stability of the prepared nanocomposites was checked on *B. Cereus* (MTCC 1305 strain) and GFP expressing *E. coli* (MTCC 433 strain) for their long term use. It was observed that the bacterial growth was equally arrested in presence of the nanocomposites irrespective of their time of preparation (**Figure 3.11**). It has already

been documented that the stability of copper oxide NPs was enhanced in the presence of molecular iodine.[21]

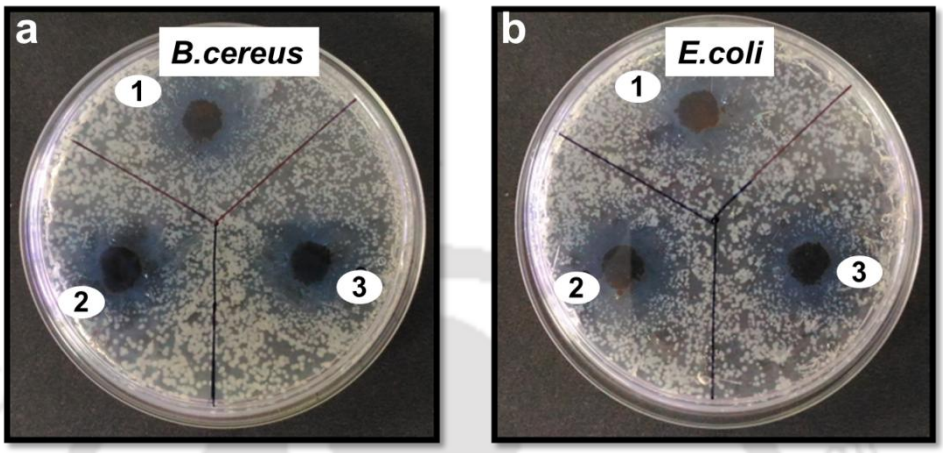

Figure 3.11. Plates with growth of both Gram positive *B.cereus* and (a) Gram negative *E.coli*, (b) showing zone of inhibition around (1) freshly prepared, (2) 2 months' old and (3) 3 months' old Sand-Fe-Cu-nanocomposites.

The antibacterial efficacies of Sand-Fe-nanocomposites and Sand-Cu-nanocomposites were also tested separately and described as control experiments. (**Figure 3.12**). There were clear zones of inhibition of bacterial growth around Sand-Cu-NP and Sand-Fe-Cu-nanocomposites on both the plates containing GPC & GNB but no zone of inhibition around copper solution and Sand-Fe-NP, thus establishing the role of CuNP as antibacterial agent. The antibacterial activity of molecular iodine was not examined separately as it has been documented that molecular iodine alone at a concentration that had been used in the study exhibited minimal bactericidal properties in comparison to that of the Sand-Fe-Cu-nanocomposites.[21]

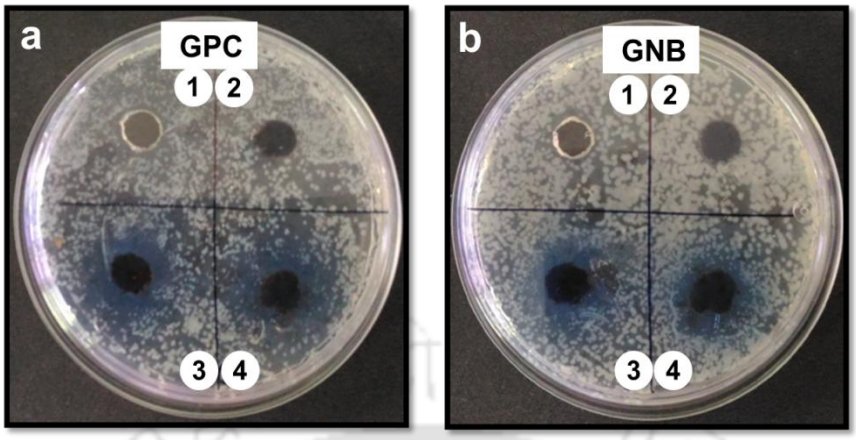

Figure 3.12. Photograph of plates representing the results of control experiments on both GPC (a) and GNB (b), where 1-copper solution, 2-Sand-Fe-nanocomposites, 3- Sand-Cu-nanocomposites and 4-Sand-Fe-Cu-nanocomposites.

3.6. Conclusion

A co-precipitation as well as chemical reduction method was used to prepare Fe-Cu bimetallic nanocomposites on sand in aqueous medium under normal environmental conditions. From the results obtained, it was evident that "Sand-Fe-Cu-nanocomposites" as such or prepared after ball milling of sand was an effective microorganism exterminator that exhibited a strong antimicrobial activity against a wide range of microbes including multidrug resistant bacteria and also fungus that are mostly clinical isolates. The particle size of the nanocomposites was decreased to 11.8 ± 1.6 nm after ball milling of sand. Such investigations attribute development of new "Sand-Fe-Cu-nanocomposites" having potential for multifaceted applications.

3.7. References

1. Mudur, G. *BMJ*. **2003**, *326*(7402), 1284.
2. Baptista, P. V., McCusker, M. P., Carvalho, A., Ferreira, D. A., Mohan, N. M., Martins, M., & Fernandes, A. R. *Front.Microbiol.*, **2018**, *9*, 1441.
3. Hemeg, H. A. *International Journal of Nanomedicine*, **2017**, *12*, 8211–8225.
4. Morones, J. R.; Elechiguerra, J. L.; Camacho A. et al., *Nanotechnology*, **2005**, *16*(10), 2346–2353.

5. Conde, J.; de la Fuente, JM; Baptista, PV. *Front.Pharmacol*. **2013**, *4*(134).

6. Banoee, M.; Seif, S.; Nazari, Z. E.; Jafari-Fesharaki, P.; Shahverdi, H. R.; et al. *J Biomed Mater Res B Appl Biomater*, **2010**, *93* (2), 557–61.

7. Seil, J.T.; Webster TJ. *Int J Nanomedicine*, **2012**, *7*, 2767–81.

8. Borzabadi-Farahani, A.; Borzabadi E; Lynch E.. *Acta Odontol Scand*. **2013**, *72* (6), 413–417.

9. AshaRani, P. V.; Mun, G. L. K.; Hande, M. P.; Valiyaveettil, S. *ACS Nano,* **2009**, *3*(2), 279–290.

10. Park, M.V.D.Z.; Neigh, A.M.; Vermeulenet J.P. et al. *Biomaterials*, **2011**, *32*(36), 9810–9817.

11. Cady, N. C.; Behnke, J. L.; Strickland, A. D. *Adv. Funct. Mater.* **2011**, *21* (13), 2506−2514.

12. Turnlund, J. R.. *Am. J. Clin. Nutr*. **1998**, *67* (5), 960S−964S.

13. Theivasanthi, T.; Alagar, M. *Ann. Biol. Res.* **2011**, *2* (3), 368−373.

14. Jia, B.; Mei, Y.; Cheng, L.; Zhou, J.; Zhang, L. *ACS Appl. Mater. Interfaces*, **2012**, *4* (6), 2897−2902.

15. Ren, G.; Hu, D.; Cheng, E. W. C.; Vargas-reus, M. A.; Reip, P.; Allaker, R. P. *Int. J. Antimicrob. Agents*, **2009**, *33*, 587−590.

16. Yoon, K. Y.; Hoon Byeon, J.; Park, J. H.; Hwang, J. *Sci. Total Environ*. **2007**, *373* (2−3), 572−575.

17. Perdikaki, A.; Galeou, A.; Pilatos, G.; Karatasios, I.; Kanellopoulos, N. K.; Prombona, A.; Karanikolos, G. N. *ACS Appl. Mater. Interfaces*, **2016**, *8* (41), 27498−27510.

18. Mahmoodi, S.; Elmi, A.; Hallaj-nezhadi, S. *J. Mol. Pharm. Org. Process Res.* **2018**, *6* (1), 1−7.

19. Santo, C. E.; Taudte, N.; Nies, D. H.; Grass, G. *Appl. Environ. Microbiol*. **2008**, *74* (4), 977−986.

20. Rtimi, S.; Konstantinidis, S.; Britun, N.; Bensimon, M.; Khmel, I.; Nadtochenko, V. Appl. *Catal. B*, **2018**, *239* (30), 245−253.

21. Mallick, S.; Sharma, S.; Banerjee, M.; Ghosh, S. S.; Chattopadhyay, A.; Paul, A. *ACS Appl.Mater. Interfaces*, **2012**, *4* (3), 1313−1323.

22. Rtimi, S.; Nadtochenko, V.; Khmel, I.; Bensimon, M.; Kiwi, J. *Mater. Today*. **2017**, *6*, 62−74.
23. Soomro, R. A.; Sherazi, S.T. H. et al. *Adv. Mat. Lett*. **2014**, *5*(4), 191-198.
24. Gawande, M. B.; Goswami, A.; Felpin, F.-X.; Asefa, T.; Huang, X.; Silva, R.; Varma, R. S. *Chemical Reviews,* **2016**, *116* (6), 3722–3811.
25. Shelke, S. N.; Bankar, S. R.; Mhaske, G. R.; Kadam, S. S.; Murade, D. K.; et.al. *ACS Sustainable Chem. Eng*. **2014**, *2*, 1699−1706.
26. Scotti, N.; Dangate, M.; Gervasini, A.; Evangelisti, C.; Ravasio, N.; Zaccheria, F. *ACS Catal.* **2014**, *4*, 2818−2826.
27. Shim, I. W.; Noh, W. T.; Kwon, J.; Cho, J. Y.; Kim, K. S.; Kang, D. H. *Bull. Korean Chem. Soc*. **2002**, *23*, 563−566.
28. Taner, M.; Sayar, N.; Yulug, I. G.; Suzer, S. *J. Mater. Chem*. **2011**, *21*, 13150−13154.
29. Eremenko, A. M.; Petrik, I. S.; Smirnova, N. P.; Rudenko, A. V.; Marikvas, Y. S. *Nanoscale Res. Lett*. **2016**, *11* (28), 1−9.
30. Xiong, Z.; Yuan, D.; Yang, P.; Lai, B. *J. Taiwan Inst. Chem. Eng*. **2017**, *80*, 669−677.
31. Mody, V.; Siwale, R.; Singh, A.; Mody, H. *J. Pharm. Bioallied Sci.,* **2010**, *2*(4), 282.
32. Ansari, S. A. M. K.; Ficiarà, E.; Ruffinatti, F. Al.; Stura, I.; Argenziano, M.; et.al. *Materials*, **2019**, *12*, 465.
33. Ali, A.; Zafar, H.; Zia, M.; Ul Haq, I.; Phull, A.R.; Ali, J.S.; Hussain, A. *Nanotechnol. Sci. Appl.* **2016**, *9*, 49–67.
34. Kandpal, N.; Sah, N.; Loshali, R.; Joshi, R.; Prasad, J. *J. Sci. Ind. Res*. **2014**, *73*, 87−90.
35. Peternele, W.; Monge Fuentes, V.; Fascineli, M. L.; Rodrigues Da Silva, J.; Silva, R.; Lucci, C.; Bentes De Azevedo, R. *J. Nanomater*. **2014**, *94* (1), 1−10.
36. Gholinejad, M.; Saadati, F.; Shaybanizadeh, S.; Pullithadathil, B. *RSC Adv*. **2016**, *6* (6), 4983−4991.
37. Kozak, D. S.; Sergiienko, R. A.; Shibata, E.; Iizuka, A.;Nakamura, T. Sci.Rep. **2016**, *6*, 1−9.

38. Knappett, B. R.; Abdulkin, P.; Ringe, E.; Jefferson, D. A.; Lozano-Perez, S.; Rojas, T. C.; Fernández, A.; Wheatley, A. E. H. *Nanoscale*, **2013**, *5* (13), 5765.
39. Anbalagan, G.; Prabakaran, A. R.; Gunasekaran, S. *J. Appl. Spectrosc*. **2010**, *77* (1), 86−94.
40. Fernandez, R.; Martirena, F.; Scrivener, K. L. *Cem. Concr. Res*. **2011**, *41* (1), 113−122.
41. Wei, S.; Tan, W.; Zhao, W.; Yu, Y.; Liu, F.; Koopal, L. K. *Soil Sci. Soc. Am. J*. **2012**, *76* (2), 389.
42. Beddiaf, S.; Chihi, S.; Leghrieb, Y. *J. Afr. Earth Sci*. **2015**, *106*, 129−133.
43. Blanco-Andujar, C.; Ortega, D.; Pankhurst, Q. A.; Thanh, N. T. K. *J. Mater. Chem*. **2012**, *22*(25), 12498.
44. Morris, M. C.; McMurdie, H. F.; Evans, E. H.; Paretzkin, B.; Parker, H. S.; Panagiotopoulos, N. C.; Hubbard, C. R. U.S. Department of Commerce, NBS: Washington, D.C., **1981**; Vol. 37.
45. Salem, N. M.; Awwad, A. M. *Nanosci. Nanotechnol*. **2013**, *3*(3), 35−39.
46. Sukumar, U. K.; Gopinath, P. *RSC Adv*. **2016**, *6* (52), 46186−46201.
47. Zhuang, L.; Zhang, W.; Zhao, Y.; Shen, H.; Lin, H.; Liang, *J.Sci. Rep*. **2015**, *5*, 1−6.
48. Wei, H.; Hu, D.; Su, J.; Li, K. *Chin. J. Chem. Eng*. **2015**, *23* (1), 296−302.
49. Yu, X.; Cheng, G.; Zheng, S. Y. *Sci. Rep*. **2016**, *6*, 1−11.
50. Jia, B.; Qin, M.; Zhang, Z.; Cao, Z.; Wu, H.; Chen, P.; Zhang, L.; Lu, X.; Qu, X. *Cryst Eng Comm*. **2016**, *18* (8), 1376−1383.
51. Meghana, S.; Kabra, P.; Chakraborty, S.; Padmavathy, N. *RSC Adv*. **2015**, *5* (16), 12293−12299.

CHAPTER-4

Fabrication of a Hand Held Filtration Device Utilizing Sand-Fe-Cu Nanocomposite for Point-of-Use Water Filtration

Chapter 4, Potential role of as synthesized Sand-Fe-Cu-nanocomposites in purification of water has been reported. A hand held water filtration device was fabricated utilizing sand-Fe-Cu nanocomposite for point of use water filtration. A wide range of microbes responsible for waterborne diseases along with several hazardous metals were tested to ensure its filtration ability.

(Chapter 3 and 4 are merged to file an Indian patent and the combined manuscript is published)

Indian Patent Application No. 201831016639 dated May 2, 2018
https://pubs.acs.org. DOI: 10.1021/acsabm.8b00572

CHAPTER -4

4.1. Introduction

With the advent of nanoscale science and engineering, new ways of designing cost effective and biocompatible device for treatment of water have surfaced. Preference for nanomaterials are largely in part due to their large surface area, strong adsorption capacity and high reactivity.[1] According to World Health Organization (WHO) recommendation, in any 100 mL of drinking water, fecal and total coliform counts should be zero.[2] The major contaminant affecting drinking water is microorganism and removal of pathogenic microorganism is the most important step in the treatment of waste water.[2,3] A variety of techniques have earlier been used for purification of water but research is still under process with respect to combinations of different techniques to ensure availability of quality drinking water to the mass at an affordable cost.[3,4] Recently, different nanomaterials have elicited extensive research interest in the treatment of polluted water but in-spite of their promising capability several flaws have limited their utility.[1,2,4-8] In order to overcome all these shortcomings fabrication of nanocomposites is considered as a standard effective approach for water treatment.[1]

Lately, use of bimetallic nanocomposites having magnetic property has attracted increasing attention, as it exhibits superior performance compared to all other materials tested. It offers an added advantage in removal of organic contaminants.[9-13] A number of studies have been done on iron oxide nanoparticles to remove heavy metals from water. FDA (US Food and Drug Administration) also approved its use in the process of water purification.[14] Use of iron oxide nanoparticle is advantageous as it can be easily regenerated.[1,5,15-18]AgNPs are also well studied to treat waste water.[3] But report establishes that AgNPs can cause cytotoxicity and genotoxicity in human cells.[19,20] Copper can be seen as a replacement on the merit of its affordability, availability and properties similar to that of other metallic NPs. It is also a natural constituent of living

tissues and human body can resist copper toxicity to some extent.[21,22] In addition to that it has also been approved by EPA (US Environmental Protection Agency).[23] At the same time Cu NPs are known to have bactericidal effects against single strains of *E. coli*, *B. subtilis*, *Vibrio cholera*, *Pseudomonas aeruginosa*, *Syphilis*, *Typhus*, and *Staphylococcus aureus*.[24-30]

Many theories are available explaining the mechanism of antimicrobial role of Cu NPs, which has been already discussed in **Chapter 3**. Though there are many reports of effective antimicrobial property of copper, the potential utility of copper in waste water treatment is yet to be explored in detail. There is a report on *in situ* preparation of Cu NPs in cellulosic blotter paper for point-of-use water purification for killing bacteria. But possibility of clogging of the filter paper by high turbidity in water sources could limit its utility.[31]

Looking at the potential role of sand, iron and copper in purification of water, we intended to fabricate a hand held filtration device incorporating the as synthesized sand-Fe-Cu nanocomposite (discussed in **Chapter 3**) for point of use water filtration. Bimetallic Fe-Cu particles were used to treat highly toxic and refractory aromatic pollutant present in industrial sewage. Findings of the some previous studies ascertained that the catalytic reactivity and pollutant degradation capacity of bimetallic Fe-Cu particles are much higher than those of the individual components. It has also been demonstrated that pollutant removal capacity of the Fe-Cu bimetallic system can be augmented by combining some other ingredients such as nitrogen, oxygen, hydrogen peroxide, per-sulfate, ozone to it.[32,33] Iron-copper bimetallic particles can act as electrochemical cell to promote pollutant removal capacity.[34] The use of sand as an inert scalar substance offers a cost effective method of water purification. Although sand has been the prime source of water purification since ages, it does not have antimicrobial property. Moreover, very less work has been carried out by incorporating it with nanomaterials for its application. A report describing removal of bacteria and metals using iron-manganese bimetallic nanoparticles oxide coated on sand is available.[35] The present work is intended to exploit the therapeutic potential of both the metals and sand for filtration of microbes and metals and thus rendering purified water

at an affordable cost. For that, a portable filtration unit was devised holding the nanocomposites in the middle of two falcon tubes with the help of sponge. As removal of pathogenic microorganism is the most important step of water filtration, the prepared nanocomposites was first tested to filter a wide range of microbes that are known to cause waterborne diseases. These microbes were isolated from varied biological specimens of different patients' of Guwahati Neurological Research Center (GNRC) Medical Hospital, Guwahati. On confirmation of its microbial annihilation capacity, different hazardous metals were then effectively filtered through the portable device.

4.2. Outline of the Present Work

Herein, a hand held portable filtration device was fabricated exploiting the therapeutic potential of all the three key ingredients (iron, copper and sand) of the as synthesized nanocomposites for the purpose of point of use water filtration. It was tested on a wide range bacteria like *Acinetobacter baumannii, Escherichia coli, Salmonella typhi, Bacteroides fragilis, Salmonella paratyphi, Shigella dysenteriae*, and *Enterococcus faecalis*, which are predominantly responsible for waterborne diseases. Further, it was also tested on hazardous metals like nickel, zinc, and lead. Leaching of copper and iron from the nanocomposites was within the permissible limit as per Bureau of Indian Standards (BIS) for Drinking Water (IS-10500-2012, second revision) as well as the International Standards for Drinking Water.

4.3. Experimental Section

4.3.1. Materials

Materials used for synthesis of Sand-Fe-Cu nanocomposite were discussed in **Chapter 3**. Nickel chloride, lead acetate and zinc chloride powder used for the experiment were purchased from Sigma Aldrich chemical Pvt. Ltd., Kolkata, India.

4.3.2. Bacterial Strains and Media

Different species of microorganisms (*E. coli, A. baumannii, S. typhi, B. fragilis, S. paratyphi, S. dysenteriae, E. faecalis)* used in the experiments were isolated from

various patients' samples collected from patients attending Guwahati Neurological Research Center (GNRC) Medical Outdoor Clinic (North Guwahati, India) or admitted there for treatment after taking written consent from them. The media used for growth of these microorganisms were cysteine lactose electrolyte deficient CLED) agar, nutrient agar and Muller Hinton agar (MHA) purchased from Himedia, Mumbai, India. Further GFP-expressing recombinant *E. coli* (MTCC 433 Strain) and *Bacillus Cereus* (MTCC 1305) grown in nutrient agar (Himedia, Mumbai, India) were also used in the experiments.

4.3.3. Fabrication of Portable Filtration Device

The comprehensive procedure for synthesis of the Fe-Cu-nanocomposite on sand was explained in detail in **Experimental Section of Chapter 3** (3.3.3). For practical application of the as synthesized nanocomposite for water filtration, a portable filtration device was fabricated using two plastic falcon tubes holding the nanocomposites in the middle of one tube and sand in the other with the help of sponge.

4.4. Characterization

For characterization, TEM, XRD, FESEM, VSM and FACS were done and described in detail in **Experimental Section of Chapter 3 (3.4).**

4.4.1. Study of Water Filtering Capacity of the Nanocomposites

(a) The prepared bimetallic nanocomposites were used to filter bacteria especially those responsible for waterborne diseases. Before giving a trial with patients' samples, first a sample each of Gram positive and Gram negative (*B. cereus*; MTCC 1305 and *E. coli*; MTCC 433) strain was inoculated into test tubes containing 5 mL peptone and was then incubated overnight separately. Then the bacterial suspensions were filtered through a filtration device containing only (1) sand and (2) Sand-Fe-Cu-nanocomposites. The same experiment was repeated with patients' samples collected from patients attending GNRC Medical, North Guwahati for treatment after getting written consent from them. Several species of bacteria responsible for water borne diseases e.g. *Acinetobacter baumannii, Escherichia coli, Salmonella typhi, Bacteroides fragilis, Salmonella paratyphi, Shigella dysenteriae, Enterococcus faecalis* were isolated from varied

biological fluids of different patients and grown overnight in 5 mL peptone. Then the tubes were compared with the turbidity standard (McFarland 0.5) and the density of the test suspension was adjusted to that of the standard by adding more bacteria or more peptone water. Thereafter, bacterial suspensions were filtered through sand and the prepared nanocomposites and filtrates were plated in nutrient agar plate and re-incubated overnight at 37°C. Also the optical density (OD) of the filtrates was measured at 595 nm using an UV- visible spectrophotometer (Lambda; Perkin-Elmer, Fremont, CA, USA).

(b) The prepared nanocomposites were also tested for its ability to filter metals. Three metal ions of nickel, lead and zinc were tested for this purpose. Solutions (1g in 10 mL of Milli-Q water) of nickel chloride, lead acetate and zinc chloride were allowed to filter through sand and the prepared nanocomposites separately and the UV absorbance of the filtrate was measured on UV−visible spectrophotometer (Lambda; Perkin-Elmer, Fremont, CA, USA). To find out the concentration of above metals in the filtrate, solutions of different concentrations, for example, 10 ppm, 50 ppm and 100 ppm solutions of the nickel, lead and zinc were prepared and allowed to filter through the hand held filtration device containing sand and the nanocomposites respectively. The concentrations of the metals in the filtrates were measured by atomic absorption spectroscopy (Varian AA-240, Atomic Absorption Spectrophotometer with GTA 120, Netherland).

4.4.2. Study of Magnetic Property

To study the magnetic property, the nanocomposites were placed on a filter paper and with the help of magnetic bar it was observed for being attracted towards the magnet completely. Also, the used nanocomposites were collected with the magnetic bar from the filtration device followed by repeated washing with Milli-Q water and then drying in hot air oven for reusing it in the filtration device.

4.4.3. Vibrating Sample Magnetometer (VSM)

Further, magnetic moment of the nanocomposites was also measured with the help of vibrating sample magnetometer (VSM, *Lakeshore, Model: 7410 series*).

4.4.4. Study to Check Reusability of Sand-Fe-Cu-nanocomposites after Washing

To demonstrate the reusability of nanocomposites, filtration was carried out with as synthesized sand Fe-Cu-nanocomposites, where after 1st set of filtration, the procedure was repeated twice following washing (washing 1 and 2) of the same nanocomposites. For filtration, briefly, 1 g of each freshly prepared sand Fe-Cu- nanocomposites and raw sand were taken in the filtration device separately. Then through these respective filtration units 5 mL of bacterial suspensions (both GPC and GNB) were allowed to filter separately. The filtrates were collected and absorbance was measured at 595 nm in UV spectrophotometer (Lambda; Perkin-Elmer, Fremont, CA, USA). Thereafter to utilize the nanocomposites for further usage, the nanocomposites were separated from the device with the help of a magnetic bar and were washed several times with Milli-Q water followed by drying in hot air oven at 37 °C. The dried nanocomposites were again placed in the filtration device and filtration was carried out. The procedure was repeated to check the efficacy of the nanocomposites after washing.

4.4.5. Atomic Absorption Spectroscopy to Check Leaching of Metals in the Filtrate

To check the leaching of copper and iron from the Sand-Fe-Cu-nanocomposites, atomic absorption spectroscopy (Varian AA-240, Atomic Absorption Spectrophotometer with GTA 120, Netherland) was performed. For this, 1g of nanocomposites was kept overnight with 5 mL Milli-Q water in a test tube, thereafter centrifuged after shaking and atomic absorption spectroscopy was done to see concentrations of iron and copper in the supernatant.

4.5. Results and Discussions

Based on the observed merit of the broad spectrum antimicrobial activity of the nanocomposites towards a wide range of bacteria, application of the same in purification of water was tested. The schematic representation of the application of the sand-Fe-Cu nanocomposite for purification of water has been illustrated in **Figure 4.1**.

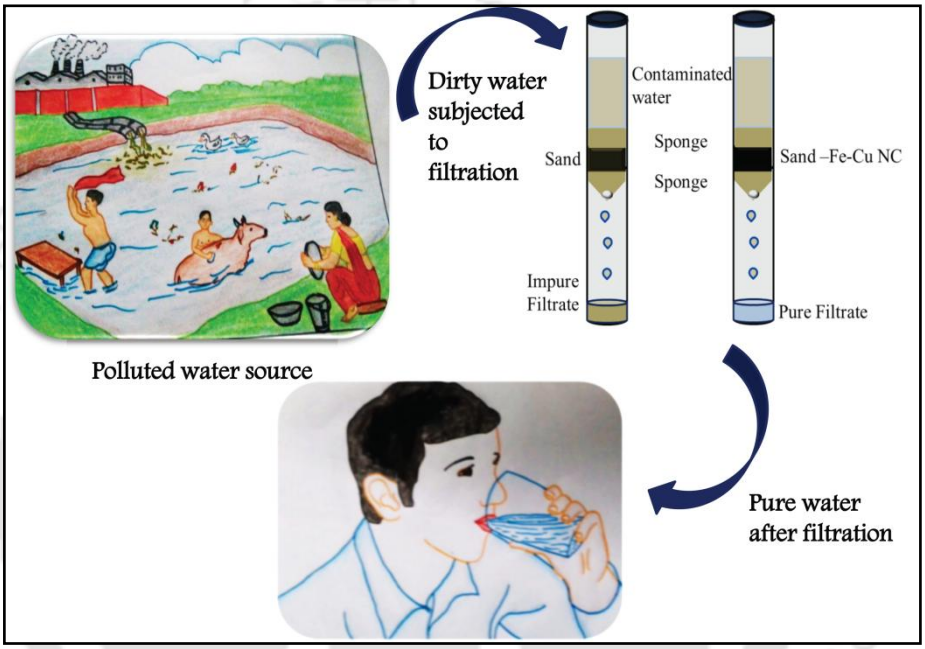

Figure 4.1. Schematic representation of application of sand-Fe-Cu nanocomposite for point-of-use water purification**.**

For this, a hand held filtration device was designed with two plastic falcon tubes with an opening at the bottom. 1 g of sand and 1 g of the prepared nanocomposites were placed in tubes 1 and 2 respectively using two pieces of colorless sponges to assess the filtration capacity of both sand and the nanocomposites independently (**Figure 4.2**).

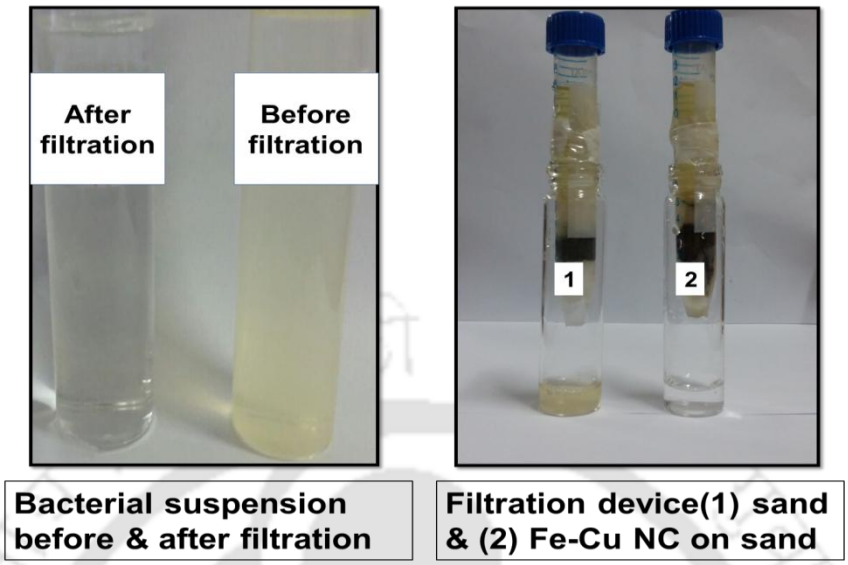

Figure 4.2. Photograph of filtration device with the filtrate.

Then the solutions to be filtered were poured slowly from the top and the filtrates were collected in separate glass tubes at the bottom. Then 5 mL of bacterial suspensions in peptone, both Gram positive (*B. cereus*; MTCC 1305 strain) and Gram negative (*E. coli* MTCC 433 strain) bacteria were filtered through the filtration device in a subsequent order, then plated and incubated on agar plates. The culture plates inoculating nanocomposites filtrate didn't show any bacterial growth after re-incubation whereas plates with sand filtrate showed significant growth of bacteria similar to that of control bacteria (**Figure 4.3**).

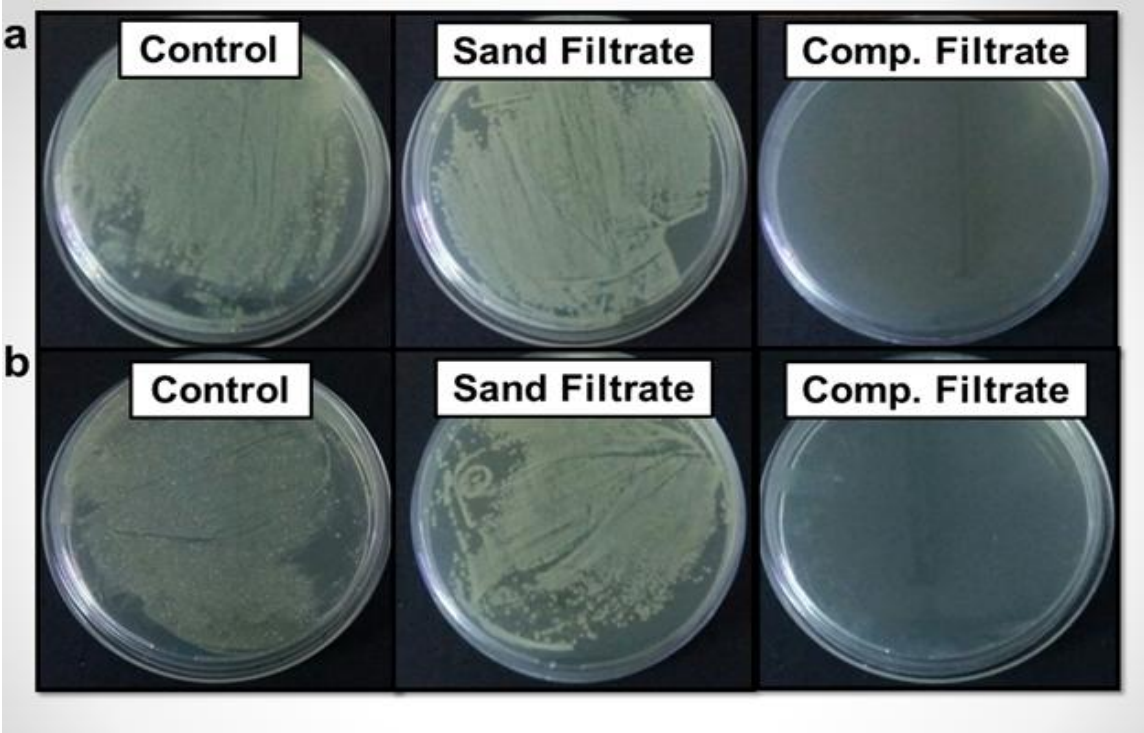

Figure 4.3. Results of bacterial filtrate re-incubation where (a) represents Gram positive (*B. cereus*) with its control, sand filtrate and composite filtrate and (b) represents Gram negative (*E. coli*) with its control, sand filtrate and composite filtrate.

For practical application, the same experiments were repeated with different patients' samples. Several species of bacteria responsible for waterborne diseases e.g., *Acinetobacter baumannii, Escherichia coli, Salmonella typhi, Bacteroides fragilis, Salmonella paratyphi, Shigella dysenteriae* and *Enterococcus faecalis* were first isolated and filtered through sand and the prepared nanocomposites separately and the filtrates were plated on nutrient agar plates and kept for overnight incubation. The culture plates with the nanocomposites filtrates after re-incubation didn't show any growth of bacteria as is evident in **Figure 4.4**.

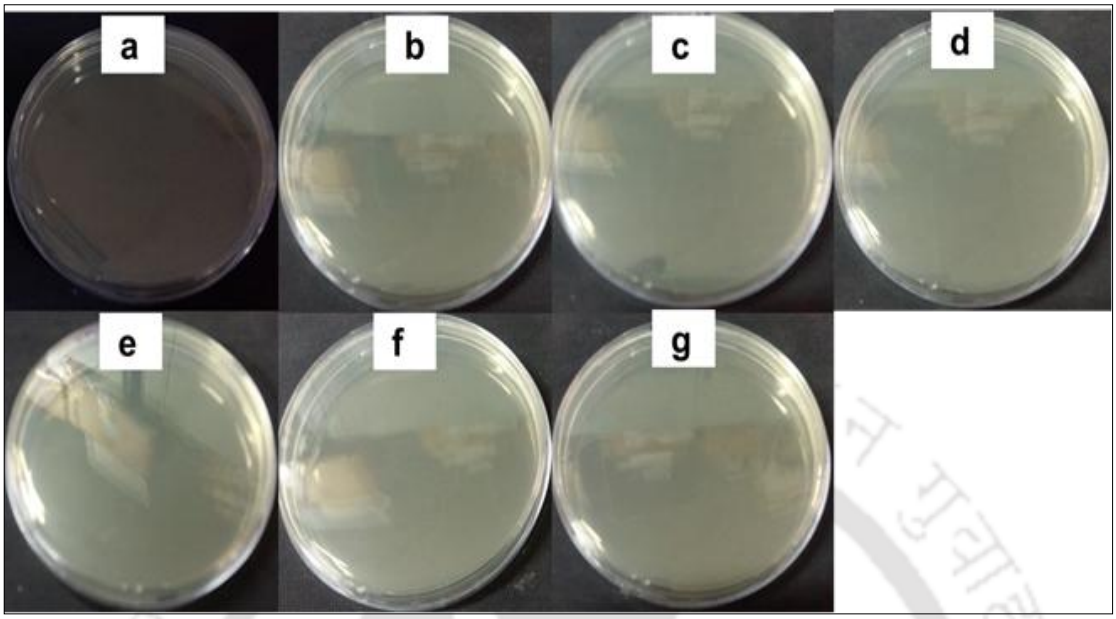

Figure 4.4. Results of re-incubation of the nanocomposites filtrate of bacterial suspensions where (a) represents plate of *A. baumannii*, (b) *E. coli*, (c) *S. typhi*, (d) *B. fragilis*, (e) *S. paratyphi*, (f) *S. dysenteriae*,(g) *E. faecalis*.

Thereafter, to substantiate the above findings, UV absorbance of the filtrates was measured at 595 nm. As illustrated in **Figure 4.5**, the absorbance of the nanocomposites treated filtrate was significantly less than the control sample. Sand, being known water filtration material showed higher absorbance value than the nanocomposites treated filtrate, which illustrated nanocomposites as a better material for water purification. It can be inferred from the above findings that 1 g of nanocomposites could effectively filter 150 million/mL of bacteria, which was calculated by comparing the bacterial suspensions (in peptone) with the turbidity standard (McFarland 0.5, which corresponds to bacterial concentration of 150 million/mL). The above protocol is followed as a standard procedure in medical microbiological lab.[36]

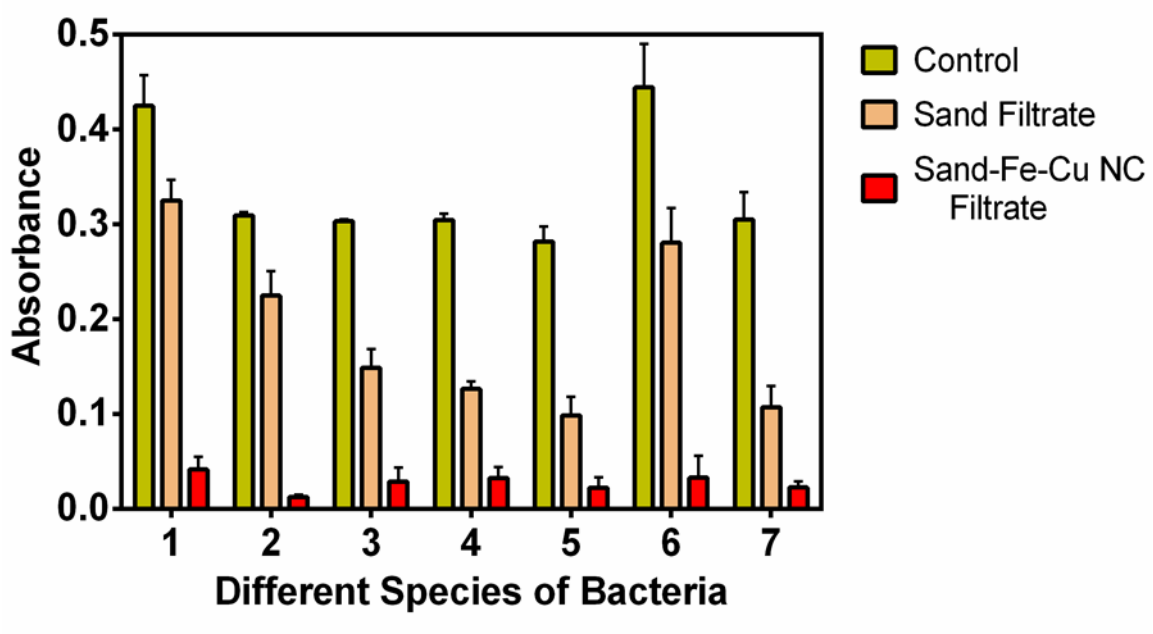

Figure 4.5. Graphical presentation of UV absorbance of different bacterial suspension in peptone before and after filtration through sand and nanocomposites, where 1- *A. baumannii*, 2- *E. coli*, 3- *S. typhi*, 4- *B. fragilis*, 5-*S. paratyphi*, 6- *S. dysenteriae*, 7-*E. faecalis*. UV absorbance of the filtrates was measured at 595 nm.

After obtaining significant results in the filtration of various microbes, the nanocomposites were tested next for the removal of heavy metals like nickel, lead and zinc from water. For this, aqueous samples with different concentrations of metals (1g in 10 mL of Milli-Q water) were passed through the filtration device containing only sand and nanocomposites separately. Afterwards, upon measuring the UV absorbance at 395 nm (nickel), 225 nm (lead) and 400 nm (zinc) of the collected filtrates, it was observed that, there was significant reduction of absorbance value due to the respective metals in nanocomposites treated filtrates (**Figure 4.6**). The intensity of the UV absorbance of the filtrate obtained after filtration through nanocomposites was reduced more as compared to that of sand filtrate in case of all the three metallic solutions. Thus, it can be inferred here that filtration through the nanocomposites was more effective than the only sand.

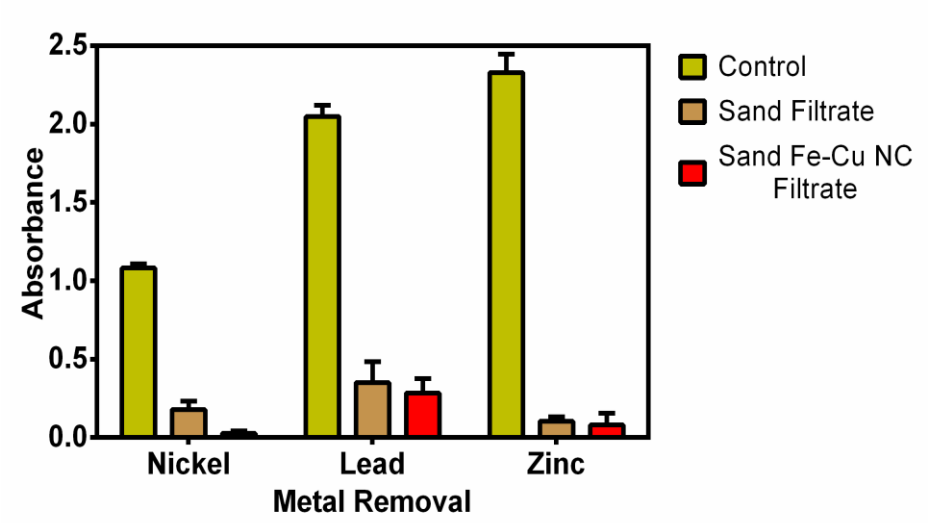

Figure 4.6. Graphical presentation of the UV absorbance of the prepared metallic solutions and the filtrates of sand and nanocomposites measured at 395 nm (nickel), 225 nm (lead) and 400 nm (zinc).

Further, for calculating the metal removal capacity, atomic absorption spectroscopy was performed for both sand and nanocomposites treated filtrates. On passing 10, 50 and 100 ppm of each metal through the sand and nanocomposites filled filtration device, removal of ~ 90.3%,~ 99.1%, and~ 95% of nickel, lead and zinc, respectively, was accomplished (**Figure 4.7d-f**). The blue line in **Figure 4.7(d-f)** signifies concentrations of nickel, lead and zinc respectively i.e. control in ppm (10, 50, 100 ppm) before filtration. After filtration of 10, 50 and 100 ppm solution of the respective metals, concentrations of the metals in the filtrates of sand and Sand-Fe-Cu-nanocomposites were visibly reduced. The red line in **Figure 4.7(d-f)** denotes the concentration in ppm of nickel, lead and zinc respectively following filtration through only sand and the green line in Figure **4.7(d-f)** represent concentration (ppm) of nickel, lead and zinc respectively in the Sand-Fe-Cu-nanocomposite filtrate, which confirms effective metal purging capacity of the nanocomposites. Therefore, the prepared nanocomposites could be beneficial for house hold use as a simple and cost effective water filtration device.

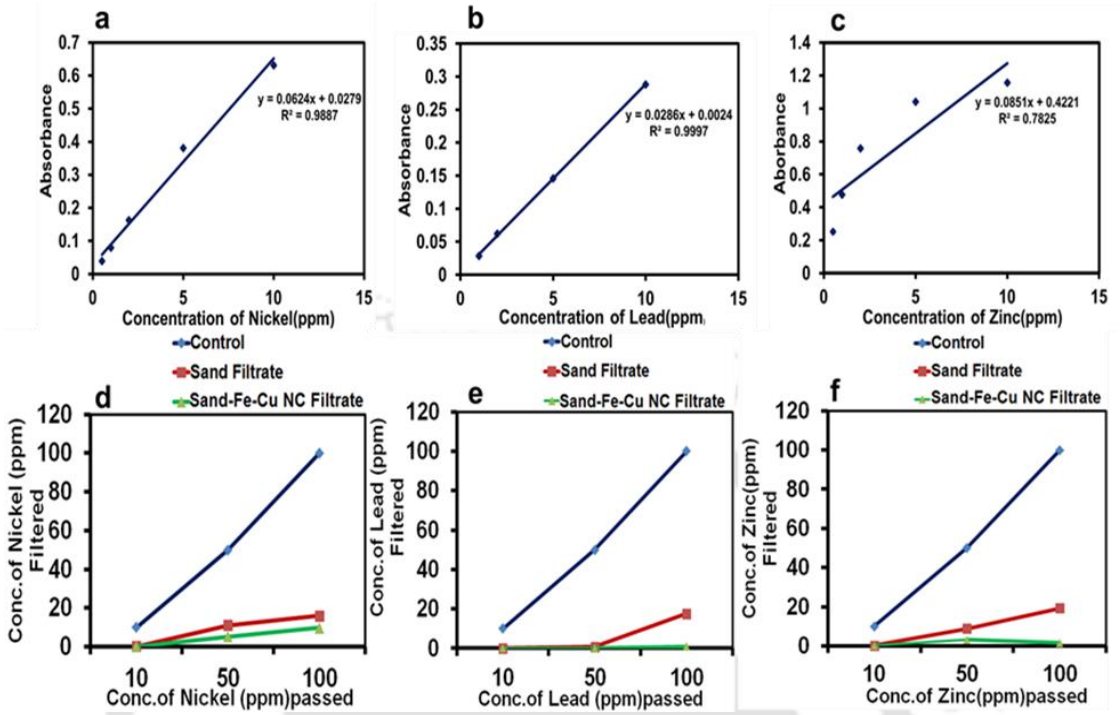

Figure 4.7. Results of atomic absorption spectroscopy where (a, b & c) represents the standard graph of nickel, lead and zinc, respectively and (d, e & f) represents the results of filtration of nickel, lead and zinc respectively through sand and Sand-Fe-Cu-nanocomposites. In figure d, e and f, the blue line represents the concentration of the metals before filtration i.e. the control, red line represents concentration of metals obtained after filtration through only sand and green line represents concentration of metals after filtration through Sand-Fe-Cu-nanocomposites.

Along with the antimicrobial activity and dissolved metal filtering capability, the prepared nanocomposites would be more suitable for practical application, if it could be manipulated by external magnetic field. For this, the magnetic property of the nanocomposites was examined by both magnetic bar and VSM. As illustrated in **Figure 4.8a** and **Figure 4.8b**, all the nanocomposites were attracted by the magnetic bar confirming the strong magnetic nature of the nanocomposites. Moreover, the saturation magnetization of the synthesized Sand-Fe-Cu-nanocomposites was also measured by vibrating sample magnetometer and found to be 4.2618 emu/g at ambient temperature (**Figure 4.8c**).

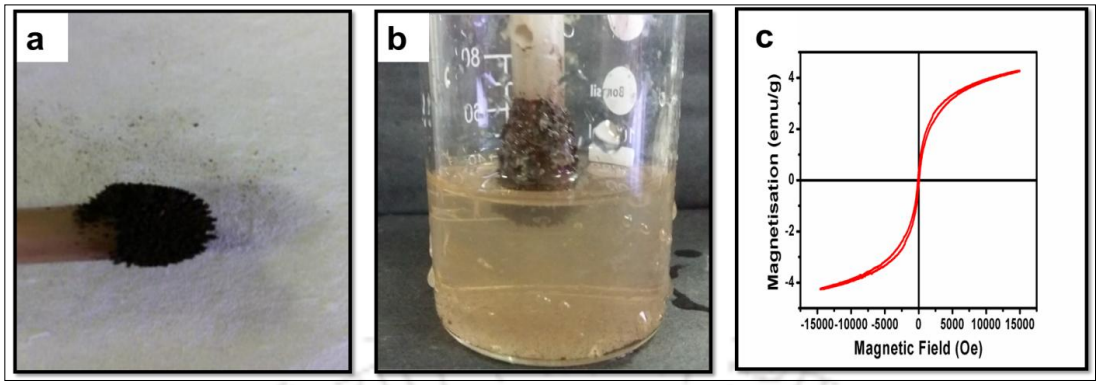

Figure 4.8. (a) Photograph showing holding of the nanocomposites by a magnetic bar, (b) Magnetic bar along with the nanocomposites after washing and (c) Magnetization curve of the iron oxide magnetic particles of the nanocomposites.

Normally, separation and recovery of the nanomaterials from the contaminated water is a challenging task due to their tiny sizes. The magnetic property of the nanocomposites was utilized for its easy separation and recovery from the system for the purpose of recycling. To exhibit the recyclable property of the nanocomposites, bacterial suspensions were filtered through raw sand and sand-Fe-Cu-nanocomposites after washing them. On filtering bacterial suspensions (both GPC and GNB), the absorbance of both raw sand filtrate and Sand-Fe-Cu-nanocomposites filtrate decreased in both GPC and GNB (**Figure 4.9**) as compared to that of control bacterial suspension. In all the 3 sets of experiments i.e., with fresh nanocomposites, nanocomposites used after 1st washing and also with nanocomposites after 2nd washing, revealed significant reduction of absorbance after treatment with Sand-Fe-Cu-nanocomposites. Though it was observed that the sand alone was capable of filtering bacteria efficiently in all the cases but superior filtration capability was observed with Sand-Fe-Cu-nanocomposites with significant differences after 1st washing. Even after comparing the results of sand filtrate and Sand-Fe-Cu-nanocomposites filtrate after 2nd washing, there was noticeable reduction in absorbance. Decrease in absorbance of the Sand-Fe-Cu-nanocomposites filtrate after washing indicated preservation of its bacteria filtering capacity even after its use and repeated washing thus can be recycled after washing.

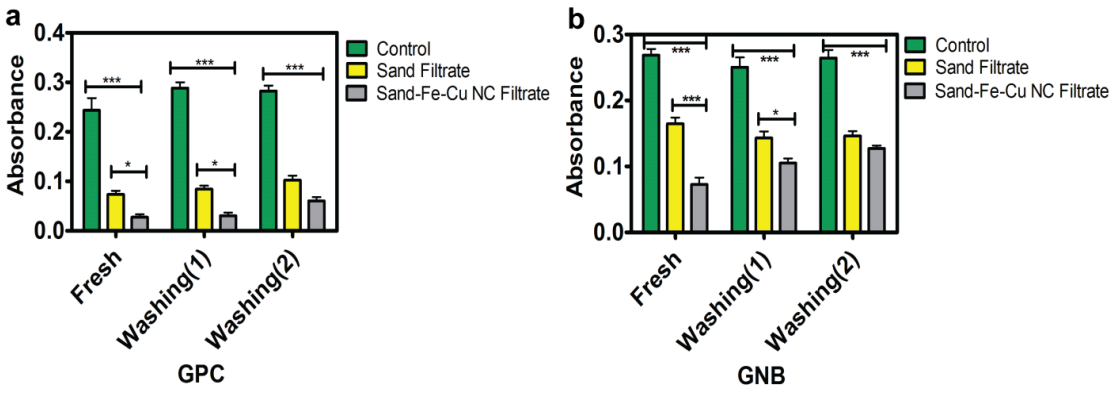

Figure 4.9. Graphical presentation of UV absorbance (measured at 595 nm) of the filtrates of bacterial suspension in peptone of both GPC (a) and GNB (b) filtered through freshly prepared nanocomposites and already used nanocomposites utilized after washing (1st and 2nd).

In order to ensure the safe utility of the prepared nanocomposites the leaching of iron and copper from the nanocomposites was tested with the help of atomic absorption spectroscopy. The results revealed release of 0.19 ppm (=0.19 mg/L) and less than 0.1 ppm (<0.1 mg/L) for copper and iron, respectively, which were within the permissible limits (1.5 mg/L for copper and 0.3 mg/L for iron according to Bureau of Indian Standards (BIS) for Drinking Water IS-10500- 2012 (second revision). And according to International Standards for Drinking Water, permissible limit for copper is 1 mg/L and that for iron is 0.3 mg/L.[37] For this, 1 g of nanocomposites was kept overnight with 5 mL Milli-Q water (described in the experimental section). The results indicated suitability of the use of the composite not only for annihilation of bacteria but also water purification (especially heavy metal removal).

4.6. Conclusion

The as synthesized Sand-Fe-Cu nanocomposite could easily be used to fabricate a hand held water filter for the purpose of point-of-use water filtration. The composites were efficient in the filtration of microbes and hazardous metals present in water. The composites demonstrated here based on non-toxic materials can be effortlessly used for purification of water in a broad range of geographical locations.

4.7. References

1. Lu, H.; Wang, J.; Stoller, M.; Wang, T.; Bao, Y.; Hao, H.; Kanchi, S. *J Env. Anal Chem*. **2016**,*2*, 10–12.
2. Tiwari, D. K.; Behari, J.; Sen, P. *Carbon Nanotub*.**2008**, *3*(3), 417–433.
3. Pradeep, T.; Anshup. *Thin Solid Films.* **2009**, *517* (24), 6441–6478.
4. Qu, X.; Alvarez, P. J. J.; Li, Q. *Water Res.* **2013**, *47* (12), 3931–3946.
5. Simeonidis, K.; Mourdikoudis, S.; Kaprara, E.; Mitrakas, M.; Polavarapu, L. *Environ. Sci. Water Res. Technol.* **2016**, *2* (1), 43–70.
6. Sreeprasad, T. S.; Gupta, S. Sen; Maliyekkal, S. M.; Pradeep, T. *J. Hazard. Mater.* **2013**, *246–247*, 213–220.
7. Savage, N.; Diallo, M. S. *J. Nanoparticle Res.* **2005**, *7* (4–5), 331–342.
8. Zhu, C.; Liu, P.; Mathew, A. P. *ACS Appl. Mater. Interfaces.* **2017**, *9* (24), 21048–21058.
9. Wang, Y.; Zhao, H.; Zhao, G. *Appl. Catal., B.* **2015**, *164*, 396–406.
10. Perdikaki, A.; Galeou, A.; Pilatos, G.; Karatasios, I.; Kanellopoulos, N. K.; Prombona, A.; Karanikolos, G. N. *ACS Appl. Mater. Interfaces.* **2016**, *8* (41), 27498–27510.
11. Lam, F. L. Y.; Hu, X. *Ind. Eng. Chem. Res.* **2013**,*52* (20), 6639-6646.
12. Marková, Z.; Šišková, K. M.; Filip, J.; Čuda, J.; Kolář, M.; Šafářová, K.; Medřík, I.; Zbořil, R. *Environ. Sci. Technol.* **2013**, *47* (10), 5285–5293.
13. Sankar, M. U.; Aigal, S.; Maliyekkal, S. M.; Chaudhary, A.; Anshup; Kumar, A. A.; Chaudhari, K.; Pradeep, T. *Proc. Natl. Acad. Sci.* **2013**, *110* (21), 8459–8464.
14. Blanco-Andujar, C.; Ortega, D.; Pankhurst, Q. A.; Thanh, N. T. K. *J. Mater. Chem.* **2012**, *22* (25), 12498.
15. Li, L.; Fan, M.; Brown, R. C.; Van Leeuwen, J.; Wang, J.; Wang, W.; Song, Y.; Zhang, P. *Crit. Rev. Environ. Sci. Technol.* **2006**, *36* (5), 405–431.
16. Tan, L.; Xu, J.; Xue, X.; Lou, Z.; Zhu, J.; Baig, S. A.; Xu, X. *RSC Adv.* **2014**, *4*, 45920-45929.
17. Ngomsik, A.F.; Bee, A.; Talbot, D.; Cote, G. *Sep. Purif. Technol.* **2012**, *86*,

(15), 1-8.

18. Sharma, Y. C.; Srivastava, V.; Singh, V. K.; Kaul, S. N.; Weng, C. H.; Srivastava, V.; Singh, V. K.; Kaul, S. N.; Weng, C. H. *Environ. Technol.* **2009**, *30*(6), 583-609.
19. AshaRani, P. V.; Mun, G. L. K.; Hande, M. P.; Valiyaveettil, S. *ACS Nano.* **2009**, *3* (2), 279–290.
20. Park, M. V. D. Z.; Neigh, A. M.; Vermeulen, J. P.; de la Fonteyne, L. J. J.; Verharen, H. W.; Briedé, J. J.; van Loveren, H.; de Jong, W. H. *Biomaterials.* **2011**, *32* (36), 9810–9817.
21. Cady, N. C.; Behnke, J. L.; Strickland, A. D. *Adv. Funct. Mater.* **2011**, *21*(13), 2506-2514.
22. Turnlund, J. R. *Am. J. Clin. Nutr.* **1998**, *67* (5 suppl.), 960S–964S.
23. Theivasanthi, T.; Alagar, M. *Ann. Biol. Res.* **2011**, *2* (3), 368–373.
24. Jia, B.; Mei, Y.; Cheng, L.; Zhou, J.; Zhang, L. *ACS Appl. Mater. Interfaces.* **2012**, *4* (6), 2897–2902.
25. Ruparelia, J. P.; Kumar, A.; Duttagupta, S. P. *Acta Biomater.* **2008**, *4*(3), 707–716.
26. Ren, G.; Hu, D.; Cheng, E. W. C.; Vargas-reus, M. A.; Reip, P.; Allaker, R. P. *Int. J. Antimicrob.* **2009**, *33*, 587–590.
27. Yoon, K. Y.; Hoon Byeon, J.; Park, J. H.; Hwang, J. *Sci. Total Environ.* **2007**, *373* (2–3), 572–575.
28. Perelshtein, I.; Applerot, G.; Perkas, N.; Wehrschuetz-Sigl, E.; Hasmann, A.; Guebitz, G.; Gedanken, A. *Surf. Coatings Technol.* **2009**, *204* (1–2), 54–57.
29. Akhavan, O.; Ghaderi, E. *Surf. Coatings Technol.* **2010**, *205* (1), 219–223.
30. Hassan, M. S.; Amna, T.; Yang, O. B.; El-Newehy, M. H.; Al-Deyab, S. S.; Khil, M. S. *Colloids Surf. B.* **2012**, *97*, 201–206.
31. Dankovich, T. A.; Smith, J. A. *Water Res.* **2014**, 15(63), 245–251.
32. Xiong, Z.; Yuan, D.; Yang, P.; Lai, B. *J. Taiwan Inst. Chem. Eng.* **2017**, *80*, 669–677.
33. Lai, B.; Zhang, Y.; Chen, Z.; Yang, P.; Zhou, Y.; Wang, J. *Appl. Catal., B.* **2014**, *144*, 816–830.

34. Hu, C.; Lo, S.; Liou, Y.; Hsu, Y. *Water Res.* **2010**, *44* (10), 3101–3108.
35. Park, S.; Lee, C.; Kim, J.; Kim, S.; Chang, Y. *Desalin Water Treat***. 2015**, *54*(12), 3380-3391.
36. Collee, J.G.; Fraser, A.G.; Marmion, B.P.; Simmons, A. Mackie & McCartney Practical Medical Microbiology. **1996,** 14th edition, 851-852.
37. Darrasse, H., Gilcreas, F. W., Hakim, K. A., Horasawa, I., Jebb, W. H. H., Modak N. V., et al. International Standards of Drinking-Water Quality. *WHO*,Geneva, **1956,** 29.

CHAPTER-5

Iron-Copper Bimetallic Nanocomposite Reinforced Dressing Materials for Infection Control and Healing of Diabetic Wound

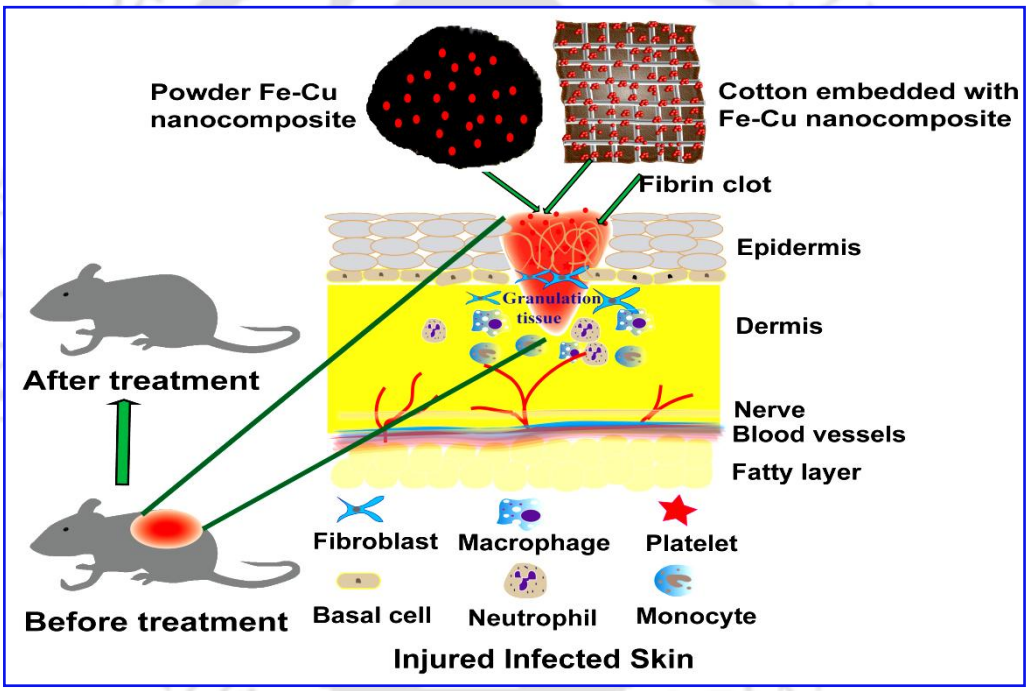

In Chapter 5, facile synthesis of iodine stabilized bimetallic dressing material in dual forms (powder and nanocomposite embedded cotton patch) have been reported. *In vitro* anti-microbial test has been performed on different clinical isolates to ascertain the antimicrobial behavior. To ensure wound healing property, *in vivo* animal experiment has been performed in diabetic Wistar Albino rats having infected wound.

(Manuscript under Minor Revision)

CHAPTER -5

5.1. Introduction

Skin plays a crucial role in protecting our body from different microbes, in addition to maintaining the homeostasis of the internal organs. Once the continuity of the skin is disrupted, it needs to be dressed quickly in order to maintain a reasonably moist environment. The dressing helps prevent infection, relieve pain, facilitate gaseous exchange, avoid scar formation, and assists in regeneration and healing of the skin.[1,2] The course of wound healing is a complex and well-organized process. Normally, it starts immediately after the injury and heals within a period of 1−12 weeks by the process of cell proliferation followed by tissue remodeling and regeneration.[3,4] Clinical challenges arise when there are superadded microbial infections and excess fluid loss from the injury sites, leading to delayed self-limiting wound healing.[5] But the exact time for healing of chronic wounds like pressure ulcers, diabetic ulcers, and vascular ulcers are difficult to anticipate as they are more susceptible to infection and are much more difficult to manage.[3,6] In India, foot ulceration is the most common complication, which affects almost 15% of diabetic patients.[7] Secondary infection in an unhealed diabetic foot ulcer is the most alarming complication that may end up with amputation of the limb, which occurs in 2.1−13.7 per 1000 diabetic patients.[8]

Till date a variety of natural polymers like polysaccharides, proteoglycans, and proteins as well as synthetic polymers have been tried for fast healing of wounds in addition to control infection.[3,9-11] However, majority of these polymers lack bioactivity and the ability to accelerate the wound healing process. A superior dressing material should be biocompatible, bio-degradable, contented and cost-effective and in addition, it should show heightened antimicrobial activity. At the same time a long shelf life and a multifaceted usage for the product are also desired. Conversely, commercially available dressing materials do not satisfy all of these criteria in a single entity; hence new materials for the purpose of wound healing are in demand now.[1] In this regard,

several engineered nanomaterials are incorporated within the polymeric network to obtain nanocomposite biomaterials that accelerate the remedial process through a continuous and steady release of therapeutics.[3,12,13]

Generally, most of the nanomaterials are prepared for surface application to diminish the side effects related with systemic use. It has been observed that topically applied antimicrobials are much more effective in curing infected granulomatous wounds than the systemically administrated antimicrobials.[3] Metallic nanoparticles have been demonstrated to be better candidates for topical use in wound healing as they show a wide range of properties, like broad spectrum antimicrobial activity, well-ordered sustained release and better mechanical strength. Metallic nanoparticles are technically and economically sustainable due to their prominent adsorption capacity.[1,3] Among the metallic nanoparticles, silver (Ag) nanoparticles has been extensively used for wound healing purpose with a few reports of copper (Cu) nanoparticles as well.[3,14-16] Silver nanoparticles (Ag NPs) have multifaceted modes of action. However, reports suggest that aggressive usage of Ag NPs in clinical practice should be restraint.[3] On the contrary, Cu NPs are considered safer as copper is an integral component of living tissues and its deficiency inhibits the wound healing process.[17,18] Moreover, human body has a mechanism of protecting against copper toxicity and can protect against excess accumulation or copper depletion by adjusting endogenous excretion.[19] It has got antimicrobial efficacy against several strains of microbes.[20-24] At the same time, Cu NPs exhibit skin re-modulation, tissue regeneration, antioxidant and anti-inflammatory properties.[16,22,25] Much lower concentration of Cu NPs is sufficient to heal a wound compared to its native form.[15] The Cu NPs, an EPA (US Environmental Protection Agency) approved material[26] has shown enhanced healing in excisional wounds of mice,[16] However, they have been less explored for wound healing[25], may be because of higher oxidation rate of Cu NPs in the presence of air and water.[27] In addition to Ag NPs and Cu NPs, reports of enhanced wound healing by iron oxide NPs[28] through increasing tissue regeneration are also available.[25,29] Therefore, research endeavors are essential to remodel a value-added dressing bed targeting both infection control and achieving faster healing of acute and chronic wounds.

Herein, synthesis of bimetallic wound healing dressing material both in powder and thin film forms has been reported which exhibited antimicrobial activity against methicillin resistant *Staphylococcus aureus* (MRSA) and displayed *in vivo* wound healing property as well. Bimetallic nanoparticles in presence of stabilizers exhibited enhanced bactericidal activity than their constituents.[30] Also, compared to single metal nanoparticle, low concentration of bimetallic nanoparticles displayed higher antimicrobial and antimycotic activities against a wide range of multidrug-resistant bacteria and fungi.[31] Therefore, emphasis has been given on preparing a biodegradable and durable bimetallic dressing bed with broad-spectrum antibacterial and antifungal properties against multidrug resistant microbes.

5.2. Outline of the Present Work

A multifunctional nanomaterial based wound healing matrix was fabricated by modified co-precipitation and chemical reduction method. The matrix comprised either of a bimetallic Fe-Cu nanocomposite powder or a wound bed made up of absorbent cotton swab impregnated with bimetallic Fe-Cu-nanocomposite. The detailed analytical studies of both the dressing materials (powder and cotton bed) were carried out with transmission electron microscopy (TEM), X-ray diffraction (XRD), field emission scanning electron microscopy (FESEM), energy-dispersive x-ray (EDX) and bright field microscopy. Both the nanocomposite powder and the nanocomposite impregnated cotton swab exhibited antimicrobial activity against Gram positive and Gram negative bacteria, including multidrug resistant bacteria (like methicillin resistant *Staphylococcus aureus*) as well against fungus isolated from different human biological samples (pus/tissue culture/urine). For real time applications, *in vivo* wound healing ability of both the dressing materials was also carried out in Wistar albino rats with infected diabetic wounds. These novel biocompatible and biodegradable dressing materials with broad spectrum antimicrobial properties have exhibited more than 20 mm in diameter zone of microbial growth inhibition against several types of microbes. Remarkably, they have also been found to assist in healing of infected diabetic wounds and show a prospect in the management of other infectious wounds.

5.3. Experimental Section

5.3.1. Materials

All reagents were used as received without further purification. The sources for the bandage materials were extra pure hydrate ferrous chloride (Loba Chemie), ferric chloride anhydrous, copper II sulphate pentahydrate ($CuSO_4.5H_2O$), 25% ammonia solution and 80% hydrazine hydrate (Merck). Iodine was purchased from Sigma Aldrich chemical Pvt. Ltd. Kolkata, India. Milli-Q grade (resistivity 18.2 MΩcm-1) water was used in all experiments.

5.3.2. Bacterial Strains and Media

Different species of microorganisms (Methicillin resistant *S.aureus*, *E.coli and C.albicans)* used in the experiments were isolated from various patients' samples collected from patients attending Guwahati Neurological Research Center (GNRC) Medical Outdoor Clinic or admitted there for treatment after taking written consent from them. The media used for growth of these microorganisms were cysteine lactose electrolyte deficient agar (CLED), nutrient agar, Muller Hinton agar (MHA) and MHA with 2% glucose and 0.5 mg/L methylene blue dye for fungus, purchased from Himedia, Mumbai, India.

5.3.3. Fabrication of Bimetallic Nanomaterial Based Dressing Material in Powder Form

For the synthesis of Fe-Cu-nanocomposites, co-precipitation[23,32,33] and chemical reduction method[23,34] with a little modification was employed. In short, 1.0 gm of $FeCl_2$ and 1.5 gm of $FeCl_3$ were dissolved in 50 mL of milli-Q grade water with constant magnetic stirring and moderate heating (60 ºC) for 3-5 min. Then 6 mL of 25% ammonium hydroxide (NH_4OH) was added to form iron oxide nanoparicles which was indicated by the formation of dark brown colored precipitation. To this medium, 250 mg of copper sulphate pentahydrate crystals were added and they were reduced by hydrazine to form bimetallic Fe-Cu-nanocomposites. 300 µL of iodine solution in ethanol (0.2 M) was added as a stabilizing agent and kept under stirring for 5 min. Then

the reaction mixture was allowed to cool at room temperature followed by centrifugation at 6000 rpm. The precipitate was washed with Milli-Q water 3 times after discarding the supernatant and then dried in hot air oven at 37 ºC.

5.3.4. Fabrication of a Dressing Bed by Impregnating Fe-Cu-nanocomposites on Absorbent Cotton Swab

For the preparation of nanomaterials impregnated dressing bed, small pieces of absorbent cotton swab (of two different sizes i.e., 1 × 1.5 inches; 66 mg by weight and 0.4 × 0.5 cm; 5.5 mg by weight) were soaked in a solution of iron (4 mL), prepared by dissolving 200 mg of $FeCl_2$ and 300 mg of $FeCl_3$ in 50 mL of Milli-Q grade water. Then the soaked cotton swabs were placed in a separate beaker where 3-4 mL of NH_4OH solution were added. When the cotton swabs turned dark brown, indicating the formation of iron oxide nanoparticals, the extra NH_4OH solution was discarded. Then fresh solution of copper sulphate (4 mL) was added. Copper sulphate solution was prepared by dissolving 50 mg of copper sulphate pentahydrate in 50 mL of Milli-Q grade water. Then 1 mL hydrazine was added. Formation of Fe-Cu-nanocomposites on cotton swab was indicated by change of color from dark brown to black. Then 0.3 mL of 0.2 M iodine solution was added to stabilize the formed nanoparticles. Throughout the whole process moderate heat (60-70 ºC) was applied by keeping the reaction mixture in a hot water bath. After completion of the reaction, the cotton swabs were removed from the beaker and washed 3 times with Milli-Q grade water to remove any extra hydrazine. Then the cotton swabs were dried in hot air oven at 37 ºC before testing.

5.4. Characterization

5.4.1. Transmission Electron Microscopy (TEM) Analysis

The probing of external morphology and crystallinity of both nanocomposites powder and nanocomposites impregnated cotton swabs were accomplished by transmission electron microscopy (TEM) and selected area electron diffraction (SAED) studies (TEM; JEM 2100; Jeol, Peabody, MA, USA). For these, the nanocomposite powders were mixed with 1 mL distilled water (added with 10 µL of 0.1% acetic acid) to extract

the nanoparticles from the composite powder mixture as they were not dispersible in water, and were drop - cast on carbon-coated copper grid for measurements following air drying. Similarly, the cotton dressing bed was cut into small pieces and soaked in water (with 0.1% acetic acid) and then the medium was drop cast. TEM & SAED images were recorded and from the corresponding particle size distribution of the obtained TEM images, size of the nanocomposites was measured.

5.4.2. Powder X-Ray Diffraction Study (XRD)

To probe the nature of the constituent materials of both the dressing materials, powder XRD were carried out at 40 kV and 40 mA on a Bruker AXS D8 Advance X-ray diffractometer with Cu Kα1 radiation (λ = 1.54060 Å).

5.4.3. Field Emission Scanning Electron Microscopy (FESEM)

The findings were further substantiated by FESEM study using field emission scanning electron microscope (FESEM), JEOL JSM-7610F. Samples were coated with platinum using sputter coater JEC-3000FC. Further, the energy dispersion X-ray spectrum (EDX) was also performed (SIGMA-01-37, ZEISS). For this, samples were coated with gold using sputter coater EDWARDS A652-01-903.

5.4.4. Confocal Laser Scanning Microscope (CLSM)

Afterwards, high resolution serial bright field images of cotton and nanocomposite impregnated cotton swabs were also collected in 5X objective of CLSM (LSM 880, Zeiss).

5.4.5. *In vitro* Study of Antimicrobial Activity

The antimicrobial activities of both the dressing materials i.e., Fe-Cu-nanocomposite powder and nanocomposite impregnated cotton swabs were determined on Gram positive cocci (GPC), Gram negative bacilli (GNB) and fungi, isolated from samples collected from patients, attending Guwahati Neurological Research Center (GNRC) Medical Outdoor Clinic, by Lawn culture method after getting written consent from them. Isolation of organisms from different clinical specimens was done by streak culture method, for which a single loop of specimen was streaked on a culture plate and

kept for overnight incubation at 37ºC. For different specimens, separate media such as Cysteine Lactose Electrolyte Deficient Agar (CLED) for urine, Nutrient Agar for blood and Sabouraud Dextrose Agar (SDA) medium for fungus were used. To study the antimicrobial activity of both Fe-Cu-nanocomposite powder and Fe-Cu-nanocomposite impregnated cotton swab, a loop of overnight grown microbial colony was inoculated in peptone (5 mL) to prepare a microbial suspension. Then with the help of a swab soaked with the microbial suspension, surface of a Mueller Hinton Agar (MHA) plate for bacteria and MHA with 2% glucose and 0.5% methylene blue for fungus, was smeared. Thereafter, the prepared dressing materials were applied over the inoculated plates followed by overnight incubation at 37 °C. Sensitivity or resistance was ascertained by presence or absence of clear zone of inhibition of bacterial growth around the prepared dressing materials after overnight incubation. To select the best matrix, i.e., powder or thin film (cotton impregnated with nanocomposites) for wound healing and to find out the role of nanoparticles, four different combinations of matrixes were tested (1) Fe-Cu-nanocomposites without iodine, (2) Cu-NPs, (3) Fe-NPs and (4) iodine stabilized Fe-Cu-nanocomposite both in powder and thin film (cotton impregnated with nanocomposites) forms.

5.4.6. Study of Stability of the Prepared Dressing Materials

Stability of both the prepared dressing materials was studied by checking the antimicrobial activity of the dressing materials after one month of preparation on methicillin resistant *S. aureus* (MRSA), *E. coli* and *Candida albicans.*

5.4.7. Quality Comparison with Commercially Available Dressing Materials

Antimicrobial activity of the commercially available dressing materials was tested on GPC (methicillin resistant *S. aureus* -MRSA), GNB (*E. coli*) and fungus (*Candida albicans*) by Lawn culture method.

5.4.8. Animal Experiment

5.4.8.A. *In vivo* Wound Healing Assessment

To assess the wound healing status and effects on dermal tissue of simple diabetic

wound and infection induced diabetic wound after application of both the prepared dressing materials, animal experiments were performed according to institutional ethical guidelines. Approval of the wound healing animal model study was obtained from the Institutional Animal Ethical Committee (IAEC), Institution of Advanced Study in Science and Technology (IASST), Guwahati, Assam. Diabetes was induced in the animals through single intraperitoneal injection of streptozotocin (55 mg/kg) dissolved in citrate buffer of pH 4.5. Diabetes induction was confirmed by determining the fasting blood glucose (FBG) levels. Animals having FBG levels more than 250 mg/dL were considered as diabetic and included in the study. The *in vivo* wound healing experiments were performed using diabetic Wistar albino rats weighing 160-180 gm to evaluate the wound healing ability of the powder Fe-Cu-nanocomposites and cotton patch impregnated with Fe-Cu-nanocomposites on healing and regeneration of the injured skin. Rats were anaesthetized using ketamine (80 mg/kg) and xylazine (10 mg/kg) cocktail and their back hair was shaved using a surgical knife and then a 2 cm diameter full thickness wound was made on the skin of dorsal side of each rat. The infection was induced by methicillin resistant *S. aureus* (MRSA) in the wounds after 24 h of inflicting the wound. Rats were divided into six groups, and four rats were assigned for each group. 3 days after inoculating the infection, treatment started as follows-

Group-I: Diabetic wounds (D.W.) with no infection and treated with normal saline topically.

Group-II: Diabetic wounds (D.W.) with infection and treated with normal saline topically.

Group-III: Diabetic wounds (D.W.) with infection and treated with 0.2 M iodine solution topically.

Group-IV: Diabetic wounds (D.W.) with infection and treated with powder Fe-Cu-nanocomposites.

Group-V: Diabetic wounds (D.W.) with infection and treated with cotton patch impregnated with Fe-Cu-nanocomposites.

Group-VI: Diabetic wounds (D.W.) with infection and treated with conventional topical antibiotic (Mupirocin).

5.4.8.B. Microbial Load Assessment of the Wound Site

Wound healing assessment and bacterial load at the wound site were determined through measuring the colony forming units (CFU) load on day 3, 7, 14 and 21st of the experimental period.

5.4.8.C. Quantitative Analysis of Pro-Inflammatory Cytokines in Blood to Assess Inflammatory Response

The inflammatory response is a critical element of wound healing and for that various inflammatory mediators are released to control the healing process. Pro-inflammatory cytokines are a group of endogenous inflammatory and immune-modulating proteins, which play important roles in the mediation of inflammation. They play a crucial role in initiating and regulating the post-injury response. At the same time, they are also involved in impaired wound healing, sepsis, abnormal scar formation and uncontrolled inflammatory response.[35] Within the cytokine network, interleukin-1b (IL-1b), interleukin-6 (IL-6) and tumour necrosis factor-a (TNF-a) play key roles in initiating an effective inflammatory response.[36-39] Since IL-1β and TNF-α are considered as the initiators of the inflammatory response, determination of the plasma levels of these two cytokines of the rats at the time points specified below was preferred.

Blood from the all the treatment groups were collected through retro orbital route at different time points (0, 3, 7, 14 and 21st day). The blood was centrifuged at 1500 rpm at 4 ºC for 5 min and the serum was collected to measure the inflammatory cytokines (IL-1β and TNF-α) by ELISA kits from R & D systems (USA). According to data supplied by the manufacturer, minimum detection limit for both IL-1β and TNF-α is less than 5 pg/mL and the intra and inter-assay precision is expressed in coefficient of variation (CV%) and proclaimed to be less than 10%. The results were presented as mean values ± SEM (standard error of the mean) of cytokine concentration.

5.4.8.D. Histopathology Assessment

At the end of the drug treatment period, skin tissues from all the treatment groups were collected and the histopathology measurement was performed in order to study the remedial outcome of the prepared dressing materials on the wound tissues microscopically. Surrounding skin of the wound areas were carefully dissected, fixed using 10% neutral buffered formalin, and finally embedded in paraffin to be preserved. Hematoxylin and eosin (H&E) staining were performed to microscopically investigate the quality of the healing process through the qualitative investigation of several parameters such as epithelization, granulation tissue, hemorrhage, inflammatory cells, necrosis, edema and thick epidermis formation. Photographs were taken from different areas of each section.

5.4.9. Toxicity Level Determination by Hemolysis Assay

The toxicity level of the prepared dressing materials was assessed by standard hemolysis assay as follows.

Impending hemolytic possibility of the prepared dressing materials was tested according to the standard protocol.[40] 5 mL of venous blood was collected in a sodium citrate vacutainer (3.8%) from a healthy volunteer. Then the sample was centrifuged at 2000 rpm for 8 min, and the cells were washed three times with sterile isotonic phosphate buffer solution (PBS) (pH 7.2 ± 0.2) following centrifugation at 1500 rpm for 5 min. Different amounts of Fe-Cu-nanocomposite powder (1 mg and 10 mg) and prepared cotton dressing bed (100 mg and 200 mg, which were the weights of Fe-Cu-nanocomposite impregnated cotton swabs) were separately incubated with 10 mL of diluted blood (dilution of 1 mL blood with 9 mL PBS). The incubation was carried out for different time points up to 24 h at 37 °C in silicon test tubes (here the weight of the cotton dressing bed corresponds to weight of cotton plus nanocomposites). Then UV absorbance of the supernatant was measured by UV−vis spectrophotometer at 540 nm at 10 min, and then at 1, 6, 12 and at 24 h following centrifugation at 1500 rpm for 10 min to see the free hemoglobin in the supernatant. Equal amount of PBS was used as

negative control and 1 mL blood mixed with 9 mL normal saline was used as positive control. Each experiment was performed in triplicate at each concentration. The absorbance of negative control was considered as zero (0) percent and positive control as 100 percent. The percentage hemolysis by the tested samples was calculated as follows-

$$\text{Hemolysis (\%)} = \frac{Absorbance\ of\ sample - Absorbance\ of\ negative\ control}{Absorbance\ of\ positive\ control - Absorbance\ of\ negative\ control} \times 100 \quad (5.1)$$

5.5. Results and Discussions

The iodine stabilized blackish Fe-Cu-nanocomposite powder and Fe-Cu-nanocomposite impregnated cotton swabs were fabricated by two–step reactions. The schematic representation of formulation and application of both the dressing materials is illustrated in **Figure 5.1**.

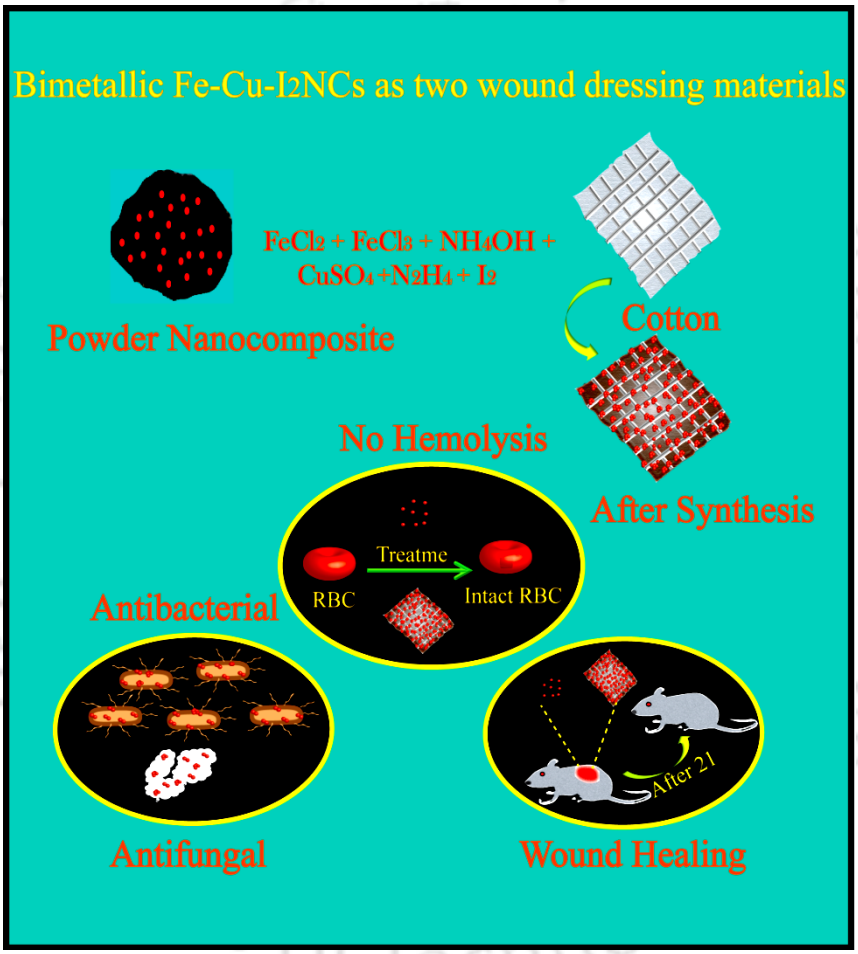

Figure 5.1. Schematic representation of synthesis of bimetallic dressing materials, both in powder form and as obtained through *in situ* synthesis on cotton swab by modified co-precipitation and chemical reduction method, and their utilization as antimicrobial agent and as dressing material for healing of wound.

Iron oxide was formed, initially of $FeCl_2$ and $FeCl_3$ by NH_4OH followed by reduction of $CuSO_4$ by N_2H_4. Following synthesis, both the dressing materials (**Figure 5.2**) were washed thoroughly with Milli-Q grade water to remove the unreacted reagents and then dried in air oven (37 ºC) before using as wound healing matrix.

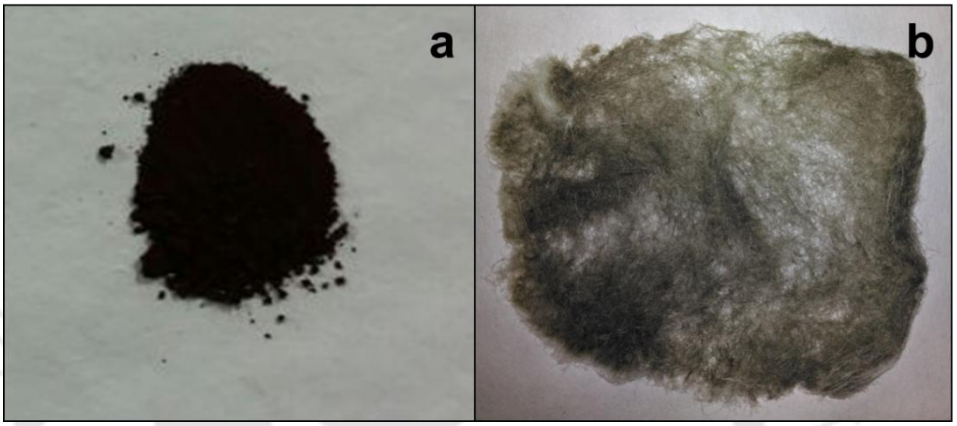

Figure 5.2. Photographs of (a) the dressing material in powder form (Fe-Cu-nanocomposite) and (b) the dressing bed prepared in cotton swab by impregnating bimetallic Fe-Cu-nanocomposite in it.

The presence of nanoparticles in Fe-Cu-nanocomposite powder was confirmed by TEM (**Figure 5.3a**). Distinct SAED patterns (**Figure 5.3b**) with lattice spacing of 0.108, 0.18 and 0.2 nm were indexed to 311, 200 and 111 planes, respectively, of Cu in cubic (fcc) structures. Whereas the values of 0.128 (311) for Cu_2O and 0.127 (104), 197 (112) and 0.205 (012) reflections were for CuO.[41,42] Again the diffraction with prominent ring with interplanar spacing value of 0.171 nm was indexed to 511 planes of Fe_3O_4[43], which confirmed the presence of iron oxide and copper oxide nanoparticles along with Cu in zero oxidation state. The average particle size of the nanoparticles in the prepared powder form of nanocomposites was found to be of 10.4 ± 4.4 nm (**Figure 5.3c**), as calculated from TEM images using Image J software. Similarly, the TEM of Fe-Cu-nanocomposite impregnated cotton swabs were also conducted (**Figure 5.3d**), which validated the synthesis of spherical Fe- Cu containing nanoparticles on cotton swab. At the same time, the diffraction patterns in SAED (**Figure 5.3e**), showed prominent rings with interplanar spacing value of 0.128 and 0.211 nm corresponding to

311 and 200 planes for Cu_2O. The values of 0.107, 0.12, 0.19 nm corresponding to 311, 220 and 111 planes for Cu in cubic (fcc) structures and diffraction at 0.126, 0.157, 0.196, 0.208 nm corresponding to 104, 220, 112 and 012 planes were for CuO.[41,42] Again, the lattice spacing of 0.157 and 0.171 were indexed to 440 and 511 planes of Fe_3O_4[43] and hence confirmed the presence of both Fe and Cu oxide nanoparticles along with Cu in zero oxidation state. The average size of the nanoparticles in the nanocomposites prepared *in situ* on cotton swab was found to be of 14.4± 5.8 nm, as observed in particle size distribution histogram (**Figure 5.3f**).

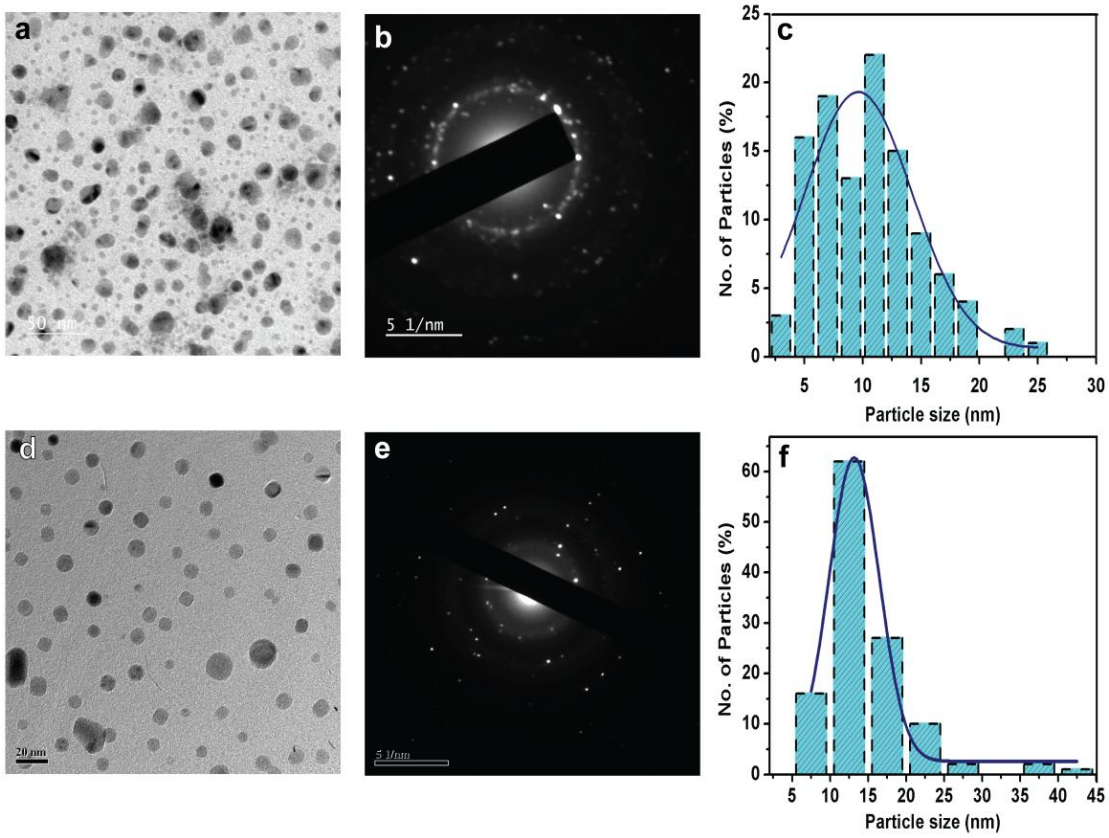

Figure 5.3. (a) TEM image, (b) SAED image and (c) histogram showing particle size distribution of bimetallic Fe-Cu-nanocomposite powder. (d) TEM image, (e) SAED image and (f) histogram showing particle size distribution of Fe-Cu-nanocomposite prepared *in situ* on cotton swab.

Subsequently, powder XRD pursued on both the dressing materials also established the existence of iron oxide and copper oxide NPs in them.

The XRD patterns of Fe-Cu-nanocomposite powder (**Figure 5.4a**) showed diffraction at 2θ values of 24.1^0 (012), 33.3^0 (104), 35.6^0 (110), 40.2^0 (113), 43.2^0 (202), 49.3^0 (024), 54.2^0 (116), 57.6^0 (018), 62.8^0 (214), 64.0^0 (300) and 72.0^0 (119), which suggested the formation of Fe_2O_3. The presence of Fe_3O_4 NPs were confirmed by the peaks obtained at 17.9^0 (111), 21.3^0 (020), 30.5^0 (220), 35.6^0 (311), 43.2^0 (400), 54.2^0 (422), 57.6^0 (511) and 62.8^0 (440).[44-50] Existence of cupric oxide (CuO) and cuprous oxide (Cu_2O) NPs were validated with peaks at 2θ value of 33.3^0 (-110), 35.6^0 (002/11-1), 46.3^0 (-112), 49.3^0 (-202), 57.6^0 (002/202), 61.3^0 (-113), 68.0^0 (113), 75.4^0 (-222) and 36.5^0 (111), 61.3^0 (220), 72.0^0 (311), 75.4^0 (222), respectively.[51-52] Plain cotton swab (**Figure 5.4b**) showed major diffraction at 15.1^0 (101), 16.9^0 (10$\underline{1}$), 23.1^0 (002) and 34.8^0 (040) due to cellulose I.[53] Similarly, powder XRD was also conducted on Fe-Cu-nanocomposite impregnated cotton swab (**Figure 5.4c**) where diffractions at 2θ values of 33.6^0 (104), 41.5^0 (113), 43.7^0 (202), 49.8^0 (024), 54.6^0 (116), 57.7^0 (018), 63.0^0 (214), 64.3^0 (300) and 72.4^0 (119) indicated the formation of Fe_2O_3 NPs whereas peaks at 30.8^0 (220), 43.7^0 (400), 54.6^0 (422), 57.7^0 (511), and 63.0^0 (440) were for Fe_3O_4.[44-50] The peaks at 2θ values of 33.6^0 (-110), 49.8^0 (-202), 53.8^0 (020/20-2), 57.7^0 (002/202), 61.5^0 (-113) and 75.5^0 (-222) suggested the existence of CuO NPs whereas formation of Cu_2O was corroborated by peaks at 2θ values of 36.0^0 (111), 61.5^0 (220), 72.4^0 (311) and 75.5^0 (222).[51-52] Diffraction from cellulose I of cotton swab was observed at 16.6^0 (101) and 23.1^0 (002).[53] The values in the parentheses represent the planes of diffractions as observed in XRD.

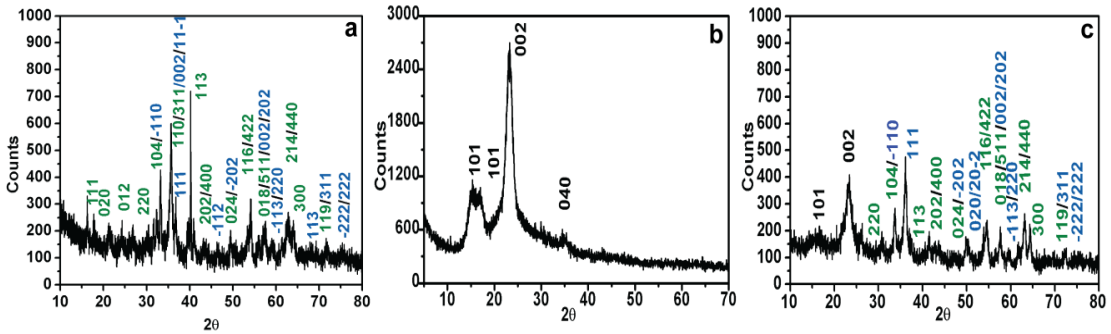

Figure 5.4. XRD patterns of (a) Fe-Cu-nanocomposite powder, (b) plain cotton and (c) Fe-Cu-nanocomposite embedded cotton swab, where peaks marked in black indicate diffractions due to cellulose, green for Fe_2O_3/Fe_3O_4 and blue is for Cu_2O/CuO.

Findings were further supported by field emission scanning electron microscopy (FESEM) of both Fe-Cu-nanocomposite powder and Fe-Cu-nanocomposite impregnated cotton swab. The field emission scanning electron micrograph of Fe-Cu-nanocomposite powder (**Figure 5.5a**) along with its magnified image (**Figure 5.5b**) clearly demonstrated the nanocomposite formation. Next the field emission scanning electron micrograph of only cotton was carried out (**Figure 5.5c**, with magnified image inset), which showed surface morphology of cotton. Whereas, **Figure 5.5d** i.e., the image (with the magnified image in the inset) of Fe-Cu-nanocomposite impregnated cotton revealed nanocomposite formation on the cotton. The formation of nanoparticles was evident on each of the strands of cotton where nanoparticles were found to be mostly agglomerated.

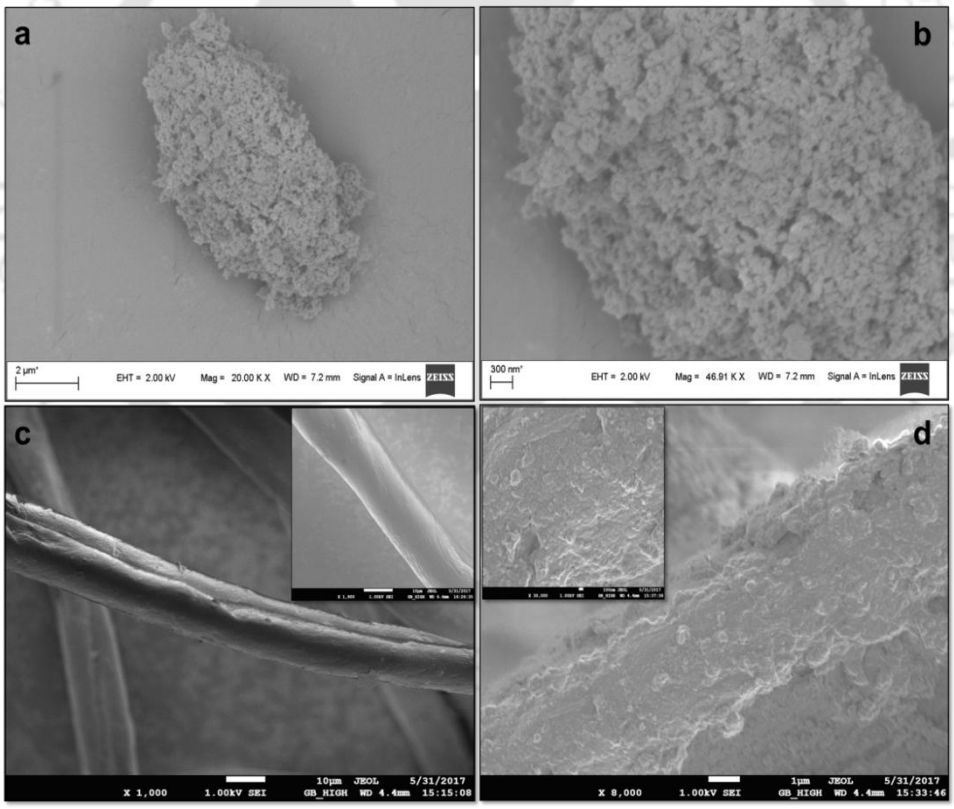

Figure 5.5. FESEM image of (a) Fe-Cu-nanocomposite powder and (b) magnified image of the same FESEM image of (c) cotton (inset is the magnified image) and (d) that of Fe-Cu-nanocomposite impregnated cotton swab. Insets represent magnified images of those in (c) and (d), respectively.

To find out the element distribution, the energy dispersive X-ray spectrum (EDX) was also pursued during FESEM analysis from which the existence of both iron and copper in both the dressing materials was confirmed. In the powder nanocomposite 16.9 and 31.9 in weight % of iron and copper, respectively were estimated (**Figure 5.6b**), whereas 15.2 and 20.5 in weight % of iron and copper were found in case of nanocomposite impregnated cotton (**Figure 5.6d**).

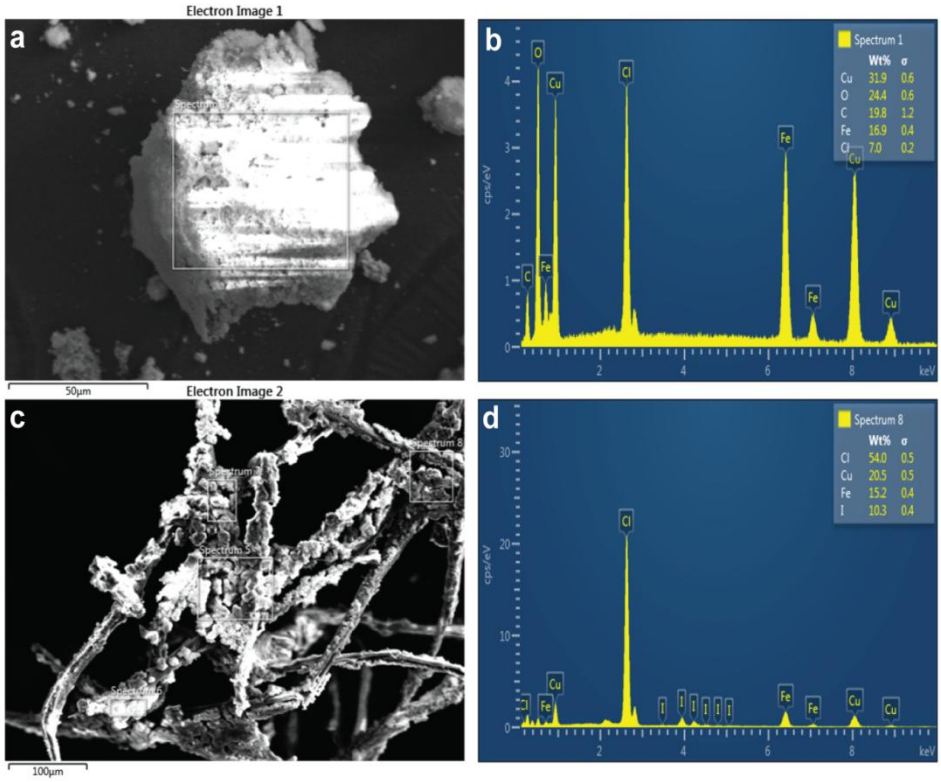

Figure 5.6. (a) FESEM micrograph of Fe-Cu-nanocomposite powder and (b) EDX result for a specific spot on the nanocomposite. (c) FESEM micrograph of Fe-Cu-nanocomposite impregnated cotton swab and (d) EDX result for a specific spot on the nanocomposite impregnated cotton.

To further support the findings, bright field images of plain cotton and nanocomposites impregnated cotton swabs were captured in confocal microscope (as depicted in **Figure 5.7a** and **Figure 5.7b**), respectively, which also clearly illustrated the formation of nanocomposites on cotton fiber. The validated dressing materials were then tested for practical application, i.e., for infection control and wound healing.

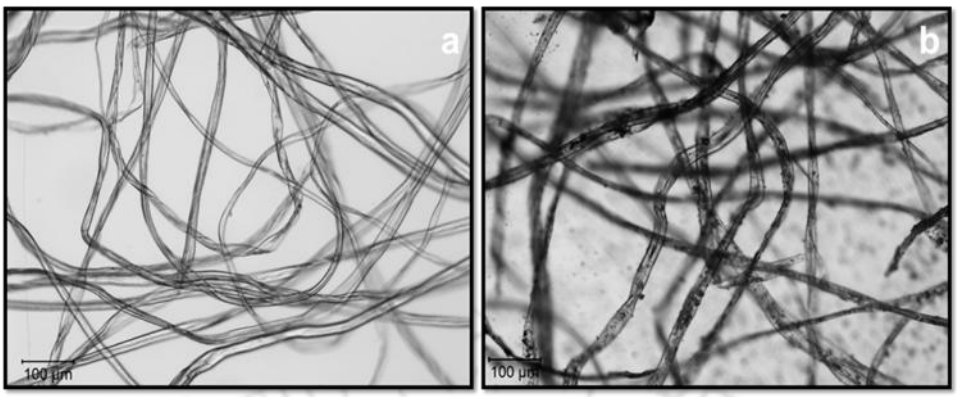

Figure 5.7. Bright field image of (a) cotton and (b) nanocomposite impregnated cotton swab recorded using the confocal microscope.

To check the efficacy of the synthesized wound healing materials (powder and cotton swab) first *in vitro* antimicrobial property of both the dressing materials were tested on pathogenic strains of *S. aureus*, *E. coli*, as well as the opportunistic dermal pathogen *Candida albicans*. For this, different combinations such as (1) Fe-Cu-nanocomposites without iodine, (2) Cu-NPs, (3) Fe-NPs and (4) iodine stabilized Fe-Cu-nanocomposites both in powder and cotton impregnated with nanocomposites were tested on both GPC and GNB. It was observed that both Fe-Cu-nanocomposite powder and nanocomposite impregnated cotton swab stabilized with iodine demonstrated better results than the other materials. The Fe-Cu-nanocomposite powder showed a zone of inhibition of 25 mm (**Figure 5.8a 4**) against Gram positive methicillin resistant *S. aureus* and 22 mm (**Figure 5.8b 4**) against Gram negative *E. coli*. Further, the Fe-Cu-nanocomposite impregnated cotton swab showed a clear zone of inhibition of 26 mm against both Gram positive (**Figure 5.8c 4**) and Gram negative organisms (**Figure 5.8d 4**). Cu NPs (both powder and Cu NPs impregnated cotton) showed a zone of inhibition of about 10 mm against both GPC and GNB, which was noticeably less than that of Fe-Cu-nanocomposites (both powder and nanocomposite impregnated cotton). Whereas minimum zone of inhibition was observed in case of powder Fe NPs; however, the Fe NPs impregnated cotton failed to arrest the growth of both GPC and GNB as observed in **Figure 5.8c 3** and **Figure 5.8d 3**. The antimicrobial response produced by other materials, for which tests were carried out, was less compared to Fe-Cu-

nanocomposite that was stabilized by 0.2 M molecular iodine. This was observed for both the powder form of nanocomposite and the nanocomposite impregnated cotton. This is probably because of synergistic action of Cu NPs and iodine. Thus, iodine stabilized Fe-Cu-nanocomposite powder and Fe-Cu-nanocomposite impregnated cotton swab, which exhibited better antimicrobial activity against GPC and GNB, were chosen as two dressing materials for further experiments.

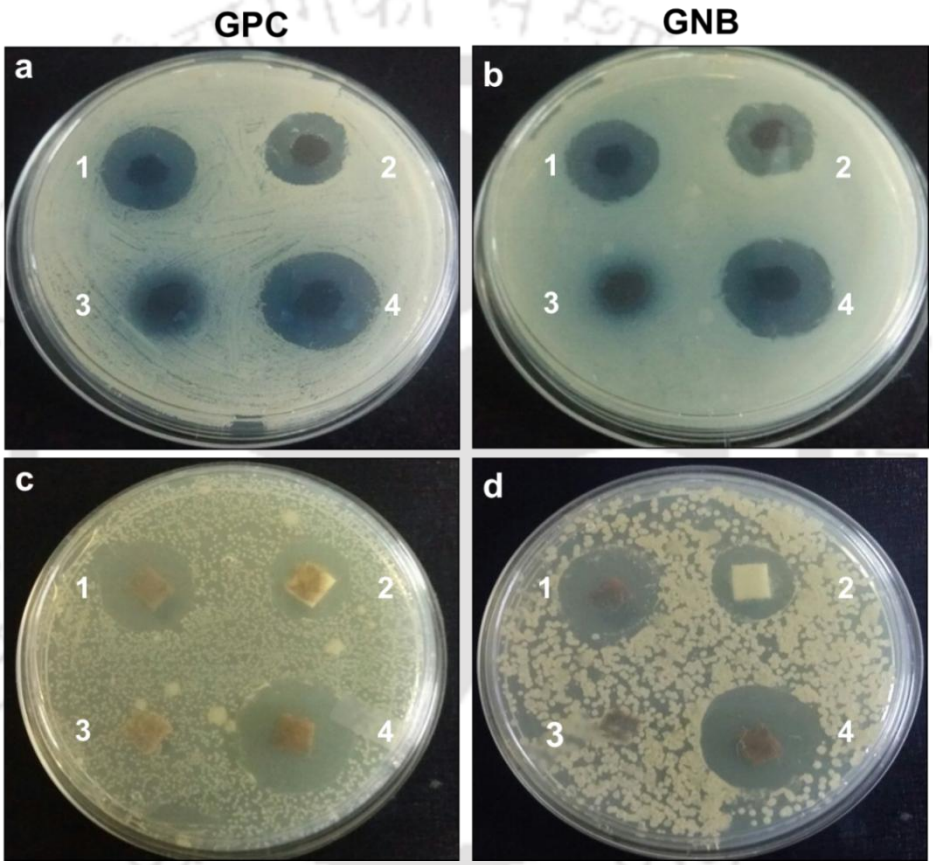

Figure 5.8. Antibacterial activity of the nanocomposite powder on (a) Gram positive cocci (methicillin resistant *Staphylococcus aureus*) and (b) Gram negative bacilli (*Escherichia coli*). Antibacterial activity of cotton swabs embedded with nanocomposite on (c) Gram positive cocci (methicillin resistant *Staphylococcus aureus*) and (d) Gram negative bacilli (*Escherichia coli*) plated on MHA where (1) represents Fe-Cu-nanocomposites without iodine, (2) Cu NPs, (3) Fe NPs and (4) iodine stabilized Fe-Cu-nanocomposite.

Subsequently, both the dressing materials were tested on fungus (*Candida albicans*), which also displayed antifungal activity with a clear zone of inhibition of about 20 mm (**Figure 5.9a & 5.9b**). All the organisms tested here were isolated from

urine samples of patients. Thus, both the dressing materials (powder and cotton swab) were proved to be efficient antimicrobial agent against pathogenic strains of *S. aureus*, *E. coli*, and the opportunistic dermal pathogen *Candida albicans*.

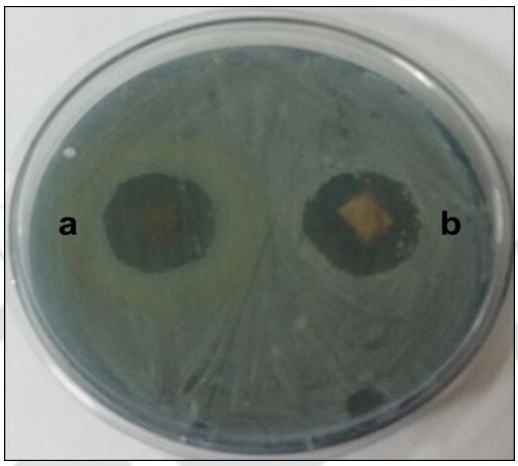

Figure 5.9. Antimicrobial activity of (a) bimetallic Fe-Cu-nanocomposite powder and (b) cotton swabs embedded with bimetallic Fe-Cu-nanocomposites on fungus (*Candida albicans*) as plated on MHA with 2% glucose and 0.5% methylene blue.

Following *in vitro* antimicrobial experiments of all the prepared dressing materials on methicillin resistant *S. aureus* and *E. coli*, the zone of inhibition of microbial growth (both GPC and GNB) produced by each prepared material was measured and statistical analysis was done. As illustrated in **Figure 5.10**, there was noticeable difference between the zone of inhibition produced by iodine stabilized Fe-Cu-nanocomposites (both powder and impregnated cotton forms) and the other materials like Fe NPs, Cu NPs, and Fe-Cu-nanocomposites prepared without iodine. The statistically significant difference in the microbial growth arrest produced by Fe-Cu-nanocomposite (which was stabilized by adding 0.2 M molecular iodine) and Fe-Cu- nanocomposite that was prepared without adding iodine (both powder and cotton) on both GPC and GNB suggested that molecular iodine might have a role in the observed activity. It has been already documented that iodine has capacity to arrest growth of microbes; however, at a concentration that had been used in the study, only iodine exhibited minimal bactericidal properties.[23,34] Consequently, it can be assumed

that besides providing stability, molecular iodine had enhanced the antimicrobial property of both the dressing materials, and may be through a synergistic action. Thus, all the findings of the *in vitro* antimicrobial study supported the utility of both the dressing materials to control infection caused by multi drug resistant strains of bacteria as well as fungus.

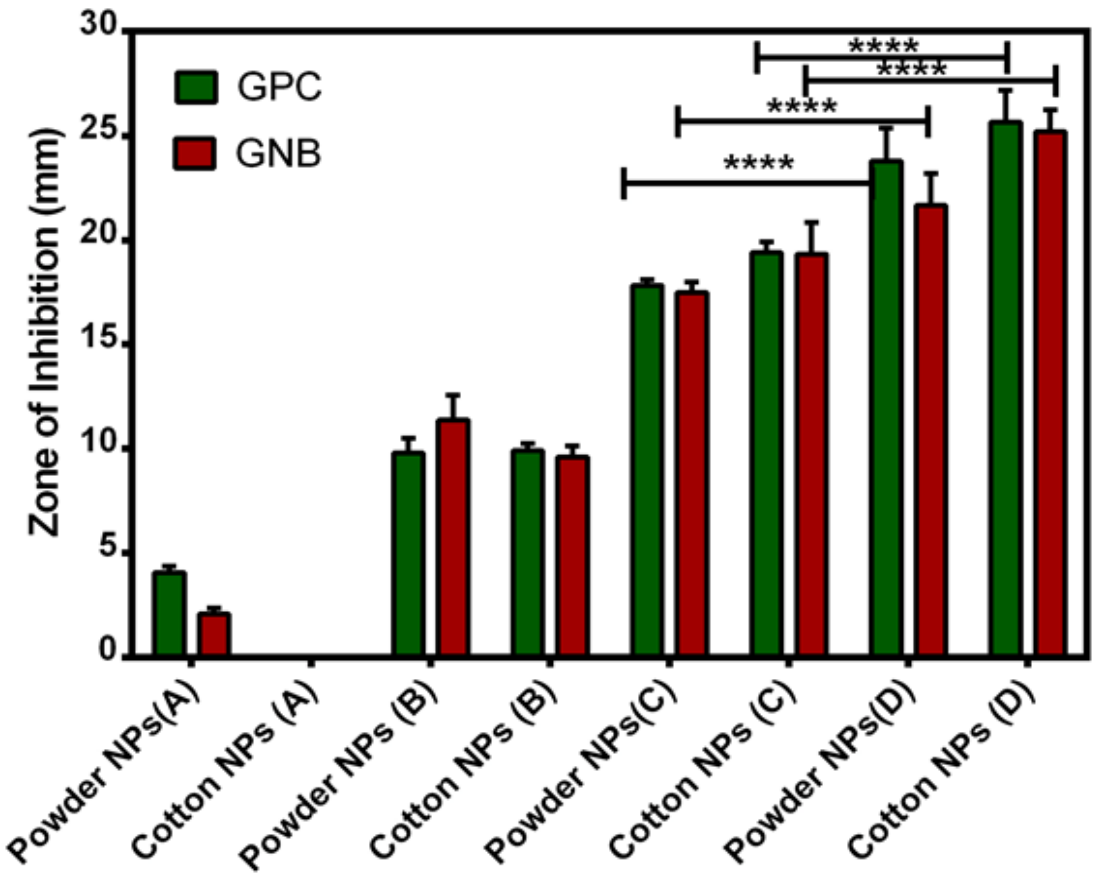

Figure 5.10 . Comparison of the antimicrobial activities (in terms of zone of inhibition) of the (different) prepared materials against methicillin resistant *S. aureus* (GPC) and *E. coli* (GNB). Here powder NPs (A) represents FeNPs in powder form, cotton NPs (A) represents FeNPs impregnated cotton, powder NPs (B) represents CuNPs in powder form, cotton NPs (B) represents CuNPs impregnated cotton, powder NPs (C) represents Fe-Cu-nanocomposite in powder form prepared without iodine, cotton NPs (C) represents Fe-Cu-nanocomposite impregnated cotton prepared without iodine, powder NPs (D) represents powder Fe-Cu-nanocomposite stabilized with iodine and cotton NPs (D) represents Fe-Cu-nanocomposite impregnated cotton stabilized with iodine.

Both copper and iron NPs are prone to oxidation in presence of air and water, which make them unstable.[27,29] As mentioned earlier, iodine was used to make them stable herein. However, it was deemed necessary to check the stability over a longer period of time. For this, both the dressing materials were tested after one month of their preparations and verified their antimicrobial property on methicillin resistant *S. aureus* (GPC), *E. coli* GNB) and *Candida albicans* (fungus). It was observed that the microbial growth was equally arrested in presence of both the dressing materials irrespective of their time of preparation (**Figure 5.11**). The results thus indicated that their stability did not get affected even one month after preparation.

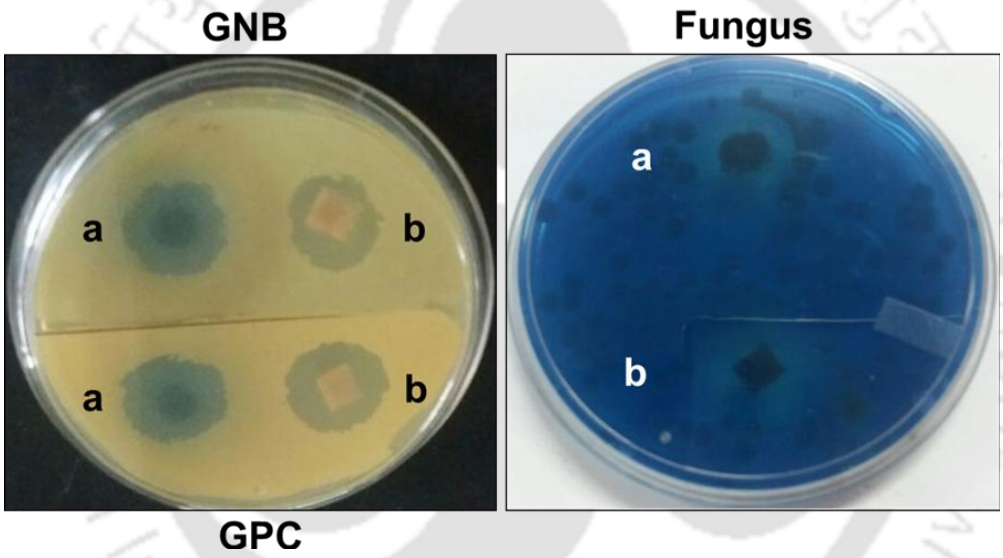

Figure 5.11. Plate with growth of both GPC (*S.aureus*)-lower left, GNB (*E.coli*)-upper left and fungus (*C.albicans*)-right, showing clear zone of inhibition around (a) powder NPs and (b) cotton NPs tested one month after preparation.

Next, the antimicrobial capability of both the dressing materials was compared with a commercially available dressing material. It was observed that, the zones of microbial growth inhibition produced by both Fe-Cu-nanocomposite powder (**Figure 5.12a-left**) and Fe-Cu-nanocomposite impregnated cotton (**Figure 5.12a-right**) were noticeably bigger than that produced by the commercial dressing bed (**Figure 5.12b**), as tested on both GPC (**Figure 5.12a** and **Figure 5.12b-top**) and GNB (**Figure 5.12a** and **Figure 5.12b-bottom**). With the use of the current dressing materials, a zone of

inhibition of 25-26 mm against GPC and 22 mm against GNB was observed. However in case of commercial dressing material, though in case of GPC (**Figure 5.12b-top**), the zone of inhibition was almost similar to that of the current dressing materials, but in case of GNB (**Figure 5.12b-bottom**), there was noticeably minimal zone of inhibition observed. Further, the commercial material failed to arrest the growth of fungus (**Figure 5.12d**); whereas, both the nanocomposites in powder form (**Figure 5.12c-left**) and nanocomposite impregnated cotton (**Figure 5.12c-right**) produced a visible zone of fungal growth arrest of about 20 mm diameter. Thus, both the dressing materials can be considered to have broad spectrum antimicrobial affect.

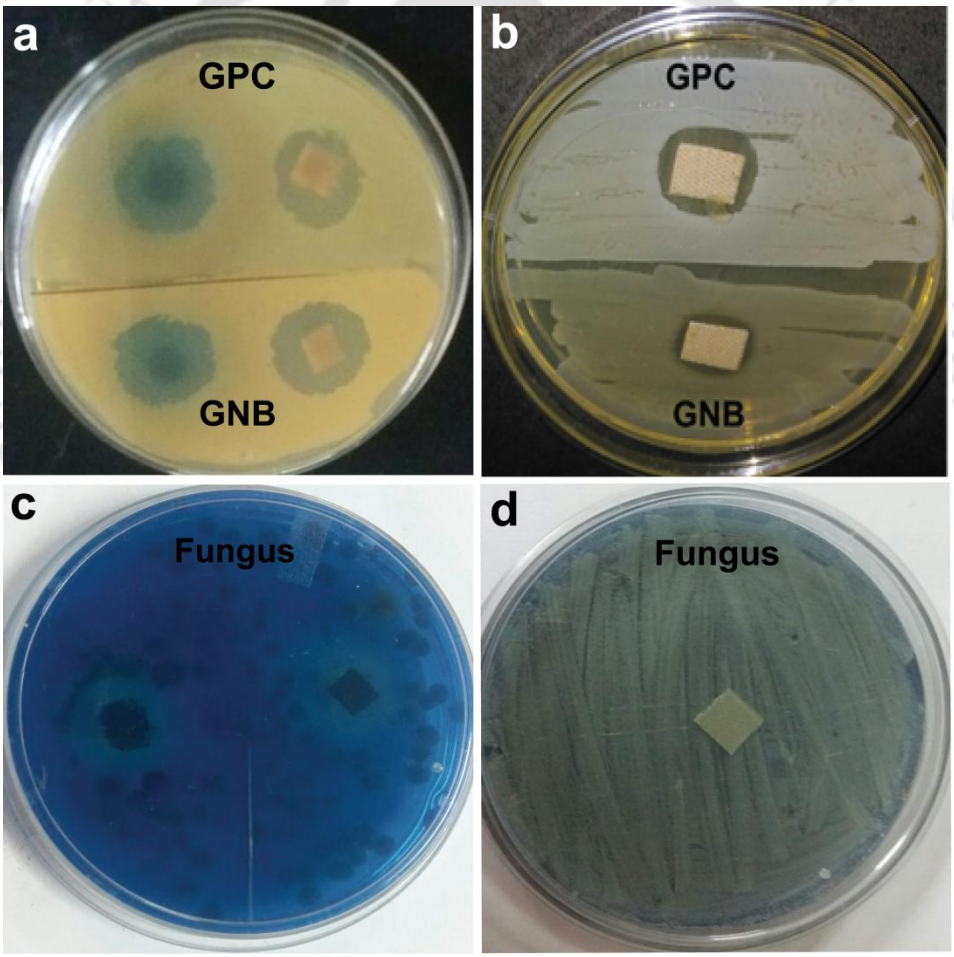

Figure 5.12. Antimicrobial activity of commercially available dressing material along with Fe-Cu-nanocomposite powder and Fe-Cu-nanocomposite embedded cotton on methicillin resistant *S. aureus* (GPC) *E. coli* (GNB) and fungus (*Candida albicans*).

Based on the accomplishment of the *in vitro* antimicrobial study, the next target was to check the efficacy of both the dressing materials on animal model for *in vivo* wound healing assessment. Considering the high prevalence of diabetic foot ulcer [7,8] and chances of development of secondary infection of these wounds, the healing ability of both the dressing materials were examined in infected diabetic wounds. For this, diabetes was introduced in these animal models following inflicting wound and inducing infection by methicillin resistant *S. aureus* (MRSA). Then to assess the remedial effects of the dressing materials on dermal tissues of simple diabetic wound and infection induced diabetic wound, experiments were performed with 24 Wistar albino rats. The rats were divided into six groups. Subsequently, treatment started with the dressing materials as described in the experimental section. The total treatment period was for 21 days. It was observed that the infected diabetic wounds of the 4th and 5th groups i.e., groups treated with the prepared dressing materials (both powder nanocomposite and cotton impregnated with nanocomposite) showed faster healing (**Figure 5.13m-t**) than the 3rd group for which only iodine was used for treatment (**Figure 5.13i-l**). It is to be mentioned here that as molecular iodine is a known antimicrobial agent, the wound healing efficacy of iodine was also carried out in the animal model separately (the 3rd group here). The wounds of the 4th and 5th groups healed completely with minimum residual scar marks after 21 days, similar to that of the simple diabetic negative control group (Figure **5.13a-d**). However, infection induced diabetic wounds without any treatment revealed slower rate of healing (**Figure 5.13e-g**) and ultimately the rats succumbed to injury (**Figure 5.13h**) after 14 days of initiation of treatment. The results indicated the remedial effect of the prepared dressing materials on dermal tissue even in the presence of bacterial infection.

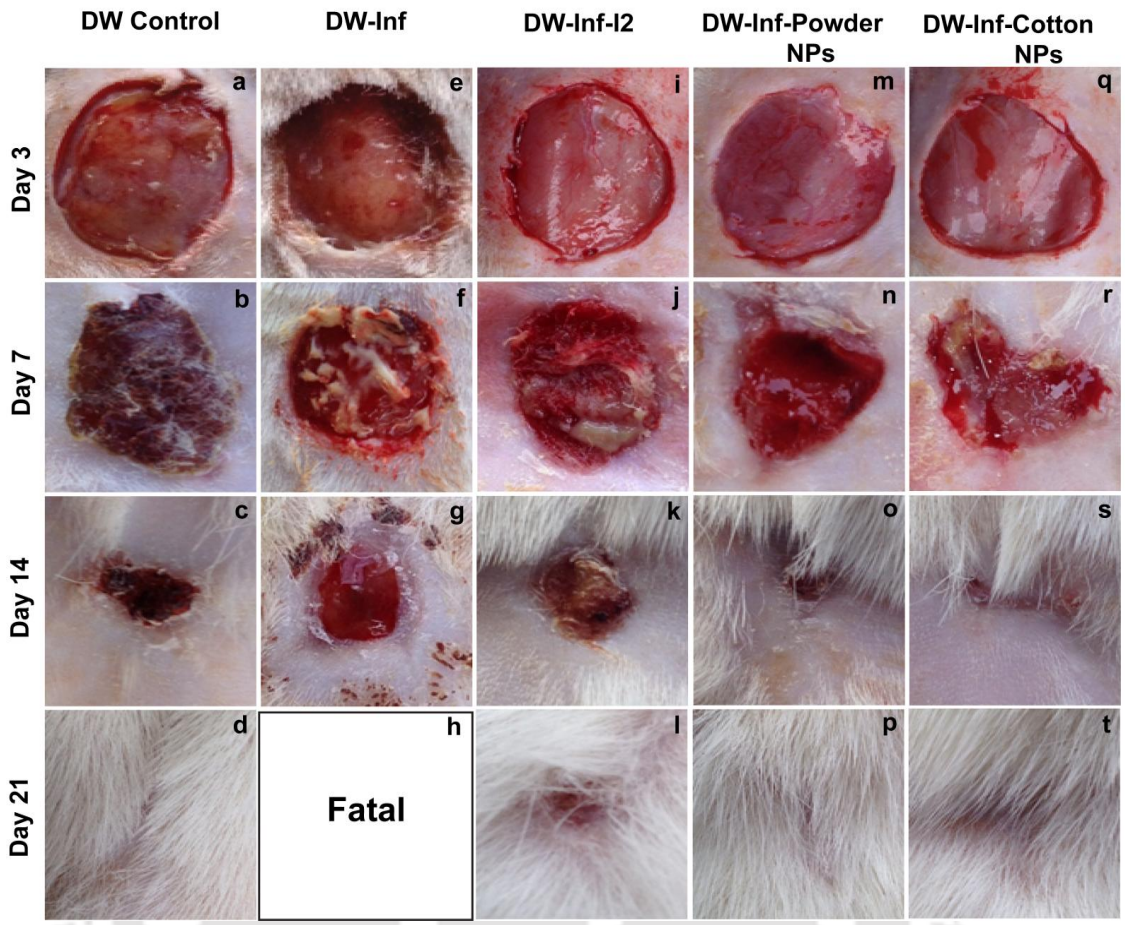

Figure 5.13. Photographs representing *in vivo* study on the effects of treatment with prepared wound healing materials on methicillin resistant *S. aureus* infection induced diabetic wounds on rats. Fig. (a-d) - represent untreated simple diabetic wound, Fig. (e-h) - represent untreated infected diabetic wound, Fig. (i-l) - represent infected diabetic wound treated with 0.2 M iodine solution, Fig. (m-p) -represent infected diabetic wound treated with powder nanocomposite and Fig. (q-t) - represent infected diabetic wound treated with nanocomposite impregnated cotton swab. Wound photographs of the rats taken on day 3 (Fig. a, e, i, m and q), day 7 (Fig. b, f, j, n, and r), day 14 (Fig. c, g, k, o and s) and day 21 (Fig. d, h, l, p and t) of initiation of treatment.

To compare the effectiveness of wound healing property of the prepared dressing materials with conventional antibiotics, topical antibiotic (Mupirocin) was chosen. Interestingly, it was found that the prepared dressing materials displayed almost similar action with that of mupirocin (**Figure 5.14**). Although on day 7 (**Figure 5.14d-f**) wounds treated with antibiotic appeared better that the wounds treated with the prepared dressing materials; however, at the end of day 21 (**Figure 5.14j-l**) these

wounds appeared to be healed completely in comparison to the wounds treated with antibiotic. In the group treated with antibiotic, evidence of residual scar was noticed (**Figure 5.14j**).

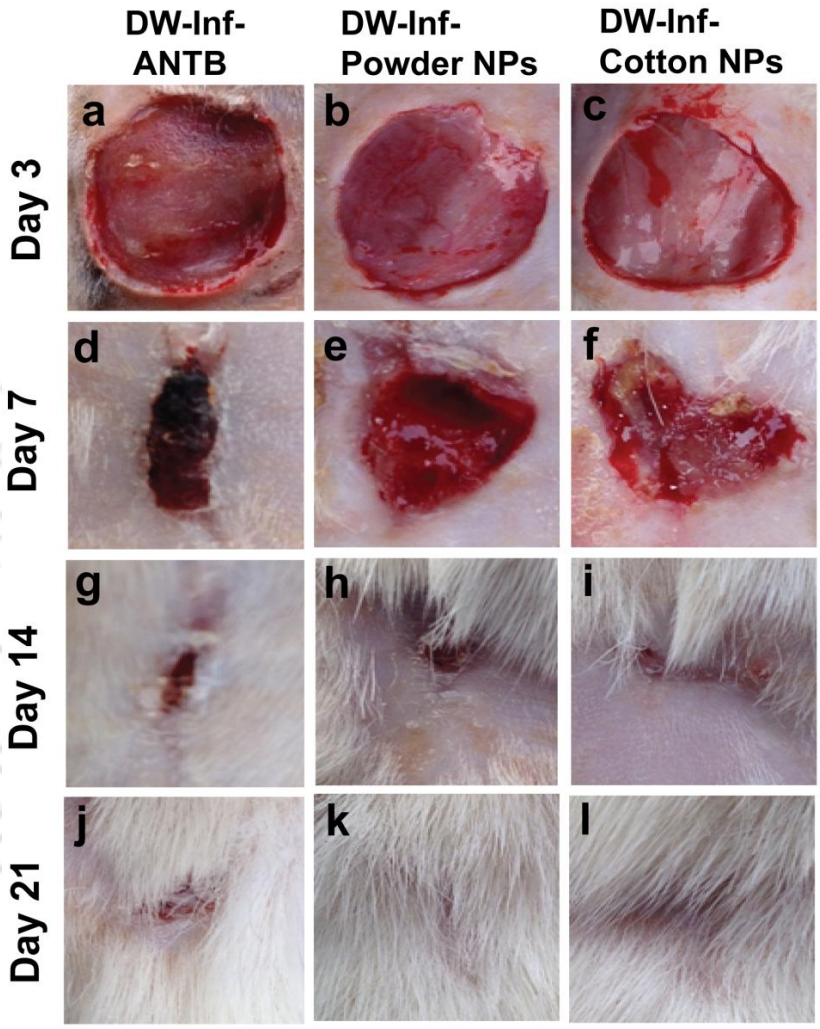

Figure 5.14. Photographic images showing comparison of the effects of treatment with conventional topical antibiotic and the currently reported wound healing materials on methicillin resistant *S. aureus* induced diabetic wound on rats.

Simultaneously, with the *in vivo* wound healing assessment, microbial load assessment of the wound site was also performed by measuring the colony forming units (CFU) load on day 3, 7, 14 and 21st of the experimental period. The microbial

assessment of the wound site of different groups revealed that, from day 7 onwards, the number of colony started decreasing in all the treated groups (i.e., groups treated with iodine solution (0.2 M), Mupirocin, powder nanocomposite and nanocomposite impregnated cotton). It was observed that, there was statistically significant reduction in the colony count between the treated and untreated groups on day 14 and day 21. Even both the treated groups i.e., group treated with nanocomposite powder and nanocomposite impregnated cotton showed significant decrease in number of bacterial colonies in comparison to the group treated with only iodine (**Figure 5.15**), which also confirmed that iodine alone at a concentration that had been used in the study exhibited insignificant antimicrobial efficacy.

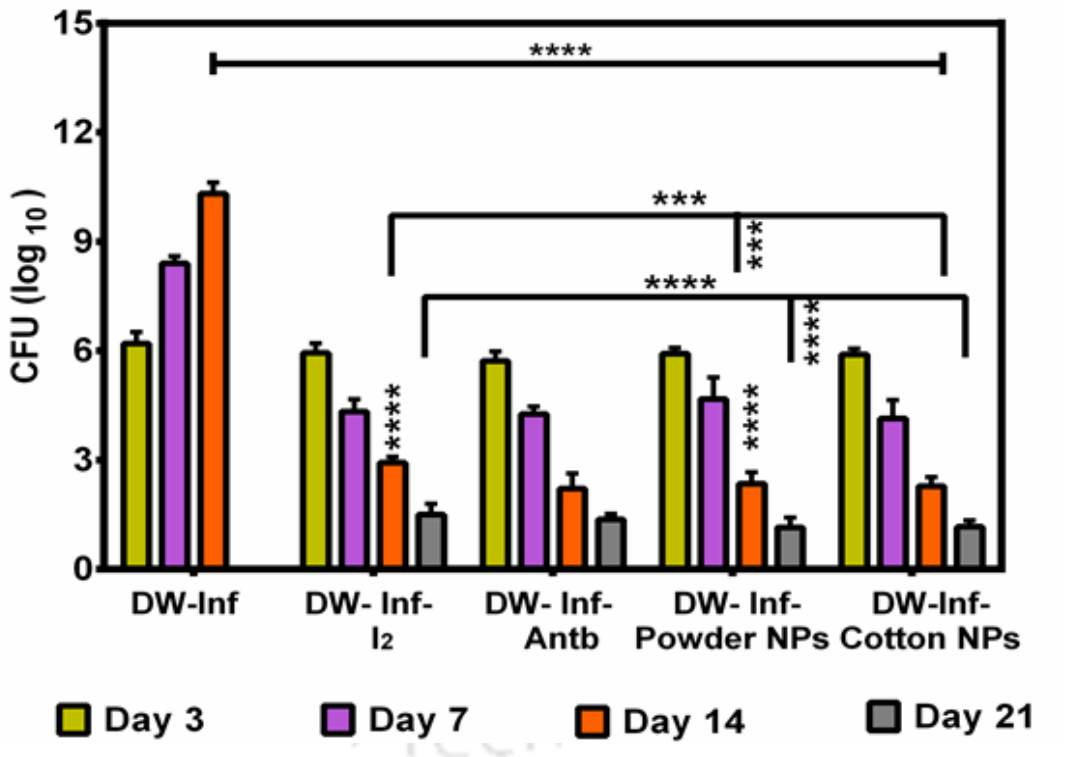

Figure 5.15. Number of colony forming bacteria at the wound site of different infected groups on day 3, 7, 14 and 21 where, DW-Inf represents rat with infected diabetic wound, DW-Inf-I_2- rat with infected diabetic wound treated with iodine, DW-Inf-Antb- rat with infected diabetic wound treated with conventional topical antibiotic, DW-Inf-powder NPs- rat with infected diabetic wound treated with nanocomposites powder and DW-Inf-Cotton NPs- rat with infected diabetic wound treated with nanocomposites impregnated cotton.

Concurrently with the *in vivo* animal experiments, estimation of the serum cytokines was done. As pro-inflammatory cytokines, mainly IL-1β and TNF-α, play crucial roles in wound healing, serum level estimation of the same was done at different time-point intervals during the experiment to probe the probable role of the dressing materials in altering cytokine levels in blood. As illustrated in **Figure 5.16**, there was significant reduction in the amount of both IL-1β and TNF-α between the treated groups i.e., groups treated with only iodine solution (0.2M), treated with mupirocin, treated with powder nanocomposite and nanocomposite impregnated cotton. In all the groups (except control group), both plasma IL-1β and TNF-α reached their maximum level on day 3 and thereafter, they gradually decreased and touched the normal limit on day 21 except for the untreated infected group where an increasing trend was noticed. Even there was a significant difference between the group treated with iodine and the groups treated with both dressing materials. So the findings supported that both the dressing materials could control infection and thus helped in healing the wounds by modulating serum levels of cytokines.

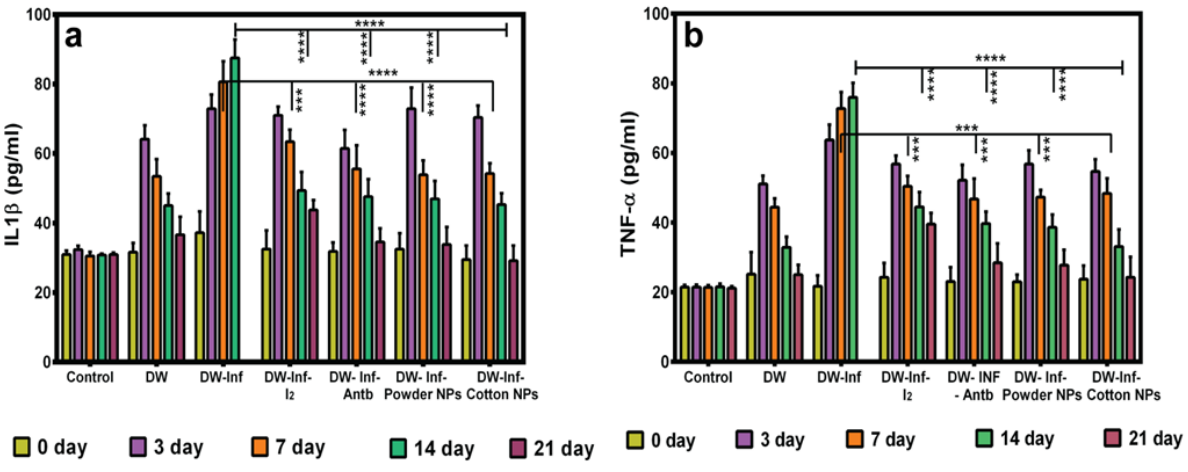

Figure 5.16. Serum values of (a) IL-1β and (b) TNF-α of different tested groups on day 0, 3, 7, 14 and 21, where control represents normal rat, DW- rat with diabetic wound, DW-Inf- rat with infected diabetic wound, DW-Inf-I_2- rat with infected diabetic wound treated with iodine, DW-Inf-Antb- rat with infected diabetic wound treated with conventional topical antibiotic, DW-Inf-powder NPs- rat with infected diabetic wound treated with nanocomposite powder and DW-Inf-Cotton NPs- rat with infected diabetic wound treated with nanocomposite impregnated cotton.

Next, to study the cellular manifestations of infections, representative hematoxylin and eosin (H and E) stained histopathological examination was done at the end of the drug treatment. The images of non-infected diabetic wound (DW Control) showed normal skin with intact epidermis, dermis, a few hair follicles and sebaceous glands. There was no discernible inflammation in the mentioned sections (**Figure 5.17a-d**). Section from the untreated infected diabetic wound (DW + Inf) showed ulcerated skin with heavy infiltrations of inflammatory cells, mostly polymorphs along with the presence of edema, hemorrhages, necrosis and suppuration (**Figure 5.17e-h**). However, sections from all the treated groups (i.e., with 0.2 M iodine, powder nanocomposite and nanocomposite impregnated cotton bed) did not show any inflammatory activity except for a few minute foci of degenerating polymorphs, which is a sign of healing process. No hemorrhage, edema and necrosis were observed at the wound site (**Figure 5.17i-t**). The results once again established the therapeutic utility of both the dressing materials against infected wound not only by annihilation of bacteria but also by modulating the inflammation.

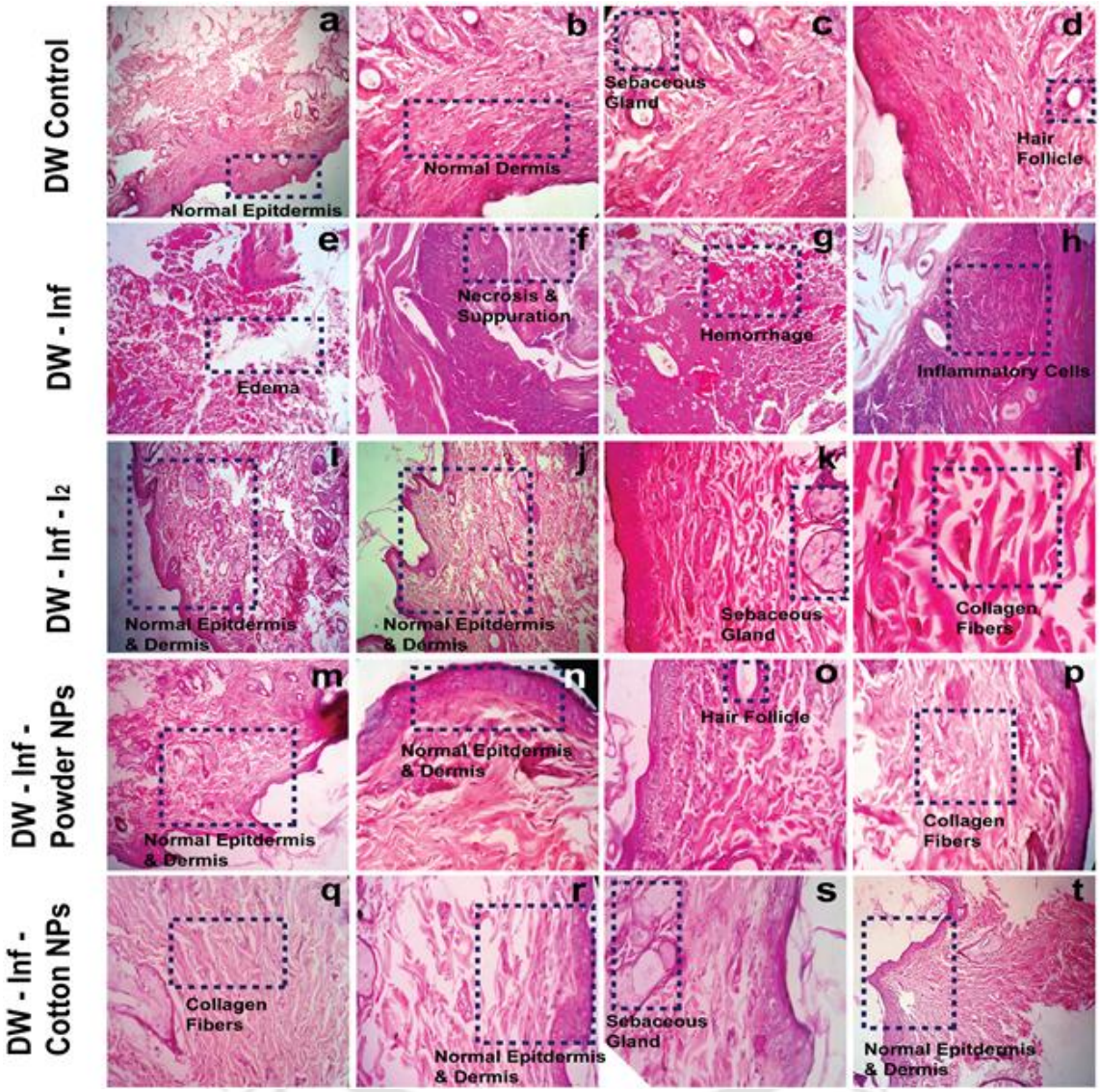

Figure 5.17. Hematoxylin and eosin (H and E) staining of dermal tissue of rats where tissues were collected from (a-d) uninfected simple diabetic wound (DW Control), (e-h)) infected untreated diabetic wound (DW-Inf), (i-l) infected diabetic wound treated with (0.2 M) iodine (DW-Inf-I_2), (m-p) infected diabetic wound treated with nanocomposite powder (DW-Inf-Powder NPs) and (q-t) infected diabetic wound treated with cotton embedded with nanocomposite (DW-Inf-Cotton NPs).

After obtaining satisfactory results in animal model for *in vivo* wound healing and infection control, impending hemolytic possibilities by the use of the dressing materials

were assessed in order to ensure the safe utility of the same. For this purpose, the toxicity level of the prepared dressing materials was assessed by standard hemolysis assay. Findings of the hemolysis assay revealed that both the prepared dressing materials exhibited low to mild hemolytic activity (percentage hemolysis) towards human erythrocytes. The tested samples demonstrated concentration-dependent hemolysis of human erythrocytes (**Figure 18a and 18b**). Both the components of the prepared dressing materials, namely, iron and copper, are regarded as biocompatible and safe as both Fe and Cu are considered as essential elements for living organisms and are natural constituent of plant and animal tissues. Also, human body has mechanisms to protect against copper toxicity to some extent. Moreover, cotton swabs that were used in the experiment are considered as bio-inert and safe, as they have been used as dressing materials safely since ages. The permissible limit of hemolysis for blood containing biomaterial is 5%,[54] whereas both the dressing materials of our experiment exhibited a maximum of 0.29 % (nanocomposites powder) and 0.32 % (cotton impregnated with nanocomposites) of hemolysis. Hence the results of our study indicated that both the prepared dressing materials do not have hemolytic components on their surface and can possibly be used for infection control and healing of wound.

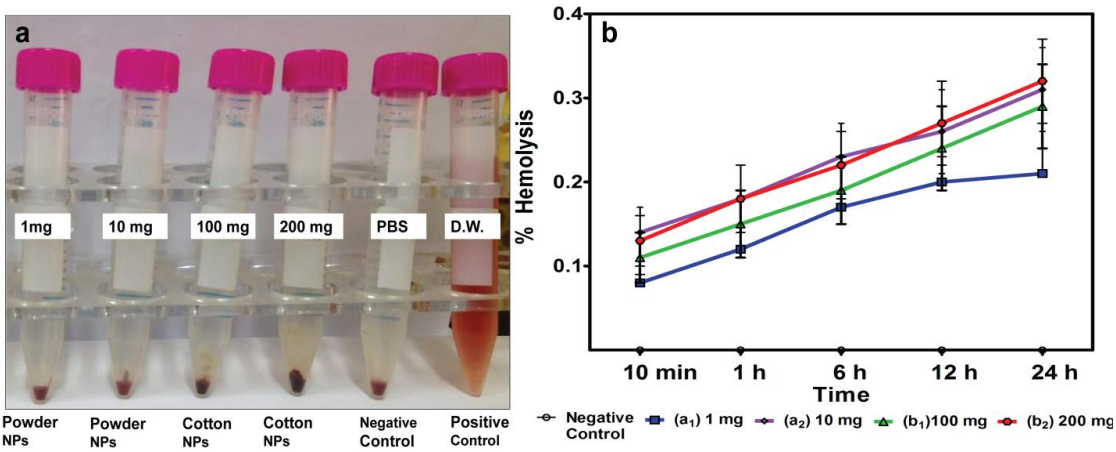

Figure 5.18. (a) Photograph of time dependent hemolysis test samples. (b) Graphical presentation of the hemolysis test results where (a_1) and (a_2) represent concentrations of powder nanocomposite; whereas (b_1) and (b_2) represent nanocomposite embedded cotton swabs used for the experiment.

5.6. Conclusion

Several dressing materials are commercially available, and at the same time, research is being pursued to formulate new materials for better and faster healing of wounds. However, an important challenge is to attain multifunctional property in the same matrix that not only can control infection by resistant strain of microbes, but also can assist in faster healing. In this context, a bimetallic multifunctional dressing material was prepared both in powder and thin film forms that exhibited antimicrobial activity against a wide range of microbes, including methicillin resistant *Staphylococcus aureus* (MRSA) and at same time displayed *in vivo* wound healing property. The prepared biocompatible dressing materials may be useful for management of both acute and chronic infected wounds. Thus, trials of these engineered dressing materials at human level may have a promising future in delivering a healing touch at an affordable cost.

5.7. References

1. Díez-Pascual, A. M.; Díez-Vicente, A. L. *Biomacromolecules* **2015**, *16* (9), 2631–2644.
2. Jones, I.; Currie, L.; Martin, R. *Br. J. Plast. Surg.* **2002**, *55*, 185–193.
3. Parani, M.; Lokhande, G.; Singh, A.; Gaharwar, A. K. *ACS Appl. Mater. Interfaces* **2016**, *8* (16), 10049–10069.
4. Gurtner GC , Werner S, Barrandon Y, L. M. *Nature.* **2008**, *15* (453), 314–321.
5. Paul, W.; Sharma, C. P. *Trends Biomater. Artif. Organs* **2004**, *18* (1), 18–23.
6. Harding, K. G.; Morris, H. L.; Patel, G. K. *BMJ* **2002**, *324* (January), 160–163.
7. Shahi, S. K.; Kumar, A.; Kumar, S.; Singh, S. K.; Gupta, S. K.; Singh, T. *J. Diabet. Foot Complicat.* **2012**, *4* (4), 83–91.
8. Singh, N.; Armstrong, D.G.; Lipsky, B.A. *JAMA.* **2005**, *293* (2), 217-228.
9. Chattopadhyay, S.; Raines, R. T. *Biopolymers.* **2014**, *101* (8), 821–833.
10. Liane I.F. Moura , Ana M.A. Dias, E. C.; Sousa, H. C. de. *Acta Biomater.* **2013**, *9* (7), 7093–7114.
11. Hu, M. S.; Maan, Z. N.; Wu, J. C.; Rennert, R. C.; Hong, W. X.; Lai, T. S.; Cheung,

A. T. M.; Walmsley, G. G.; Chung, M. T.; McArdle, A.; et al. *Ann. Biomed. Eng.* **2014**, *42* (7), 1494–1507.

12. Zhang, L.; Webster, T. J. *Nano Today* **2009**, *4* (1), 66–80.
13. Carrow, J. K.; Gaharwar, A. K. *Macromol. Chem. Phys.* **2015**, *216* (3), 248–264.
14. Mei, L.; Lu, Z.; Zhang, X.; Li, C.; Jia, Y. *ACS Appl. Mater. Interfaces* **2014,** 6, 15813-15821.
15. Tiwari, M.; Narayanan, K.; Thakar, MB.; Jagani, HV.; Venkata, R. J. *IET Nanobiotechnol* **2014**, 8 (4), 230-7.
16. Rakhmetova, A. A.; Alekseeva, T. P.; Bogoslovskaya, O. A.; Leipunskii, I. O.; Ol'khovskaya, I. P.; Zhigach, A. N.; Glushchenko, N. N. *Nanotechnol Russ* **2010**, *5* (3–4), 271–276.
17. Lansdown, AB. *Crit Rev Toxicol* **1995**, 25 (5), 397-462.
18. Lansdown, A. B. G.; Sampson, B.; Rowe, A. *J. Anat.* **1999**, *195* (3), 375–38.
19. Turnlund, J. R. *Am. J. Clin. Nutr.* **1998**, *67* (5 suppl.), 960S-964S.
20. Yoon, K. Y.; Hoon Byeon, J.; Park, J. H.; Hwang, J. *Sci. Total Environ.* **2007**, *373* (2–3), 572–575.
21. Perelshtein, I.; Applerot, G.; Perkas, N.; Wehrschuetz-Sigl, E.; Hasmann, A.; Guebitz, G.; Gedanken, A. *Surf. Coatings Technol.* **2009**, *204* (1–2), 54–57.
22. Rajeshkumar, S.; Rinitha, G. *OpenNano* **2018**, *3* (March), 18–27.
23. Das, M.; Goswami, U.; Ghosh, S.S.; Chattopadhyay, A. *ACS Appl. Bio.Mater* ***2018***, *1* (6), 2153-2166.
24. Jia, B.; Mei, Y.; Cheng, L.; Zhou, J.; Zhang, L. *ACS Appl. Mater. Interfaces* **2012**, *4* (6), 2897–2902.
25. Babushkina, I. V.; Gladkova, E. V.; Mamonova, I. A. *World J. Med. Sci*. **2013**, *8* (4), 318–321.
26. Theivasanthi, T.; Alagar, M. *Ann Bio Res* **2011**, *2* (3), 368–373.
27. Datta, K. K. R.; Kulkarni, C.; Eswaramoorthy, M. *Chem comm* **2010**, 4, 4–7.
28. Ziv-Polat, O.; Topaz, M.; Brosh, T.; Margel, S. *Biomaterials* **2010**, *31* (4), 741–747.
29. Gupta, A. K.; Gupta, M. *Biomaterials* **2005**, *26* (18), 3995–4021.

30. Taner, M.; Sayar, N.; Yulug, I. G.; Suzer, S. *J. Mater. Chem.* **2011**, *902874* (35), 2193–2201.
31. Eremenko, A. M.; Petrik, I. S.; Smirnova, N. P.; Rudenko, A. V.; Marikvas, Y. S. *Nanoscale Res. Lett.* **2016**, *11* (1), 1–9.
32. Kandpal, N.; Sah, N.; Loshali, R.; Joshi, R.; Prasad, J. *J. Sci. Ind. Res.* **2014**, *73*, 87–90.
33. Peternele, W.; Monge Fuentes, V.; Fascineli, M. L.; Rodrigues Da Silva, J.; Silva, R.; Lucci, C.; Bentes De Azevedo, R. *J. Nanomater.* **2014**, *94* (1), 10.
34. Mallick, S.; Sharma, S.; Banerjee, M.; Ghosh, S. S.; Chattopadhyay, A.; Paul, A. *ACS Appl. Mater. Interfaces* **2012**, *4* (3), 1313–1323.
35. Tian, J.; Wong, K. K. Y.; Ho, C. M.; Lok, C. N.; Yu, W. Y.; Che, C. M.; Chiu, J. F.; Tam, P. K. H. *ChemMedChem* **2007**, *2* (1), 129–136.
36. Blackwell, T. S.; Christman, J. W. *Br. J. Anaesth.* **1996**, *77* (1), 110–117.
37. Gogos, C. A.; Drosou, E.; Bassaris, H. P.; Skoutelis, A. *J. Infect.Dis.* **2002**, *181* (1), 176–180.
38. Fernandes, A. A. M.; Carvalho, L. J. D. M.; Zanini, G. M.; Ventura, A. M. R. D. S.; Souza, J. M.; Cotias, P. M.; Silva-Filho, I. L.; Daniel-Ribeiro, C. T. *Clin. Vaccine Immunol.* **2008**, *15* (4), 650–658.
39. Goddard, A.; Leisewitz, A. L.; Kjelgaard-Hansen, M.; Kristensen, A. T.; Schoeman, J. P. *PLoS One* **2016**, *11* (3), 1–15.
40. Kalita, S.; Devi, B.; Kandimalla, R.; Sharma, K. K.; Sharma, A.; Kalita, K.; Kataki, A. C.; Kotoky, J. *Int J Nanomedicine* **2015**, 2971–2984.
41. Gholinejad, M.; Saadati, F.; Shaybanizadeh, S.; Pullithadathil, B. *RSC Adv.* **2016**, *6* (6), 4983–4991.
42. Kozak, D. S.; Sergiienko, R. A.; Shibata, E.; Iizuka, A.; Nakamura, T. *Sci. Rep.* **2016**, *6*, 1–9.
43. Knappett, B. R.; Abdulkin, P.; Ringe, E.; Jefferson, D. A.; Lozano-Perez, S.; Rojas, T. C.; Fernández, A.; Wheatley, A. E. H. *Nanoscale* **2013**, *5* (13), 5765.

44. Blanco-Andujar, C.; Ortega, D.; Pankhurst, Q. A.; Thanh, N. T. K. *J. Mater. Chem.* **2012**, *22* (25), 12498.
45. Morris, M. C.; McMurdie, H. F.; Evans, E. H.; Paretzkin, B.; Parker, H. S.; Panagiotopoulos, N. C.; Hubbard, C. R. U.S. Department of Commerce, NBS: Washington, D.C., **1981**; Vol. 37.
46. Salem, N. M.; Awwad, A. M. *Nanosci. Nanotechnol.* **2013**, *3* (3), 35–39.
47. Sukumar, U. K.; Gopinath, P. *RSC Adv.* **2016**, *6* (52), 46186–46201.
48. Zhuang, L.; Zhang, W.; Zhao, Y.; Shen, H.; Lin, H.; Liang, J. *Sci. Rep.* **2015**, *5*, 1–6.
49. Wei, H.; Hu, D.; Su, J.; Li, K. *Chinese J. Chem. Eng.* **2015**, *23* (1), 296–302.
50. Yu, X.; Cheng, G.; Zheng, S. Y. *Sci. Rep.* **2016**, *6* (May), 1–11.
51. Jia, B.; Qin, M.; Zhang, Z.; Cao, Z.; Wu, H.; Chen, P.; Zhang, L.; Lu, X.; Qu, X. *Cryst Eng Comm* **2016**, *18* (8), 1376–1383.
52. Meghana, S.; Kabra, P.; Chakraborty, S.; Padmavathy, N. *RSC Adv.* **2015**, *5* (16), 12293–12299.
53. Liu, Y.; Thibodeaux, D.; Gamble, G.; Bauer, P.; VanDerveer, D. *Appl. Spectrosc.* **2012**, *66* (8), 983–986.
54. Singhal, J. P.; Ray, A. R. *Biomaterials* **2002**, *23* (4), 1139–1145.

CHAPTER-6

Overview and Future Prospects

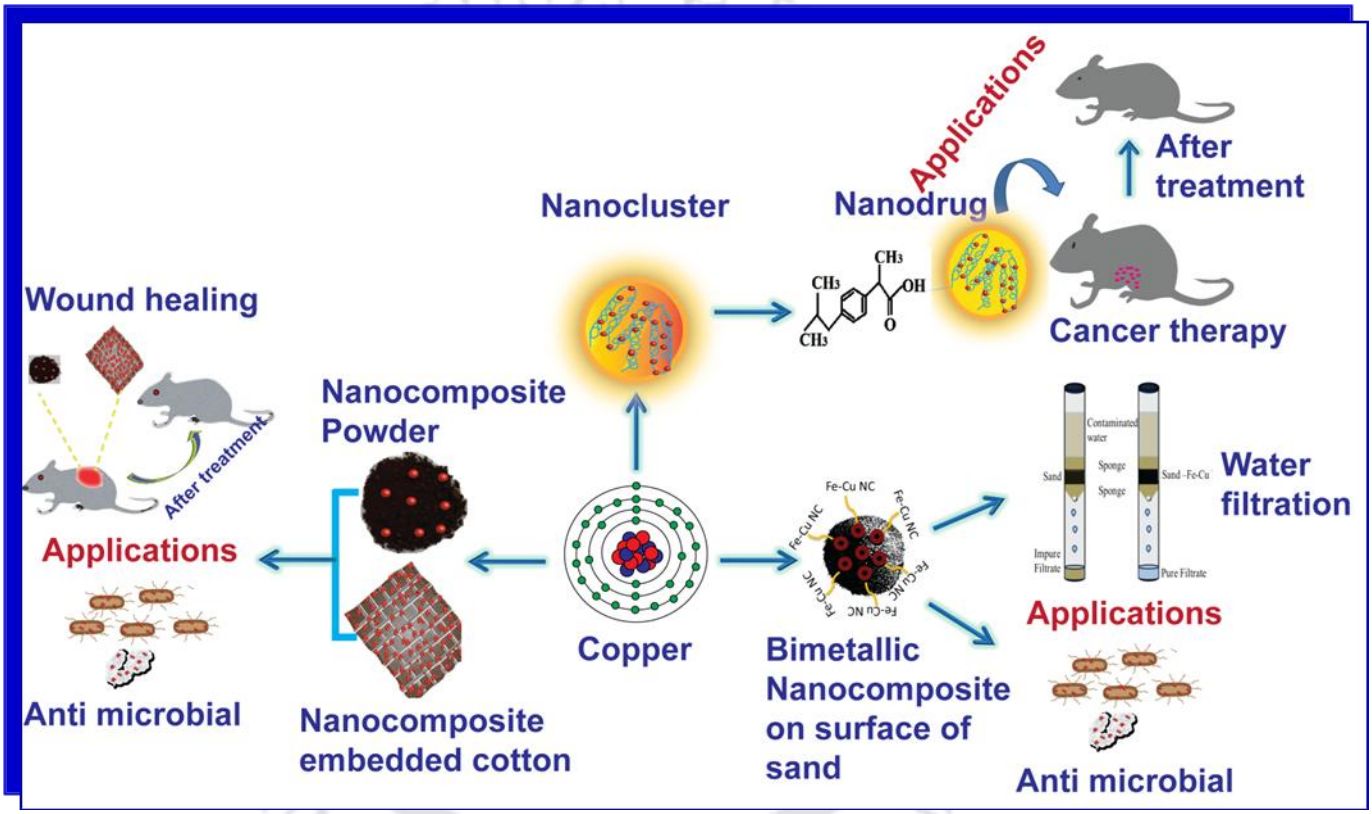

Chapter 6, concisely summarize of the current study and introduces the scope for future work.

CHAPTER -6

6.1. Summary of the Thesis

In recent years, nanoscale objects achieve enormous significance because of their superior physicochemical and mechanical properties and because of these exclusive properties they are extremely in demand for applications in various disciplines including biomedical healthcare system. Lately, copper in nanoplatform have drawn much attention because of their natural abundance and affordability besides their other unique properties.

The present thesis predominantly highlights on development of copper based nanomaterials, functionalizing with other materials and thus fabricating different composite nanoparticles with potential biomedical applications in cancer chemotherapy, annihilation of a wide range of clinical isolates including multi drug resistant organisms, point-of-use water filtration and wound healing. As several projects related to cancer therapy were under trial, preference was given to fabricate a nanodrug for cancer theranostics. As a key to the successful cancer therapy, combination chemotherapy was achieved with BSA-Cu NC encapsulated ibuprofen, a non steroidal anti-inflammatory drug, by an easy, rapid, and affordable approach. The formulated biocompatible nanodrug displayed superior therapeutic efficiency on *in vitro* HeLa cell lines as well as *in vivo* experiments on DLA bearing mice. Experiment results were supported with detailed molecular mechanisms.

In view of the antimicrobial property of the copper nanoparticles, subsequently a bimetallic nanocomposite was formulated to negate multidrug resistant organisms. Emergence of the multi drug resistant bacterial strains, associated with unavailability of newer antimicrobial agents, project an alarming panorama in infection management. Therefore, a simple and rapid attempt was made to formulate a bimetallic nanocomposite blending copper with iron and sand particles to achieve a product with multifaceted utility. The resultant nanocomposite ascertained superior antimicrobial efficacy against various clinical isolates including methicillin resistant *S. aureus*

(MRSA) as well as fungus isolated from real patients' samples. Next the bacterial annihilation property of the nanocomposite was exploited for purification of water. For this a portable hand held filtration device was fabricated with some materials of regular use for point-of-use water filtration at an affordable cost. A wide range of microbes, responsible for waterborne diseases were tested effectively through this filtration device along with few hazardous metals, establishing the successful potentiality of the nanocomposite in water filtration.

In the subsequent study, comparable technique was employed for synthesis of a dressing material in dual forms for assisting wound healing. Bimetallic Fe-Cu nanocomposites in powder form and nanocomposite embedded cotton patch were fabricated for *in vivo* animal testing. Both the materials exhibited wound healing property, even superior to the conventional antibiotic ointment, when tested in infected diabetic wound.

6.2. Future Prospects

The potential scopes of present work based on the current findings are as follows:

- Combination therapy with different chemotherapeutic agents may bring new hope in cancer therapy by reducing the adverse effects of conventional drug regime, thus decreasing the morbidity and mortality from cancer.
- Synthesis of luminescent metal nanoclusters on selected templates may bring a paradigm shift in medical diagnostic field. For example, use of aptamer as a template for synthesis of metal nanoclusters, may help to diagnose some homicidal viruses and bacteria like HIV, HCV, *Salmonella typhi,* at an early stage, thus preventing spreading the diseases.
- Researchers may be persuaded to develop wound healing dressing materials on cotton or adhesive strips.
- Surface modification of metal nanomaterials to enhance their properties, may open up a wide range of application prospects in many health care devices.

PUBLICATIONS

Publications based on the works reported in the thesis:

1. **Das, M**.; Goswami, U.; Ghosh, SS.; Chattopadhyay, A. Bimetallic Fe−Cu Nanocomposites on Sand Particles for the Inactivation of Clinical Isolates and Point-of-Use Water Filtration. ***ACS Applied Bio Materials*** **(2018). DOI: 10.1021/acsabm.8b00572.**
2. **Das, M**.; Goswami, U.; Kandimalla, R.; Kalita, S.; Ghosh, SS.; Chattopadhyay A. Iron-Copper Bimetallic Nanocomposite Reinforced Dressing Materials for Infection Control and Healing of Diabetic Wound (***Under Minor Revision***)

Patents filed:

1. Chattopadhyay, A.; Ghosh, S.S.; **Das, M.** and Goswami, U. A Composition for Filtration of Microorganism and Heavy Metals and A Process Thereof**.** ***Applied.*** (Application No.: **201831016639** dated May 02, 2018).
2. Chattopadhyay, A.; Ghosh, S.S.; **Das, M**.; Goswami, U.; Kandimalla, R.; Kalita, S. Bimetallic Nanocomposite Based Wound Healing System and Method of Manufacture Thereof**.** ***Applied.*** (Application No. **201931014175** dated April 08, 2019).

Manuscript ready for publication:

1. **Das, M**.; Goswami, U.; Bhattacharyya, S.; Kandimalla, R.; Chattopadhyay, A.; Ghosh, S.S. Integration of Nonsteroidal Anti-Inflammatory Drug (NSAID) with Luminescent Copper for *in vivo* Cancer Therapy in Mouse Model.

RSC | Advancing the Chemical Sciences

Royal Society of Chemistry
Thomas Graham House
Science Park
Milton Road
Cambridge
CB4 0WF

Tel: +44 (0)1223 420 066
Fax: +44 (0)1223 423 623
Email: contracts-copyright@rsc.org

www.rsc.org

Acknowledgements to be used by RSC authors

Authors of RSC books and journal articles can reproduce material (for example a figure) from the RSC publication in a non-RSC publication, including theses, without formally requesting permission providing that the correct acknowledgement is given to the RSC publication. This permission extends to reproduction of large portions of text or the whole article or book chapter when being reproduced in a thesis.

The acknowledgement to be used depends on the RSC publication in which the material was published and the form of the acknowledgements is as follows:

- For material being reproduced from an article in *New Journal of Chemistry* the acknowledgement should be in the form:
  - [Original citation] - Reproduced by permission of The Royal Society of Chemistry (RSC) on behalf of the Centre National de la Recherche Scientifique (CNRS) and the RSC
- For material being reproduced from an article *Photochemical & Photobiological Sciences* the acknowledgement should be in the form:
  - [Original citation] - Reproduced by permission of The Royal Society of Chemistry (RSC) on behalf of the European Society for Photobiology, the European Photochemistry Association, and RSC
- For material being reproduced from an article in *Physical Chemistry Chemical Physics* the acknowledgement should be in the form:
  - [Original citation] - Reproduced by permission of the PCCP Owner Societies
- For material reproduced from books and any other journal the acknowledgement should be in the form:
  - [Original citation] - Reproduced by permission of The Royal Society of Chemistry

The acknowledgement should also include a hyperlink to the article on the RSC website.

The form of the acknowledgement is also specified in the RSC agreement/licence signed by the corresponding author.

Except in cases of republication in a thesis, this express permission does not cover the reproduction of large portions of text from the RSC publication or reproduction of the whole article or book chapter.

A publisher of a non-RSC publication can use this document as proof that permission is granted to use the material in the non-RSC publication.

VAT Registration Number: GB 342 1764 71 Registered Charity Number: 207890

RSC | Advancing the Chemical Sciences

Royal Society of Chemistry
Thomas Graham House
Science Park
Milton Road
Cambridge
CB4 0WF

Tel: +44 (0)1223 420 066
Fax: +44 (0)1223 423 623
Email: contracts-copyright@rsc.org

www.rsc.org

Acknowledgements to be used by RSC authors

Authors of RSC books and journal articles can reproduce material (for example a figure) from the RSC publication in a non-RSC publication, including theses, without formally requesting permission providing that the correct acknowledgement is given to the RSC publication. This permission extends to reproduction of large portions of text or the whole article or book chapter when being reproduced in a thesis.

The acknowledgement to be used depends on the RSC publication in which the material was published and the form of the acknowledgements is as follows:

- For material being reproduced from an article in *New Journal of Chemistry* the acknowledgement should be in the form:
  - [Original citation] - Reproduced by permission of The Royal Society of Chemistry (RSC) on behalf of the Centre National de la Recherche Scientifique (CNRS) and the RSC
- For material being reproduced from an article *Photochemical & Photobiological Sciences* the acknowledgement should be in the form:
  - [Original citation] - Reproduced by permission of The Royal Society of Chemistry (RSC) on behalf of the European Society for Photobiology, the European Photochemistry Association, and RSC
- For material being reproduced from an article in *Physical Chemistry Chemical Physics* the acknowledgement should be in the form:
  - [Original citation] - Reproduced by permission of the PCCP Owner Societies
- For material reproduced from books and any other journal the acknowledgement should be in the form:
  - [Original citation] - Reproduced by permission of The Royal Society of Chemistry

The acknowledgement should also include a hyperlink to the article on the RSC website.

The form of the acknowledgement is also specified in the RSC agreement/licence signed by the corresponding author.

Except in cases of republication in a thesis, this express permission does not cover the reproduction of large portions of text from the RSC publication or reproduction of the whole article or book chapter.

A publisher of a non-RSC publication can use this document as proof that permission is granted to use the material in the non-RSC publication.

VAT Registration Number: GB 342 1764 71 Registered Charity Number: 207890

RSC | Advancing the Chemical Sciences

Royal Society of Chemistry
Thomas Graham House
Science Park
Milton Road
Cambridge
CB4 0WF

Tel: +44 (0)1223 420 066
Fax: +44 (0)1223 423 623
Email: contracts-copyright@rsc.org

www.rsc.org

Acknowledgements to be used by RSC authors

Authors of RSC books and journal articles can reproduce material (for example a figure) from the RSC publication in a non-RSC publication, including theses, without formally requesting permission providing that the correct acknowledgement is given to the RSC publication. This permission extends to reproduction of large portions of text or the whole article or book chapter when being reproduced in a thesis.

The acknowledgement to be used depends on the RSC publication in which the material was published and the form of the acknowledgements is as follows:

- For material being reproduced from an article in *New Journal of Chemistry* the acknowledgement should be in the form:
  - [Original citation] - Reproduced by permission of The Royal Society of Chemistry (RSC) on behalf of the Centre National de la Recherche Scientifique (CNRS) and the RSC
- For material being reproduced from an article *Photochemical & Photobiological Sciences* the acknowledgement should be in the form:
  - [Original citation] - Reproduced by permission of The Royal Society of Chemistry (RSC) on behalf of the European Society for Photobiology, the European Photochemistry Association, and RSC
- For material being reproduced from an article in *Physical Chemistry Chemical Physics* the acknowledgement should be in the form:
  - [Original citation] - Reproduced by permission of the PCCP Owner Societies
- For material reproduced from books and any other journal the acknowledgement should be in the form:
  - [Original citation] - Reproduced by permission of The Royal Society of Chemistry

The acknowledgement should also include a hyperlink to the article on the RSC website.

The form of the acknowledgement is also specified in the RSC agreement/licence signed by the corresponding author.

Except in cases of republication in a thesis, this express permission does not cover the reproduction of large portions of text from the RSC publication or reproduction of the whole article or book chapter.

A publisher of a non-RSC publication can use this document as proof that permission is granted to use the material in the non-RSC publication.

VAT Registration Number: GB 342 1764 71 Registered Charity Number: 207890